Prepared for submission to JHEP version "00z"; July 20, 2018; JLAB-THY-18-XXXX

Semi-Inclusive Deep Inelastic Scattering in Wandzura-Wilczek-type approximation

S. Bastami[a] **H. Avakian**[b] **A. V. Efremov**[c] **A. Kotzinian**[d,e] **B. U. Musch**[f] **B. Parsamyan**[k] **A. Prokudin**[g,b] **M. Schlegel**[h] **G. Schnell**[i] **P. Schweitzer**[a,j] **K. Tezgin**[a]

[a] *Department of Physics, University of Connecticut, Storrs, CT 06269, U.S.A.*
[b] *Thomas Jefferson National Accelerator Facility, Newport News, VA 23606, U.S.A.*
[c] *Joint Institute for Nuclear Research, Dubna, 141980 Russia*
[d] *Yerevan Physics Institute, Alikhanyan Brothers St., 375036 Yerevan, Armenia*
[e] *INFN, Sezione di Torino, 10125 Torino, Italy*
[f] *Institut f́ur Theoretische Physik, Universit́at Regensburg, 93040 Regensburg, Germany*
[g] *Division of Science, Penn State Berks, Reading, PA 19610, USA*
[k] *CERN, 1211 Geneva 23, Switzerland*
[h] *Department of Physics, New Mexico State University, Las Cruces, NM 88003-001, USA*
[i] *Department of Theoretical Physics, University of the Basque Country UPV/EHU, 48080 Bilbao, Spain, and IKERBASQUE, Basque Foundation for Science, 48013 Bilbao, Spain*
[j] *Institute for Theoretical Physics, Universit́at T́ubingen, D-72076 T́ubingen, Germany*

E-mail: saman.bastami@uconn.edu, avakian@jlab.org, efremov@theor.jinr.ru, aram.kotzinian@cern.ch, bmusch@b-mu.de, bakur@cern.ch, prokudin@jlab.org, schlegel@nmsu.edu, gunar.schnell@desy.de, peter.schweitzer@phys.uconn.edu, kemal.tezgin@uconn.edu

Abstract: We present the complete cross-section for the production of unpolarized hadrons in semi-inclusive deep-inelastic scattering up to power-suppressed $\mathcal{O}(1/Q^2)$ terms in the Wandzura–Wilczek-type approximation which consists in systematically assuming that $\bar{q}gq$–terms are much smaller than $\bar{q}q$–correlators. We compute all twist-2 and twist-3 structure functions and the corresponding asymmetries, and discuss the applicability of the Wandzura–Wilczek-type approximations on the basis of available data. We make predictions which can be tested by data from Jefferson Lab, COMPASS, HERMES, and the future Electron-Ion Collider. The results of this paper can be readily used for phenomenology and for event generators, and will help to improve our understanding of the TMD theory beyond leading twist.

Keywords: Wandzura–Wilczek approximation, semi-inclusive deep-inelastic scattering, transverse momentum dependent distribution and fragmentation functions, spin and azimuthal asymmetries, leading and subleading twist

Contents

1 Introduction

A great deal of what is known about the quark-gluon structure of nucleons is due to studies of parton distribution functions (PDFs) in deep-inelastic reactions. Leading-twist PDFs tell us how likely it is to find an unpolarized parton (described by PDF $f_1^a(x)$, $a = q,\, \bar{q},\, g$) or a longitudinally polarized parton (described by PDF $g_1^a(x)$, $a = q,\, \bar{q},\, g$) in a fast-moving unpolarized or longitudinally polarized nucleon, which carries the fraction x of the nucleon momentum. This information depends on the "resolution (renormalization) scale" associated with the hard scale Q of the process. Although the PDFs $f_1^a(x)$ and $g_1^a(x)$ continue being the subject of intense research (small-x, large-x, helicity sea and gluon distributions) they can be considered as rather well-known, and the frontier has been extended in the last years to go beyond the one-dimensional picture offered by those PDFs.

One way to do this consists in a systematic inclusion of transverse parton momenta $k_\perp$, whose effects manifest themselves in terms of transverse momenta of the reaction products in the final state. If these transverse momenta are much smaller than the hard scale Q of the process, the formal description is given in terms of transverse momentum dependent distribution functions (TMDs) and fragmentation functions (FFs), which are defined in terms of quark-quark correlators [1–5], and depend on two independent variables: for TMDs, on the fraction x of nucleon momentum carried by the parton and intrinsic transverse momentum $k_\perp$ of the parton. For FFs, on the fraction z of the parton momentum transferred to the hadron for and the transverse momentum of the hadron acquired during the fragmentation process. Being a vector in the plane transverse with respect to the light-cone direction singled out by the hard momentum flow in the process, $k_\perp$ allows us to access novel information on the nucleon spin structure through correlations of $k_\perp$ with the nucleon and/or parton spin. The latter is a well-defined concept for twist-2 TMDs interpreted in the infinite momentum frame or in the lightcone quantization formalism.

One powerful tool to study TMDs are measurements of the semi-inclusive deep-inelastic scattering (SIDIS) process. By exploring various possibilities for the lepton beam and target polarizations unambiguous information can be accessed on the 8 leading-twist TMDs [3] and, if one assumes factorization, on certain linear combinations of the 16 subleading-twist TMDs [4, 5]. It is important to stress that this information could not have been obtained without advances in target polarization techniques employed in the HERMES, COMPASS and JLab experiments [6–8]. Complementary information can be obtained from the Drell–Yan process [9], and e^+e^- annihilation [10].

In QCD the TMDs are independent functions. Each TMD contains unique information on a different aspect of the nucleon structure. Twist-2 TMDs have partonic interpretations. Twist-3 TMDs give insights on quark-gluon correlations in the nucleon [11–13]. Besides positivity constraints [14] there is little model-independent information on TMDs. An important question with practical applications is: do useful *approximations* for TMDs exist? Experience from collinear PDFs encourages to explore this possibility: the twist-3 $g_T^a(x)$ and $h_L^a(x)$ can be respectively expressed in terms of contributions from twist-2 $g_1^a(x)$ and $h_1^a(x)$, and additional quark-gluon-quark ($\bar{q}gq$) correlations or current-quark mass terms [15, 16] (the index $a = q\,,\bar{q}$ does not include gluons for h_1^a, h_L^a and other chiral-odd TMDs below). We shall refer to the latter generically as $\bar{q}gq$–terms, keeping in mind one deals in each case with matrix elements of different operators. The $\bar{q}gq$–correlations contain new insights on hadron structure, which are worthwhile exploring for their own sake, see [17] on $g_T^a(x)$.

The striking observation is that the $\bar{q}gq$–terms in $g_T^a(x)$ and $h_L^a(x)$ are small: theoretical mechanisms predict this [18–21], and in the case of $g_T^a(x)$ data confirm or are compatible with these predictions [22–24]. This approximation ("neglect of $\bar{q}gq$–terms") is commonly known as Wandzura–Wilczek (WW) approximation [15]. The possibility to apply this type of approximation also to TMDs has been explored in specific cases in [25–31]. In both cases, PDFs and TMDs, one basically assumes that the contributions from $\bar{q}gq$–terms can be neglected with respect to $\bar{q}q$–terms. But the nature of the omitted matrix elements is different, and in the context of TMDs one often prefers to speak about WW-type approximations.

The present work is the first study of all SIDIS structure functions up to twist-3 in a unique approach. Our results are of importance for measurements performed or in preparation at HERMES, COMPASS, Jefferson Lab (JLab) with 12 GeV beam-energy upgrade, or proposed in the long-term (Electron Ion Collider), and provide helpful input for the development of Monte Carlo event generators [32].

Our predictions, whether confirmed or not supported by current and future experimental data, will in any case provide a useful benchmark, and call for dedicated theoretical studies to explain (i) why the pertinent $\bar{q}gq$–terms are small or (ii) why they are sizable. In either case our results will deepen the understanding of $\bar{q}gq$–correlations, pave the way towards testing the validity of the TMD factorization approach at subleading twist, and help us to guide further developments.

In this work, after introducing the SIDIS process and defining TMDs and FFs (Sec. 2), we shall introduce the WW(-type) approximations, and review what is presently known about them from experiment and theory (Sec. 3). We will show that under the assumption of the validity of these approximations all leading and subleading SIDIS structure functions are described in terms of a basis of 6 TMDs and 2 FFs (Sec. 4), and review how these basis functions describe available data (Sec. 5). We will systematically apply the WW and/or WW-type approximations to SIDIS structure functions at leading (Sec. 6) and subleading (Sec. 7) twist, and conclude with a critical discussion (Sec. 8). The Appendices A and B contain technical details. In App. C we describe an open-source package implemented in `mathematica` [33] (already available) and `Python` (to be released in the near future) that is made publicly available on `github.com`: https://github.com/prokudin/WW-SIDIS

2 The SIDIS process in terms of TMDs and FFs

In this section we review the description of the SIDIS process, define structure functions, PDFs, TMDs, FFs and recall how they describe the SIDIS structure functions.

2.1 The SIDIS process

The SIDIS process $lN \to l'hX$ is sketched in Fig. 1. Here, l and P are the momenta of the incoming lepton and nucleon, l' and P_h are the momenta of the outgoing lepton and produced hadron. The virtual-photon momentum $q = l - l'$ defines the z-axis, and l' points in the direction of the x-axis from which azimuthal angles are counted. The relevant kinematic invariants are

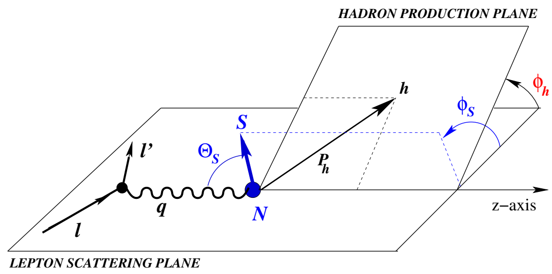

Figure 1. Kinematics of the SIDIS process $lN \to l'hX$ in the 1-photon exchange approximation.

$$x = \frac{Q^2}{2\,P\cdot q}, \quad y = \frac{P\cdot q}{P\cdot l}, \quad z = \frac{P\cdot P_h}{P\cdot q}, \quad Q^2 = -q^2. \tag{2.1}$$

Note that we consider the production of unpolarized hadrons in DIS of charged leptons (electrons, positrons, muons) at $Q^2 \ll M_Z^2$ in the single-photon exchange approximation, where M_Z denotes the mass of the Z^0 electroweak gauge boson. In addition to x, y, z the cross section is also differential in the azimuthal angle ϕ_h of the produced hadron, the square of its momentum component P_{hT} perpendicular with respect to the virtual-photon momentum. The cross section is also differential with respect to the azimuthal angle ψ_l characterizing the overall orientation of the lepton scattering plane around the incoming lepton direction. The angle is calculated with respect to an arbitrary reference axis, which in case of transversely polarized targets is chosen to be the direction of S_T. In the DIS limit $\psi_l \approx \phi_S$, where the latter is the azimuthal angle of the spin-vector defined as in Fig. 1. It is convenient to define the unpolarized lepton–quark scattering subprocess cross section

$$\frac{d\hat{\sigma}}{dy} = \frac{4\pi\alpha_{em}^2}{x\,y\,Q^2}\left(1 - y + \frac{1}{2}y^2\right). \tag{2.2}$$

To leading order in $1/Q$ the SIDIS cross-section is given by

$$\begin{aligned}\frac{d^6\sigma_{\rm leading}}{dx\,dy\,dz\,d\psi_l\,d\phi_h\,dP_{hT}^2} = \frac{1}{4\pi}\,\frac{d\hat{\sigma}}{dy}\,F_{UU}(x,z,P_{hT}^2)\Bigg\{&\,1 + \cos(2\phi_h)\,p_1\,A_{UU}^{\cos(2\phi_h)}\\ &+S_L\sin(2\phi_h)\,p_1\,A_{UL}^{\sin(2\phi_h)} + \lambda\,S_L\,p_2\,A_{LL}\\ &+S_T\sin(\phi_h-\phi_S)\,A_{UT}^{\sin(\phi_h-\phi_S)} + S_T\sin(\phi_h+\phi_S)\,p_1\,A_{UT}^{\sin(\phi_h+\phi_S)}\\ &+S_T\sin(3\phi_h-\phi_S)\,p_1\,A_{UT}^{\sin(3\phi_h-\phi_S)} + \lambda\,S_T\cos(\phi_h-\phi_S)\,p_2\,A_{LT}^{\cos(\phi_h-\phi_S)}\Bigg\}.\end{aligned} \tag{2.3a}$$

Here F_{UU} is the structure function due to transverse polarization of the virtual photon (sometimes denoted as $F_{UU,T}$), and we neglect $1/Q^2$ corrections in kinematic factors and a structure function (sometimes denoted as $F_{UU,L}$) arising from longitudinal polarization of the virtual photon (and another structure function $\propto S_T\,\sin(\phi_h - \phi_S)$, see below). The structure functions (and asymmetries) also depend on Q^2 via the scale dependence of TMDs and FFs, which we do not show in formulas throughout this work.

At subleading order in the $1/Q$ expansion one has

$$\frac{d^6\sigma_{\text{subleading}}}{dx\,dy\,dz\,d\psi_l\,d\phi_h\,dP_{hT}^2} = \frac{1}{4\pi}\,\frac{d\hat{\sigma}}{dy}\,F_{UU}(x,z,P_{hT}^2)\Big\{\cos(\phi_h)\,p_3\,A_{UU}^{\cos(\phi_h)}$$
$$+\lambda\sin(\phi_h)\,p_4\,A_{LU}^{\sin(\phi_h)} + S_L\sin(\phi_h)\,p_3\,A_{UL}^{\sin(\phi_h)} + \lambda\,S_L\cos(\phi_h)\,p_4\,A_{LL}^{\cos(\phi_h)}$$
$$+S_T\sin(2\phi_h-\phi_S)\,p_3\,A_{UT}^{\sin(2\phi_h-\phi_S)} + S_T\sin(\phi_S)\,p_3\,A_{UT}^{\sin(\phi_S)}$$
$$+\lambda\,S_T\cos(\phi_S)\,p_4\,A_{LT}^{\cos(\phi_S)} + \lambda\,S_T\cos(2\phi_h-\phi_S)\,p_4\,A_{LT}^{\cos(2\phi_h-\phi_S)}\Big\} \tag{2.3b}$$

Neglecting $1/Q^2$ corrections, the kinematic prefactors p_i are given by

$$p_1 = \frac{1-y}{1-y+\frac{1}{2}\,y^2}\,, \quad p_2 = \frac{y(1-\frac{1}{2}\,y)}{1-y+\frac{1}{2}\,y^2}\,, \quad p_3 = \frac{(2-y)\sqrt{1-y}}{1-y+\frac{1}{2}\,y^2}\,, \quad p_4 = \frac{y\sqrt{1-y}}{1-y+\frac{1}{2}\,y^2}\,, \tag{2.4}$$

and the asymmetries are defined as follows

$$A_{XY}^{\text{weight}} \equiv A_{XY}^{\text{weight}}(x,z,P_{hT}) = \frac{F_{XY}^{\text{weight}}(x,z,P_{hT})}{F_{UU}(x,z,P_{hT})}. \tag{2.5}$$

Here the first subscript $X = U(L)$ denotes the unpolarized beam (longitudinally polarized beam with helicity λ). The second subscript $Y = U(L \text{ or } T)$ refers to the target, which can be unpolarized (longitudinally or transversely polarized with respect to virtual photon). The superscript "weight" indicates the azimuthal dependence with no index indicating an isotropic angular distribution of the produced hadrons.

In the partonic description the structure functions in (2.3a) are "twist-2." Those in (2.3b) are "twist-3" and contain a factor M_N/Q in their definitions, see below, where M_N is the nucleon mass. In our treatment to $1/Q^2$ accuracy we neglect two structure functions due to longitudinal virtual-photon polarization, which contribute at order $\mathcal{O}(M_N^2/Q^2)$ in the partonic description of the process, one being $F_{UU,L}$ and the other contributing to the $\sin(\phi_h - \phi_S)$ angular distribution [5].

Experimental collaborations often define asymmetries in terms of counts $N(\phi_h)$. This means the kinematic prefactors p_i and $1/(x\,y\,Q^2)$ are included in the numerators or denominators of the asymmetries which are averaged over y within experimental kinematics. We will call the corresponding asymmetries $A_{XY,\langle y\rangle}^{\text{weight}}$. For instance, in the unpolarized case one has

$$N(x,\dots,\phi) = \frac{N_0(x,\dots)}{2\pi}\left(1+\cos\phi\;A_{UU,\langle y\rangle}^{\cos\phi_h}(x,\dots)+\cos 2\phi\;A_{UU,\langle y\rangle}^{\cos 2\phi_h}(x,\dots)\right) \tag{2.6}$$

where N_0 denotes the total (ϕ_h–averaged) number of counts and the dots indicate further kinematic variables in the kinematic bin of interest (which may also be averaged over). It would be preferable if asymmetries were analyzed with known kinematic prefactors divided out on event-by-event basis. One could then directly compare asymmetries $A_{XY}^{\rm weight}$ measured in different experiments and kinematics, and focus on effects of evolution or power suppression for twist-3. In practice, often the kinematic factors were included. We will define and comment on the explicit expressions as needed.

For completeness we remark that after integrating the cross section over transverse hadron momenta one obtains

$$\frac{d^4\sigma_{\rm leading}}{dx\,dy\,dz\,d\psi_l} = \frac{1}{2\pi}\,\frac{d\hat{\sigma}}{dy}\;F_{UU}(x,z)\biggl\{\;1+\lambda\,S_L\,p_2\,A_{LL}\biggr\} \tag{2.7a}$$

$$\frac{d^4\sigma_{\rm subleading}}{dx\,dy\,dz\,d\psi_l} = \frac{1}{2\pi}\,\frac{d\hat{\sigma}}{dy}\;F_{UU}(x,z)\biggl\{S_T\sin(\phi_S)\,p_3\,A_{UT}^{\sin(\phi_S)}+\lambda\,S_T\cos(\phi_S)\,p_4\,A_{LT}^{\cos(\phi_S)}\biggr\} \tag{2.7b}$$

where (and analogous for the other structure functions)

$$F_{UU}(x,z) = \int d^2P_{hT}\;F_{UU}(x,z,P_{hT}) \tag{2.8}$$

and the asymmetries are defined as

$$A_{XY}^{\rm weight}(x,z) = \frac{F_{XY}^{\rm weight}(x,z)}{F_{UU}(x,z)}\,. \tag{2.9}$$

The connection of "collinear" SIDIS structure functions in (2.7a, 2.7b) to those known from inclusive DIS is established by integrating over z and summing over hadrons as

$$\sum_h\int dz\;z\;F_{UU}(x,z) \quad\equiv\quad 2\,x\,F_1(x)\;, \tag{2.10a}$$

$$\sum_h\int dz\;z\;F_{LL}(x,z) \quad\equiv\quad 2\,x\,g_1(x)\;, \tag{2.10b}$$

$$\sum_h\int dz\;z\;F_{LT}^{\cos\phi_S}(x,z) \;\equiv\; -\gamma\;2\,x\biggl(g_1(x)+g_2(x)\biggr)\;, \tag{2.10c}$$

$$\sum_h\int dz\;z\;F_{UT}^{\sin\phi_S}(x,z) \;=\; 0\,, \tag{2.10d}$$

where $\gamma = 2M_Nx/Q$ signals the twist-3 character of $F_{LT}^{\cos\phi_S}(x,z)$. Notice that $F_{UT}^{\sin\phi_S}(x,z)$ has no DIS counterpart due to time-reversal symmetry of strong interactions, and terms suppressed by $1/Q^2$ are consequently neglected throughout this work including the twist-4 DIS structure function $F_L(x)$.

2.2 TMDs, FFs and structure functions

TMDs are defined in terms of light-front correlators

$$\Phi(x,\boldsymbol{k}_\perp)_{ij} = \int\frac{d\xi^-d^2\boldsymbol{\xi}_\perp}{(2\pi)^3}\;e^{ik\xi}\;\langle N(P,S)|\bar{\psi}_j(0)\,\mathcal{W}_{(0,\,\infty)}\mathcal{W}_{(\infty,\xi)}\,\psi_i(\xi)|N(P,S)\rangle\bigg|_{\substack{\xi^+=0\\ k^+=xP^+}} \tag{2.11}$$

where the Wilson-lines refer to the SIDIS process [34]. For a generic four-vector a^μ we define the light-cone coordinates $a^\mu = (a^+, a^-, a_\perp)$ with $a^\pm = (a^0 \pm a^3)/\sqrt{2}$. The light-cone direction is singled out by the virtual-photon momentum and transverse vectors like $\boldsymbol{k}_\perp$ are perpendicular to it. In the virtual-photon–nucleon center-of-mass frame, the nucleon and the partons inside it move in the (+)–lightcone direction, while the struck quark and the produced hadron move in the (−)–light-cone direction. In the nucleon rest frame the polarization vector is given by $S = (0, \boldsymbol{S}_T, S_L)$ with $\boldsymbol{S}_T^2 + S_L^2 = 1$.

The 8 leading-twist TMDs [3] are projected out from the correlator (2.11) as follows (blue: T-even TMDs, red: T-odd TMDs; all TMDs depend on x, $k_\perp$, renormalization scale and carry a flavor index which we do not indicate for brevity):

$$\frac{1}{2}\,\mathrm{Tr}\Big[\gamma^+\,\Phi(x,\boldsymbol{k}_\perp)\Big] = f_1 - \frac{\varepsilon^{jk}k_\perp^j S_T^k}{M_N}\,f_{1T}^\perp\,, \tag{2.12a}$$

$$\frac{1}{2}\,\mathrm{Tr}\Big[\gamma^+\gamma_5\,\Phi(x,\boldsymbol{k}_\perp)\Big] = S_L\,g_1 + \frac{\boldsymbol{k}_\perp\cdot\boldsymbol{S}_T}{M_N}\,g_{1T}^\perp\,, \tag{2.12b}$$

$$\frac{1}{2}\,\mathrm{Tr}\Big[i\sigma^{j+}\gamma_5\,\Phi(x,\boldsymbol{k}_\perp)\Big] = S_T^j\,h_1 + S_L\,\frac{k_\perp^j}{M_N}\,h_{1L}^\perp + \frac{\kappa^{jk}S_T^k}{M_N^2}\,h_{1T}^\perp + \frac{\varepsilon^{jk}k_\perp^k}{M_N}\,h_1^\perp\,, \tag{2.12c}$$

and the 16 subleading-twist TMDs [2, 5] are given by

$$\frac{1}{2}\mathrm{Tr}\Big[1\,\Phi(x,\boldsymbol{k}_\perp)\Big] = \frac{M_N}{P^+}\Big[\quad e - \frac{\varepsilon^{jk}k_\perp^j S_T^k}{M_N}\,e_T^\perp\Big], \tag{2.12d}$$

$$\frac{1}{2}\mathrm{Tr}\Big[i\gamma_5\Phi(x,\boldsymbol{k}_\perp)\Big] = \frac{M_N}{P^+}\Big[S_L e_L + \frac{\boldsymbol{k}_\perp\cdot\boldsymbol{S}_T}{M_N}\,e_T\Big], \tag{2.12e}$$

$$\frac{1}{2}\mathrm{Tr}\Big[\gamma^j\,\Phi(x,\boldsymbol{k}_\perp)\Big] = \frac{M_N}{P^+}\Big[\frac{k_\perp^j}{M_N}f^\perp + \varepsilon^{jk}S_T^k f_T + S_L\frac{\varepsilon^{jk}k_\perp^k}{M_N}f_L^\perp - \frac{\kappa^{jk}\varepsilon^{kl}S_T^l}{M_N^2}f_T^\perp\Big], \tag{2.12f}$$

$$\frac{1}{2}\mathrm{Tr}\Big[\gamma^j\gamma_5\Phi(x,\boldsymbol{k}_\perp)\Big] = \frac{M_N}{P^+}\Big[S_T^j\,g_T + S_L\,\frac{k_\perp^j}{M_N}g_L^\perp + \frac{\kappa^{jk}S_T^k}{M_N^2}\,g_T^\perp + \frac{\varepsilon^{jk}k_\perp^k}{M_N}\,g^\perp\Big], \tag{2.12g}$$

$$\frac{1}{2}\mathrm{Tr}\Big[i\,\sigma^{jk}\gamma_5\Phi(x,\boldsymbol{k}_\perp)\Big] = \frac{M_N}{P^+}\Big[\frac{S_T^j k_\perp^k - S_T^k k_\perp^j}{M_N}\,h_T^\perp - \varepsilon^{jk}\,h\Big], \tag{2.12h}$$

$$\frac{1}{2}\mathrm{Tr}\Big[i\,\sigma^{+-}\gamma_5\,\Phi(x,\boldsymbol{k}_\perp)\Big] = \frac{M_N}{P^+}\Big[S_L\,h_L + \frac{\boldsymbol{k}_\perp\cdot\boldsymbol{S}_T}{M_N}\,h_T\Big], \tag{2.12i}$$

where $\kappa^{jk} \equiv (k_\perp^j k_\perp^k - \frac{1}{2}\,\boldsymbol{k}_\perp^2\delta^{jk})$. The indices j, k, l refer to the plane transverse with respect to the light-cone, $\epsilon^{ij} \equiv \epsilon^{-+ij}$ and $\epsilon^{0123} = +1$. Dirac-structures not listed in (2.12a–2.12i) are twist-4 [4]. Integrating out transverse momenta in the correlator (2.11) leads to the "usual" PDFs known from collinear kinematics [16, 35], namely at twist-2 level

$$\frac{1}{2}\,\mathrm{Tr}\Big[\gamma^+\,\Phi(x)\Big] = f_1\,, \tag{2.13a}$$

$$\frac{1}{2}\,\mathrm{Tr}\Big[\gamma^+\gamma_5\,\Phi(x)\Big] = S_L\,g_1\,, \tag{2.13b}$$

$$\frac{1}{2}\,\mathrm{Tr}\Big[i\sigma^{j+}\gamma_5\,\Phi(x)\Big] = S_T^j\,h_1\,, \tag{2.13c}$$

and at twist-3 level

$$\frac{1}{2}\,\mathrm{Tr}\Big[\,1\;\Phi(x)\Big] \;=\; \frac{M_N}{P^+}\;e\;, \tag{2.13d}$$

$$\frac{1}{2}\,\mathrm{Tr}\Big[\gamma^j\gamma_5\;\Phi(x)\Big] \;=\; \frac{M_N}{P^+}\;S_T^j\,g_T\;, \tag{2.13e}$$

$$\frac{1}{2}\,\mathrm{Tr}\Big[\,i\,\sigma^{+-}\gamma_5\;\Phi(x)\Big] \;=\; \frac{M_N}{P^+}\;S_L\,h_L\,. \tag{2.13f}$$

Other structures drop out either due to explicit $k_\perp$–dependence, or due to the sum rules [5]

$$\int d^2\boldsymbol{k}_\perp\;f_T^a(x,k_\perp^2) = \int d^2\boldsymbol{k}_\perp\;e_L^a(x,k_\perp^2) = \int d^2\boldsymbol{k}_\perp\;h^a(x,k_\perp^2) = 0 \tag{2.14}$$

imposed by time reversal constraints.

The fragmentation functions are similarly defined in terms of the correlator

$$\Delta(z,\boldsymbol{P}_\perp)_{ij} = \sum_X\int\frac{d\xi^+d^2\boldsymbol{\xi}_\perp}{2z(2\pi)^3}\,e^{ip\xi}\,\langle 0|\mathcal{W}_{(\infty,\xi)}\psi_i(\xi)\,|h,X\rangle\,\langle h,X|\bar\psi_j(0)\mathcal{W}_{(0,\infty)}|0\rangle\Big|_{\substack{\xi^-=0\\ p^-=P_h^-/z\\ \boldsymbol{p}_\perp=-\boldsymbol{P}_\perp/z.}} \tag{2.15}$$

In this work we will consider only unpolarized final-state hadrons. If the produced hadron moves fast in the $(-)$ light-cone direction, the twist-2 FFs are projected out as

$$\frac{1}{2}\mathrm{Tr}[\gamma^-\Delta(z,\boldsymbol{P}_\perp)] \;=\; D_1\,, \tag{2.16a}$$

$$\frac{1}{2}\mathrm{Tr}[i\sigma^{j-}\gamma_5\Delta(z,\boldsymbol{P}_\perp)] \;=\; \epsilon^{jk}\,\frac{P_\perp^k}{zm_h}H_1^\perp\;, \tag{2.16b}$$

and at twist-3 level

$$\frac{1}{2}\,\mathrm{Tr}\Big[\,1\;\Delta(z,\boldsymbol{P}_\perp)\Big] \;=\; \frac{M_h}{P_h^-}\;E\;, \tag{2.16c}$$

$$\frac{1}{2}\,\mathrm{Tr}\Big[\;\gamma^j\;\Delta(z,\boldsymbol{P}_\perp)\Big] \;=\; -\frac{P_\perp^j}{zP_h^-}\;D^\perp\;, \tag{2.16d}$$

$$\frac{1}{2}\,\mathrm{Tr}\Big[\gamma^j\gamma_5\,\Delta(z,\boldsymbol{P}_\perp)\Big] \;=\; \varepsilon^{jk}\,\frac{P_\perp^k}{zP_h^-}\;G^\perp\;, \tag{2.16e}$$

$$\frac{1}{2}\,\mathrm{Tr}\Big[i\,\sigma^{jk}\gamma_5\,\Delta(z,\boldsymbol{P}_\perp)\Big] \;=\; -\varepsilon^{jk}\,\frac{M_h}{P_h^-}\;H\;. \tag{2.16f}$$

The FFs depend on z, $P_\perp$, renormalization scale, quark flavor and type of hadron which we do not indicate for brevity. Integration over transverse hadron momenta leaves us with $D_1(z)$, $E(z)$, $H(z)$ while the other structures drop out due to their $P_\perp$ dependence.

The structure functions in Eqs. (2.3a, 2.3b) are described in the Bjorken limit at tree level in terms of convolutions of TMDs and FFs. We define the unit vector $\hat{\boldsymbol{h}} = \boldsymbol{P}_{hT}/P_{hT}$ and use the following convolution integrals (see Appendix B.1 for details)

$$\mathcal{C}\Big[\omega\;f\;D\Big] = x\sum_a e_a^2\int d^2\boldsymbol{k}_\perp d^2\boldsymbol{P}_\perp\;\delta^{(2)}(z\boldsymbol{k}_\perp+\boldsymbol{P}_\perp-\boldsymbol{P}_{hT})\;\omega\;f^a(x,\boldsymbol{k}_\perp^2)\;D^a(z,\boldsymbol{P}_\perp^2)\;, \tag{2.17}$$

where ω is a weight function which in general depends on $\boldsymbol{k}_\perp$ and $\boldsymbol{P}_\perp$. The 8 leading–twist structure functions are

$$F_{UU} = \mathcal{C}\Big[\, \omega^{\{0\}}\, f_1 D_1 \,\Big]\,, \tag{2.18a}$$

$$F_{LL} = \mathcal{C}\Big[\, \omega^{\{0\}}\, g_1 D_1 \,\Big]\,, \tag{2.18b}$$

$$F_{UT}^{\sin(\phi_h+\phi_S)} = \mathcal{C}\Big[\, \omega_{\rm A}^{\{1\}}\, h_1 H_1^\perp \,\Big]\,, \tag{2.18c}$$

$$F_{UT}^{\sin(\phi_h-\phi_S)} = \mathcal{C}\Big[-\omega_{\rm B}^{\{1\}}\, f_{1T}^\perp D_1 \Big]\,, \tag{2.18d}$$

$$F_{LT}^{\cos(\phi_h-\phi_S)} = \mathcal{C}\Big[\omega_{\rm B}^{\{1\}}\, g_{1T}^\perp D_1 \Big]\,, \tag{2.18e}$$

$$F_{UU}^{\cos 2\phi_h} = \mathcal{C}\Big[\, \omega_{\rm AB}^{\{2\}}\, h_1^\perp\, H_1^\perp \,\Big]\,, \tag{2.18f}$$

$$F_{UL}^{\sin 2\phi_h} = \mathcal{C}\Big[\, \omega_{\rm AB}^{\{2\}}\, h_{1L}^\perp H_1^\perp \,\Big]\,, \tag{2.18g}$$

$$F_{UT}^{\sin(3\phi_h-\phi_S)} = \mathcal{C}\Big[\, \omega^{\{3\}}\, h_{1T}^\perp H_1^\perp \,\Big]\,. \tag{2.18h}$$

At subleading–twist we have the structure functions

$$F_{UU}^{\cos\phi_h} = \frac{2M_N}{Q}\,\mathcal{C}\Big[\; \omega_{\rm A}^{\{1\}}\Big(xh\, H_1^\perp + r_h\; f_1 \frac{\tilde{D}^\perp}{z}\Big) - \omega_{\rm B}^{\{1\}}\Big(x f^\perp D_1 + r_h\; h_1^\perp \frac{\tilde{H}}{z}\Big)\Big], \tag{2.19a}$$

$$F_{LU}^{\sin\phi_h} = \frac{2M_N}{Q}\,\mathcal{C}\Big[\; \omega_{\rm A}^{\{1\}}\Big(x\, e\, H_1^\perp + r_h\; f_1 \frac{\tilde{G}^\perp}{z}\Big) + \omega_{\rm B}^{\{1\}}\Big(x g^\perp D_1 + r_h\; h_1^\perp \frac{\tilde{E}}{z}\Big)\Big], \tag{2.19b}$$

$$F_{UL}^{\sin\phi_h} = \frac{2M_N}{Q}\,\mathcal{C}\Big[\; \omega_{\rm A}^{\{1\}}\Big(xh_L H_1^\perp + r_h\; g_1 \frac{\tilde{G}^\perp}{z}\Big) + \omega_{\rm B}^{\{1\}}\Big(x f_L^\perp D_1 - r_h\; h_{1L}^\perp \frac{\tilde{H}}{z}\Big)\Big], \tag{2.19c}$$

$$F_{LL}^{\cos\phi_h} = \frac{2M_N}{Q}\,\mathcal{C}\Big[-\omega_{\rm A}^{\{1\}}\Big(xe_L H_1^\perp - r_h\; g_1 \frac{\tilde{D}^\perp}{z}\Big) - \omega_{\rm B}^{\{1\}}\Big(x g_L^\perp D_1 + r_h\; h_{1L}^\perp \frac{\tilde{E}}{z}\Big)\Big] \tag{2.19d}$$

$$\begin{aligned} F_{UT}^{\sin\phi_S} = \frac{2M_N}{Q}\,\mathcal{C}\Big[\; & \omega^{\{0\}}\,\Big(x f_T D_1 \;- r_h\; h_1 \frac{\tilde{H}}{z}\Big) \\ & -\frac{\omega_{\rm B}^{\{2\}}}{2}\Big(xh_T H_1^\perp + r_h\, g_{1T}^\perp \frac{\tilde{G}^\perp}{z} - xh_T^\perp H_1^\perp + r_h\, f_{1T}^\perp \frac{\tilde{D}^\perp}{z}\Big)\Big]\,, \end{aligned} \tag{2.19e}$$

$$\begin{aligned} F_{LT}^{\cos\phi_S} = \frac{2M_N}{Q}\,\mathcal{C}\Big[& -\omega^{\{0\}}\,\Big(x g_T D_1 + r_h\; h_1 \frac{\tilde{E}}{z}\Big) \\ & +\frac{\omega_{\rm B}^{\{2\}}}{2}\Big(xe_T H_1^\perp - r_h\, g_{1T}^\perp \frac{\tilde{D}^\perp}{z} + xe_T^\perp H_1^\perp + r_h\, f_{1T}^\perp \frac{\tilde{G}^\perp}{z}\Big)\Big]\,, \end{aligned} \tag{2.19f}$$

$$\begin{aligned} F_{UT}^{\sin(2\phi_h-\phi_S)} = \frac{2M_N}{Q}\,\mathcal{C}\Big[\; & \frac{\omega_{\rm AB}^{\{2\}}}{2}\,\Big(xh_T H_1^\perp + r_h\, g_{1T}^\perp \frac{\tilde{G}^\perp}{z} + xh_T^\perp H_1^\perp - r_h\, f_{1T}^\perp \frac{\tilde{D}^\perp}{z}\Big) \\ & +\omega_{\rm C}^{\{2\}}\Big(x f_T^\perp D_1 - r_h\; h_{1T}^\perp \frac{\tilde{H}}{z}\Big)\Big]\,, \end{aligned} \tag{2.19g}$$

$$F_{LT}^{\cos(2\phi_h-\phi_S)} = \frac{2M_N}{Q}\,\mathcal{C}\Big[-\frac{\omega_{\rm AB}^{\{2\}}}{2}\Big(xe_T H_1^\perp - r_h\, g_{1T}^\perp\frac{\tilde D^\perp}{z} - xe_T^\perp H_1^\perp - r_h\, f_{1T}^\perp\frac{\tilde G^\perp}{z}\Big) - \omega_{\rm C}^{\{2\}}\Big(xg_T^\perp D_1 + r_h\; h_{1T}^\perp\frac{\tilde E}{z}\Big)\Big]\,, \tag{2.19h}$$

where $r_h = m_h/M_N$ and $F_{XY}^{\rm weight} \equiv F_{XY}^{\rm weight}(x,z,P_{hT})$. The tilde-functions $\tilde D^\perp$, $\tilde G^\perp$, $\tilde H$, $\tilde E$ are defined in terms of $\bar q g q$-correlators, see Sec. 3.2. The weight functions are defined as

$$\begin{aligned}
\omega^{\{0\}} &= 1\,,\\
\omega_{\rm A}^{\{1\}} &= \frac{\hat{\boldsymbol h}\cdot\boldsymbol P_\perp}{zm_h}\,,\quad \omega_{\rm B}^{\{1\}} = \frac{\hat{\boldsymbol h}\cdot\boldsymbol k_\perp}{M_N}\,,\\
\omega_{\rm A}^{\{2\}} &= \frac{2\,(\hat{\boldsymbol h}\cdot\boldsymbol P_\perp)\,(\hat{\boldsymbol h}\cdot\boldsymbol k_\perp)}{zM_Nm_h}\,,\quad \omega_{\rm B}^{\{2\}} = -\frac{\boldsymbol P_\perp\cdot\boldsymbol k_\perp}{zM_Nm_h}\,,\quad \omega_{\rm C}^{\{2\}} = \frac{2\,(\hat{\boldsymbol h}\cdot\boldsymbol k_\perp)^2-\boldsymbol k_\perp^2}{2M_N^2}\,,\\
\omega^{\{3\}} &= \frac{4\,(\hat{\boldsymbol h}\cdot\boldsymbol P_\perp)\,(\hat{\boldsymbol h}\cdot\boldsymbol k_\perp)^2 - 2\,(\hat{\boldsymbol h}\cdot\boldsymbol k_\perp)\,(\boldsymbol k_\perp\cdot\boldsymbol P_\perp) - (\hat{\boldsymbol h}\cdot\boldsymbol P_\perp)\,\boldsymbol k_\perp^2}{2zM_N^2m_h}\,,
\end{aligned} \tag{2.20}$$

and $\omega_{\rm AB}^{\{2\}} = \omega_{\rm A}^{\{2\}} + \omega_{\rm B}^{\{2\}}$. In $\omega_i^{\{n\}}$ the index $n = 0,\,1,\,2,\,3$ indicates the (maximal) power $(P_{hT})^n$ with which the corresponding contribution scales, and index i (if any) distinguishes different types of contributions at the given order n. Notice that twist-3 structure functions in Eqs. (2.19a–2.19h) contain an explicit factor M/Q. We also recall that we neglect two structure functions (denoted in [5] as $F_{UU,L}$ and $F_{UT,L}^{\sin(\phi_h-\phi_S)}$) due to longitudinal virtual-photon polarization, which are of order $\mathcal{O}(M^2/Q^2)$ in the TMD partonic description.

The structure functions surviving P_{hT}–integration of the SIDIS cross section in (2.7a, 2.7b) are associated with the trivial weights $\omega^{\{0\}}$ and expressed in terms of collinear PDFs and FFs as follows (here the sum rules (2.14) are used):

$$F_{UU}(x,z) = x\sum_a e_a^2\, f_1^a(x)\, D_1^a(z)\,, \tag{2.21a}$$

$$F_{LL}(x,z) = x\sum_a e_a^2\, g_1^a(x)\, D_1^a(z)\,, \tag{2.21b}$$

$$F_{LT}^{\cos\phi_S}(x,z) = -\frac{2M_N}{Q}\;x\sum_a e_a^2\Big(x\, g_T^q(x)\, D_1^a(z) + r_h\, h_1^a(x)\frac{\tilde E^a(z)}{z}\Big)\,, \tag{2.21c}$$

$$F_{UT}^{\sin\phi_S}(x,z) = -\frac{2\,m_h}{Q}\;x\sum_a e_a^2\, h_1^a(x)\frac{\tilde H^a(z)}{z}\,. \tag{2.21d}$$

Finally, integrating over z, summing over hadrons, and using the sum rules for the T-odd FFs, $\sum_h\int dz\;\tilde E^a(z) = 0$ and $\sum_h\int dz\;\tilde H^a(z) = 0$, we recover Eqs. (2.10a–2.10d) and obtain for the DIS structure functions

$$F_1(x) = \frac{1}{2}\sum_a e_a^2\, f_1^a(x)\,, \tag{2.22a}$$

$$g_1(x) = \frac{1}{2}\sum_a e_a^2\, g_1^a(x)\,, \tag{2.22b}$$

$$g_2(x) = \frac{1}{2}\sum_a e_a^2\, g_T^a(x)\; - \; g_1(x)\,. \tag{2.22c}$$

Before introducing the WW-type approximations in the next section, we would like to add a comment on TMD factorization: the partonic description of the leading-twist structure functions in (2.18) is based on factorization theorems [36–40]. In contrast to this, the partonic description of the subleading-twist structure functions in (2.19) is based on the *assumption* that that SIDIS cross section factorizes.

A lot of progress has been achieved in recent years in the theoretical understanding of leading-twist observables within the TMD framework, including definition, renormalization and evolution of leading-twist TMDs [41–43], NLO corrections within the TMD framework [44], and phenomenological fits with evolution [45, 46]. In contrast to this, the theory for subleading-twist TMD observables is only poorly developed. Still to the present day, the state-of-the-art approach to subleading-twist TMD observables is the one of Refs. [1–5], based on a TMD tree-level formalism, which we adopt here. In fact, the results of Refs. [47, 48] indicate doubts even in the tree-level formalism. Recently, an attempt was made to remedy these doubts [49]. Keeping in mind these "words of warning," still the formulas (2.19) are the best that theory has to offer currently. We may consider (2.19) as a model itself for the twist-3 SIDIS observables. We hope that the phenomenological approach based on WW-type approximations pursued in this work might lead to more insight into these observables, and eventually might trigger more theory efforts in the future.

3 WW and WW-type approximations

In this section we will define the approximations and review what is known about them. The basic idea of the approximations is simple. One uses QCD equations of motion to separate contributions from $\bar{q}q$–terms and $\bar{q}gq$–terms and assumes that the latter can be neglected with respect to the leading $\bar{q}q$–terms with a useful accuracy (here the $\langle \ldots \rangle$ denote symbolically the matrix elements which enter the definitions of TMDs or FFs):

$$\left| \frac{\langle \bar{q}gq \rangle}{\langle \bar{q}q \rangle} \right| \ll 1 \,. \tag{3.1}$$

3.1 WW approximation for PDFs

The WW approximation applies in principle to all twist-3 PDFs, Eqs. (2.13d, 2.13e, 2.13f). It was established first for $g_T^a(x)$ [15], and later for $h_L^a(x)$ [16]. The situation of $e^a(x)$ is somewhat special, see below and the review [50].

The origin of the approximations is as follows. The operators defining $g_T^a(x)$ and $h_L^a(x)$ can be decomposed by means of QCD equations of motion in twist-2 parts, and pure twist-3 (interaction dependent) $\bar{q}gq$–terms and current-quark mass terms. We denote $\bar{q}gq$–terms and mass terms collectively and symbolically by functions with a tilde. Such decompositions are possible because $g_T^a(x)$ and $h_L^a(x)$ are "twist-3" not according to the "strict QCD definition" (twist = mass dimension of associated local operator minus its spin). Rather they are classified according to the "working definition" of twist [51] (a function is "twist t" if, in addition to overall kinematic prefactors, it contributes to cross sections in a partonic description suppressed by $(M/Q)^{t-2}$ where M is a generic hadronic and Q the hard scale).

The two definitions coincide for twist-2 quantities, but higher-twist observables in general contain "contaminations" by leading twist.

In this way one obtains the decompositions and, if they apply, WW approximations [15, 16] (keep in mind here tilde terms contain pure twist-3 and current-quark mass terms)

$$g_T^a(x) = \int_x^1 \frac{dy}{y}\, g_1^a(y) + \tilde{g}_T^a(x) \overset{\text{WW}}{\approx} \int_x^1 \frac{dy}{y}\, g_1^a(y)\;, \tag{3.2a}$$

$$h_L^a(x) = 2x \int_x^1 \frac{dy}{y^2}\, h_1^a(y) + \tilde{h}_L^a(x) \overset{\text{WW}}{\approx} 2x \int_x^1 \frac{dy}{y^2}\, h_1^a(y)\;, \tag{3.2b}$$

$$x\, e^a(x) = x\, \tilde{e}^a(x) \overset{\text{WW}}{\approx} 0\,, \tag{3.2c}$$

where we included $e^a(x)$ which is a special case in the sense that it receives no twist-2 contribution. A prefactor of x is provided in (3.2c) to cancel a $\delta(x)$–type singularity [50].

The relations (3.2a–3.2c) have been derived basically using operator product expansion techniques [15, 16]. Notice that the operators defining g_T^a and and h_L^a can also be decomposed within the TMD framework by means of a combination of relations derived from the QCD equations of motion and further constraint relations, called Lorentz-Invariance Relations (LIRs), (see recent review [52] and references therein) into a twist-2 part, and dynamical twist-3 (interactions dependent) $\bar{q}gq$-terms and current-quark mass terms.

We will come back to (3.2a, 3.2b) and review the theoretical predictions and supporting experiments, but before we will introduce the WW-type approximations for TMDs and FFs.

3.2 WW-type approximations for TMDs and FFs

Analogous to WW approximations for PDFs discussed in Sec. 3.1, also certain TMDs and FFs can be decomposed in twist-2 contributions and tilde-terms. The latter may be assumed, in the spirit of (3.1), to be small. Hereby it is important to keep in mind that for each TMD or FF one deals with different types of ("unintegrated") $\bar{q}gq$–correlations, and we prefer to refer to them as WW-type approximations.

In the T-even case one obtains the following approximations, where the terms on the left-hand-side are twist-3, those on the right-hand-side (if any) are twist-2,

$$xe^q(x, k_\perp^2) \overset{\text{WW–type}}{\approx} 0, \tag{3.3a}$$

$$xf^{\perp q}(x, k_\perp^2) \overset{\text{WW–type}}{\approx} f_1^q(x, k_\perp^2), \tag{3.3b}$$

$$xg_L^{\perp q}(x, k_\perp^2) \overset{\text{WW–type}}{\approx} g_1^q(x, k_\perp^2), \tag{3.3c}$$

$$xg_T^{\perp q}(x, k_\perp^2) \overset{\text{WW–type}}{\approx} g_{1T}^{\perp q}(x, k_\perp^2), \tag{3.3d}$$

$$xg_T^q(x, k_\perp^2) \overset{\text{WW–type}}{\approx} g_{1T}^{\perp(1)q}(x, k_\perp^2), \tag{3.3e}$$

$$xh_L^q(x, k_\perp^2) \overset{\text{WW–type}}{\approx} -2\, h_{1L}^{\perp(1)q}(x, k_\perp^2), \tag{3.3f}$$

$$xh_T^q(x, k_\perp^2) \overset{\text{WW–type}}{\approx} -h_1^q(x, k_\perp^2) - h_{1T}^{\perp(1)}(x, k_\perp^2), \tag{3.3g}$$

$$xh_T^{\perp q}(x,k_\perp^2) \overset{\text{WW–type}}{\approx} h_1^q(x,k_\perp^2) - h_{1T}^{\perp(1)}(x,k_\perp^2). \tag{3.3h}$$

In the T-odd case one obtains the approximations

$$xe_L^q(x,k_\perp^2) \overset{\text{WW–type}}{\approx} 0, \tag{3.4a}$$
$$xe_T^q(x,k_\perp^2) \overset{\text{WW–type}}{\approx} 0, \tag{3.4b}$$
$$xe_T^{\perp q}(x,k_\perp^2) \overset{\text{WW–type}}{\approx} 0, \tag{3.4c}$$
$$xg^{\perp q}(x,k_\perp^2) \overset{\text{WW–type}}{\approx} 0, \tag{3.4d}$$
$$xf_L^{\perp q}(x,k_\perp^2) \overset{\text{WW–type}}{\approx} 0, \tag{3.4e}$$
$$xf_T^{\perp q}(x,k_\perp^2) \overset{\text{WW–type}}{\approx} f_{1T}^{\perp q}(x,k_\perp^2), \tag{3.4f}$$
$$xf_T^q(x,k_\perp^2) \overset{\text{WW–type}}{\approx} -f_{1T}^{\perp(1)q}(x,k_\perp^2), \tag{3.4g}$$
$$xh^q(x,k_\perp^2) \overset{\text{WW–type}}{\approx} -2\,h_1^{\perp(1)}(x,k_\perp^2). \tag{3.4h}$$

The superscript "(1)" denotes the first transverse moments of TMDs defined generically as

$$f^{(1)}(x,k_\perp^2) = \frac{k_\perp^2}{2M^2}\,f(x,k_\perp^2)\;, \quad f^{(1)}(x) = \int d^2\boldsymbol{k}_\perp f^{(1)}(x,k_\perp^2)\;. \tag{3.5}$$

Two very useful WW-type approximations follow from combining the WW approximations (3.2a, 3.2b) with the WW-type approximations (3.3e, 3.3f). This yields [2, 28, 31]

$$g_{1T}^{\perp(1)a}(x) \overset{\text{WW–type}}{\approx} x\int_x^1 \frac{dy}{y}\,g_1^a(y)\;, \tag{3.6a}$$
$$h_{1L}^{\perp(1)a}(x) \overset{\text{WW–type}}{\approx} -x^2\int_x^1 \frac{dy}{y^2}\,h_1^a(y)\;. \tag{3.6b}$$

Some of the above WW-type approximations were discussed in [2, 25–31]. WW-relations for FFs are actually not needed: in Eqs. (2.18, 2.19) either twist-2 FFs D_1^q, $H_1^{\perp q}$ enter or tilde FFs, as a consequence of how the azimuthal angles are defined [5]. For completeness we quote the WW-type approximations for FFs [5]

$$E(z,P_\perp^2) \overset{\text{WW–type}}{\approx} 0\,, \tag{3.7a}$$
$$G^\perp(z,P_\perp^2) \overset{\text{WW–type}}{\approx} 0\,, \tag{3.7b}$$
$$D^\perp(z,P_\perp^2) \overset{\text{WW–type}}{\approx} z\,D_1(z,P_\perp^2)\,, \tag{3.7c}$$
$$H(z,P_\perp^2) \overset{\text{WW–type}}{\approx} -\frac{P_\perp^2}{zM_h^2}\,H_1^\perp(z,P_\perp^2)\,. \tag{3.7d}$$

Having introduced the WW and WW-type approximations, we will review in the following what is currently known from theory and experiment about the WW(-type) approximations.

3.3 Predictions from instanton vacuum model

Insights on the relative size of hadronic matrix elements, such as Eq. (3.1), require a non-perturbative approach. It is by no means obvious which small parameter in the strong interaction regime would allow one to explain such results. An appealing non-perturbative approach is provided by the instanton model of the QCD vacuum [53–55]. This semi-classical approach assumes that properties of the QCD vacuum are dominated by instantons and anti-instantons, topological non-perturbative gluon field configurations, which form a strongly interacting medium. The approach provides a natural mechanism for dynamical chiral-symmetry breaking, the dominant feature of strong interactions in the nonperturbative regime. It was shown with variational and numerical methods that the instantons form a dilute medium characterized by a non-trivial small parameter $\rho/R \sim 1/3$ [53–55], where ρ and R denote respectively the average instanton size ρ and separation R.

Applying the instanton vacuum model to studies of $g_T^a(x)$ and $h_L^a(x)$ it was predicted that matrix elements of the $\bar{q}gq$ operators defining $\tilde{g}_T^a(x)$ [18] and $\tilde{h}_L^a(x)$ [19] are strongly suppressed by powers of the small parameter ρ/R with respect to contributions from the respective twist-2 parts, which are of order $(\rho/R)^0$. For Mellin moments it was found [18, 19]

$$\frac{\tilde{g}_T^q}{g_T^q} \sim \frac{\tilde{h}_L^q}{h_L^q} \sim \frac{\langle \bar{q}gq \rangle}{\langle \bar{q}q \rangle} \sim \left(\frac{\rho}{R}\right)^4 \log\left(\frac{\rho}{R}\right) \sim 10^{-2} \tag{3.8}$$

which strongly supports the generic approximation in Eq. (3.1) with the instanton packing fraction providing the non-trivial small parameter justifying the neglect of tilde terms. The predictions for $\tilde{g}_T^a(x)$ [18] were made before the advent of the first precise data on $g_2(x)$, which we discuss next. The instanton calculus has not yet been applied to $\tilde{e}^a(x)$.

3.4 Tests of WW approximation in DIS experiments

The presently available phenomenological information on $g_T^a(x)$ is due to measurements of the structure function $g_2(x)$, Eq. (2.22c), in DIS off various transversely polarized targets. In the WW-approximation (3.2a) one can write $g_2(x)$ as a total derivative expressed in terms of the experimentally well-known twist-2 structure function $g_1(x)$ as follows

$$g_2(x) \overset{\text{WW}}{\approx} g_2(x)_{\text{WW}} \equiv \frac{d}{dx}\left[x\int_x^1 \frac{dy}{y}\, g_1(y)\right]. \tag{3.9}$$

Data support (3.9) to a good accuracy [22–24], although especially at smaller x more stringent tests are not yet possible. Overall it has been estimated that the WW approximation for $g_2(x)$ and $g_T^a(x)$ works with an accuracy of about 40 % or better [56].

We present calculations of $g_2(x)_{\text{WW}}$ in Fig. 2. This result is obtained using the LO $g_1^a(x)$-parametrization [57]. In order to display the theoretical "uncertainty band" of this WW-approximation of about 40 % as deduced in Ref. [56] we proceed as follows: we split the 40 % uncertainty in two parts, $\varepsilon_1 = \pm 20\,\%$ and $\varepsilon_2(x) = \pm 20\,\%(1-x)^\epsilon$ with a small $\epsilon > 0$, and estimate the impact of this uncertainty as

$$g_2(x)_{\text{WW}} = (1 \pm \varepsilon_1)\frac{d}{dx}\left[x\int_x^1 \frac{dy}{y}\left(\frac{1}{2}\sum_a e_a^2\, g_1^a(y(1\pm\varepsilon_2))\right)\right]. \tag{3.10}$$

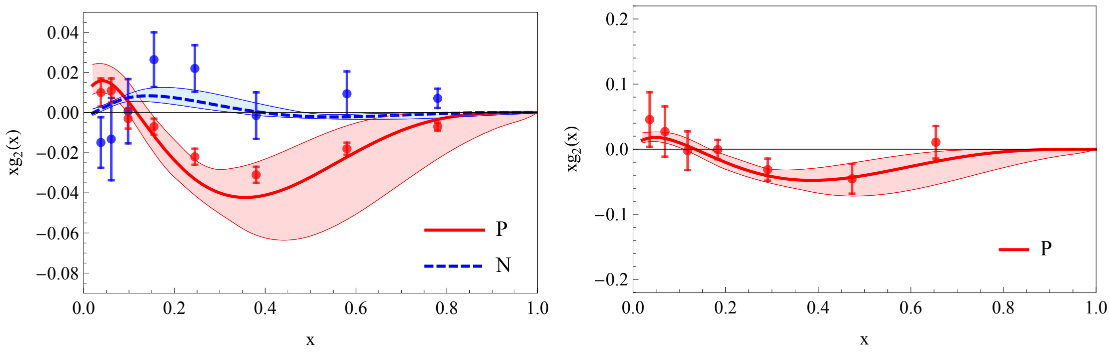

Figure 2. The structure function $xg_2(x)$ in WW-approximation at $Q^2 = 7.1\,\text{GeV}^2$, Eq. (3.9), for proton (P) and neutron (N) targets. Left panel: data from E144 and E155 experiments at $\langle Q^2 \rangle = 7.1\,\text{GeV}^2$ [22, 23]. Right panel: HERMES data for $Q^2 > 1\,\text{GeV}^2$ with $\langle Q^2 \rangle = 2.4\,\text{GeV}^2$ [24]. The estimate of the theoretical uncertainty is described in the text.

The effect of ε_1 is to change the magnitude of $g_2(x)_{\text{WW}}$, ε_2 varies the position of its zero. The x–dependence of ε_2 preserves $\lim_{x\to 1} g_2(x) = 0$; we use $\epsilon = 0.05$, which yields $\varepsilon_2 \approx 20\,\%$ up to the highest measured x–bin. The good agreement of $g_2(x)_{\text{WW}}$ with data is encouraging, and in line with theory predictions [18]. Our estimate with the splitted uncertainties $\varepsilon_{1,2}$ may overestimate in certain x–bins the 40 %–"uncertainty band" estimated in [56]. This however helps us to display a conservative estimate of possible uncertainties. We conclude that the WW–approximation works reasonably well, see Fig. 2.

Presently $h_L^a(x)$ is unknown. With phenomenological information on $h_1^a(x)$ [58–60], the WW approximation (3.2b) for $h_L^a(x)$ could be tested experimentally in Drell–Yan [61].

3.5 Tests in lattice QCD

The lowest Mellin moments of the PDF $g_T^q(x)$ were studied in lattice QCD in the quenched approximation [20] and with $N_f = 2$ flavors of light dynamical quarks [21]. The obtained results were compatible with a small $\tilde{g}_T^q(x)$. We are not aware of lattice QCD studies related to the PDF $h_L^a(x)$, and turn now our attention to TMD studies in lattice QCD.

After first exploratory investigations of TMDs on the lattice [62, 63], recent years have witnessed considerable progress and improvements with regard to rigor, realism and methodology [64–67]. However, numerical results from recent calculations are only available for a subset of observables, and the quantities calculated are not in a form that lends itself to straightforward tests of the WW-type relations as presented in this paper. Details about recent works and future perspectives are discussed at the end of this section.

For the time being, we content ourselves with rather crude comparisons based on the lattice data published in Refs. [62, 63]. These early works explored all nucleon and quark polarizations, but they used a gauge link that does not incorporate the final or initial state interactions present in SIDIS or Drell–Yan experiments. In other words, the transverse momentum dependent quantities computed in [62, 63] are not precisely the TMDs measurable in experiment. More caveats will be discussed along the way.

Let us now translate the approximations (3.6a, 3.6b) into expressions for which we have a chance to compare them with available lattice data. For that we multiply the Eqs. (3.6a, 3.6b) by x^N with $N = 0,\, 1,\, 2,\, \ldots$ and integrate over $x \in [-1, 1]$ which yields

$$\int_{-1}^{1} dx\; x^N g_{1T}^{\perp(1)q}(x) \overset{\text{WW–type}}{\approx} \frac{1}{N+2}\int_{-1}^{1} dx\; x^{N+1} g_1^q(x)\,, \tag{3.11}$$

$$\int_{-1}^{1} dx\; x^N h_{1L}^{\perp(1)q}(x) \overset{\text{WW–type}}{\approx} -\frac{1}{N+3}\int_{-1}^{1} dx\; x^{N+1}\, h_1^q(x)\,. \tag{3.12}$$

with the understanding that negative x refer to antiquark distributions $g_1^{\bar{q}}(x) = +\,g_1^q(-x)$, $h_1^{\bar{q}}(x) = -\,h_1^q(-x)$, $g_{1T}^{\perp(1)\bar{q}}(x) = -g_{1T}^{\perp(1)q}(-x)$, $h_{1L}^{\perp(1)\bar{q}}(x) = +\,h_{1L}^{\perp(1)q}(-x)$ depending on C–parity of the involved operators [2]. The right hand sides of Eqs. (3.11, 3.12) are x–moments of parton distributions, and those can be obtained from lattice QCD using well-established methods based on operator product expansion. The left hand sides are moments of TMDs in x and $\boldsymbol{k}_\perp$. We have to keep in mind that TMDs diverge for large $\boldsymbol{k}_\perp$. Therefore, without regularizing these divergences in a scheme suitable for the comparison of left and right hand side, a test of the above relations is meaningless, even before we get to address the issues of lattice calculations. Let us not give up at this point and take a look at the lattice observables of Ref. [63]. Here, the TMDs are obtained from amplitudes $\tilde{A}_i(l^2, \ldots)$ in Fourier space, where $\boldsymbol{k}_\perp$ is encoded in the Fourier conjugate variable $\boldsymbol{\ell}_\perp$, which is the transverse displacement of quark operators in the correlator evaluated on the lattice. In Fourier-space, the aforementioned divergent behavior for large $\boldsymbol{k}_\perp$ translates into strong lattice scale and scheme dependencies at short distances $\boldsymbol{\ell}_\perp$ between the quark operators. The $\boldsymbol{k}_\perp$ integrals needed for the left hand sides of Eqs. (3.11, 3.12) correspond to the amplitudes at $\boldsymbol{\ell}_\perp = 0$, where scheme and scale-dependence is greatest. In Ref. [63] Gaussian fits have been performed to the amplitudes *excluding* data at short quark separations $\boldsymbol{\ell}_\perp$. The Gaussians describe the long range data quite well and bridge the gap at short distances $\boldsymbol{\ell}_\perp$. Taking the Gaussian fit at $\boldsymbol{\ell}_\perp = 0$, we get a value which is (presumably) largely lattice scheme and scale independent. We have thus swept the problem of divergences under the rug. The Gaussian fit acts as a crude regularization of the divergences that appear in TMDs at large $\boldsymbol{k}_\perp$ and manifest themselves as short range artifacts on the lattice. Casting this line of thought into mathematics, we get

$$\int_{-1}^{1} dx\; g_{1T}^{\perp(1)q}(x) = \int_{-1}^{1} dx\; \int d^2\boldsymbol{k}_\perp \tfrac{k_\perp^2}{2M^2} g_{1T}^{\perp q}(x, k_\perp) = -2\tilde{A}_{7,q}(\ell = 0) \overset{\text{Gaussian}}{=} -c_{7,q} \tag{3.13}$$

$$\int_{-1}^{1} dx\; h_{1L}^{\perp(1)q}(x) = \int_{-1}^{1} dx\; \int d^2\boldsymbol{k}_\perp \tfrac{k_\perp^2}{2M^2} h_{1T}^{\perp q}(x, k_\perp) = -2\tilde{A}_{10,q}(\ell = 0) \overset{\text{Gaussian}}{=} -c_{10,q} \tag{3.14}$$

where the amplitudes $\tilde{A}$ and constants c are those of Ref. [63]. We have thus expressed the left hand side of Eqs. (3.11, 3.12) in terms of amplitudes $c_{7,q}$ and $c_{10,q}$ of the Gaussian fits on the lattice. Before quoting numbers, a few more comments are in order. The overall multiplicative renormalization in Ref. [63] was fixed by setting the Gaussian integral $c_{2,u-d}$ of the unpolarized TMD f_1 in the isovector channel (u-d) to the nucleon quark content, namely, to 1. One then assumes that the normalization of the lattice results for the unpolarized TMD f_1 also fixes the normalization for polarized quantities correctly. This assumption holds if renormalization is multiplicative and flavor-independent for the non-local lattice operators. This is not true for all lattice actions [64] but presumably it is true if the lattice action preserves chiral symmetry, as it does in the present case. The Gaussian fits along with the normalization prescription serve as a crude form of renormalization, and this is needed to attempt a comparison of left and right hand sides of equations Eqs. (3.11, 3.12).

There is yet another issue to be discussed. The gauge link that goes into the evaluation of the quark-quark correlator introduces a power divergence that has to be subtracted. Ref. [63] employs a subtraction scheme on the lattice but establishes no connection with a subtraction scheme designed for experimental TMDs and the corresponding gauge-link geometry. The gauge-link renormalization mainly influences the width of the Gaussian fits; the amplitudes are only slightly affected, so it may not play a big role for our discussion. Altogether, the significance of our numerical "tests" of WW-relations should be taken with a grain of salt.

For the test of E. (3.11), we use the numbers $\int dx\; g_{1T}^{\perp(1)u}(x) \overset{\text{Gaussian}}{=} -c_{7,u} = 0.1041(85)$ and $\int dx\; g_{1T}^{\perp(1)d}(x) \overset{\text{Gaussian}}{=} -c_{7,d} = -0.0232(42)$ from [63]. Lattice data for $\int dx\, x^N g_1^q(x)$ [68, 69] and $\int dx\, x^N h_1^q(x)$ [70] are available for $N = 0,\, 1,\, 2,\, 3$. These values have been computed using (quasi-) local operators which have been renormalized to the $\overline{MS}$ scheme at the scale $\mu^2 = 4\,\text{GeV}^2$. According to [69] (data set 4: with $a\, m_{u,d} = 0.020$ with $m_\pi \approx 500\,\text{MeV}$) one has $\int dx\;\, x\, g_1^{u-d}(x) = 0.257(10)$ and $\int dx\;\, x\, g_1^{u+d}(x) = 0.159(14)$. Decomposing the results from [69] into individual flavors, and inserting them into Eq. (3.11) we obtain

$$\begin{aligned}
\underbrace{\int dx\; g_{1T}^{\perp(1)u}(x)}_{=0.1041(85)\text{ Ref. [63]}} &\overset{!}{\approx} \underbrace{\frac{1}{2}\int dx\; x\, g_1^u(x)}_{=0.104(9)\text{ Ref. [69]}} \;, \\
\underbrace{\int dx\; g_{1T}^{\perp(1)d}(x)}_{=-0.0232(42)\text{ Ref. [63]}} &\overset{!}{\approx} \underbrace{\frac{1}{2}\int dx\; x\, g_1^d(x)}_{=-0.025(9)\text{ Ref. [69]}} \;,
\end{aligned} \tag{3.15}$$

which confirms the approximation (3.11) for $N = 0$ within the statistical uncertainties of the lattice calculations. In order to test (3.12) we use $\int dx\;\, h_{1L}^{\perp(1)u}(x) \overset{\text{Gaussian}}{=} -c_{10,u} = -0.0881(72)$ and $\int dx\; h_{1L}^{\perp(1)d}(x) \overset{\text{Gaussian}}{=} -c_{10,d} = 0.0137(34)$ from [63] and the lattice data $\int dx\;\, x\, h_1^u(x) = 0.28(1)$ and $\int dx\;\, x\, h_1^d(x) = -0.054(4)$ from QCDSF [70].[1] Inserting these numbers into (3.12) for the case $N = 0$ we obtain

$$\begin{aligned}
\underbrace{\int dx\; h_{1L}^{\perp(1)u}(x)}_{=-0.0881(72)\text{ Ref. [63]}} &\overset{!}{\approx} \underbrace{-\frac{1}{3}\int dx\; x\, h_1^u(x)}_{=-0.093(3)\text{ Ref. [69]}} \;, \\
\underbrace{\int dx\; h_{1L}^{\perp(1)d}(x)}_{=0.0137(34)\text{ Ref. [63]}} &\overset{!}{\approx} \underbrace{-\frac{1}{3}\int dx\; x\, h_1^d(x)}_{=0.018(1)\text{ Ref. [69]}} \;,
\end{aligned} \tag{3.16}$$

[1] These numbers are read off from a figure in [70], and were computed on a different lattice. We interpolate them to a common value of the pion mass $m_\pi \approx 500\,\text{MeV}$, and estimate the uncertainty conservatively in order to take systematic effects into account due to the use of a different lattice.

which again confirms the WW-type approximation within the statistical uncertainties of the lattice calculations.

Several more comments are in order concerning the, at first glance, remarkably good confirmation of the WW-type approximations by lattice data in Eqs. (3.15, 3.16).

First, the relations refer to lattice parameters corresponding to pion masses of 500 MeV. We do not need to worry about that too much. The lattice results do provide a valid test of the approximations in a "hadronic world" with somewhat heavier pions and nucleons. All that matters in our context is that the relative size of $\bar{q}gq$–matrix elements is small with respect to $\bar{q}q$–matrix elements.

Second, we have to revisit carefully which approximations the above lattice calculations actually test. As mentioned above, in the lattice study [62, 63], a specific choice for the path of the gauge link was chosen, which is actually different from the paths required in SIDIS or Drell–Yan. With the path choice of [62, 63] there are effectively only (T-even) A_i amplitudes, the B_i amplitudes are absent. Therefore the test (3.15) of the WW-type approximation (3.11) actually constitutes a test of the WW-approximation (3.2a) and confirms earlier lattice work [20, 21], cf. Refs. [29, 30] and Sec. 3.6. Similarly, the test (3.16) of the WW-type approximation (3.12) actually constitutes a test of the WW-approximation (3.2b). The latter however has not been reported previously in literature, and is a new result.

Third, to be precise: Eqs. (3.15, 3.16) test the first Mellin moments of the WW approximations (3.2a, 3.2b), which corresponds to the Burkhardt-Cottingham sum rule for $g_T^a(x)$ and an analogous sum rule for $h_L^a(x)$, see [51] and references there in. In view of the long debate on the validity of those sum rules [50, 71, 72], this is in an interesting result in itself.

It is important to stress that in view of the pioneering and exploratory status of the TMD lattice calculations [62, 63], this is already a remarkable and very interesting result. Thus, apart from the instanton calculus [19], also lattice data provide support for the validity of the WW approximation (3.2b). At the same time, however, we also have to admit that we do not really reach our goal of testing the WW-type approximations on the lattice. We have to wait for better lattice data. Meanwhile we may try to gain insights into the quality of WW-type approximations from models.

3.6 Tests in models

Effective approaches and models such as bag [16, 73–75], spectator [76], chiral quark-soliton [77], or light-cone constituent [78, 79] models support the approximations (3.2a, 3.2b) for PDFs within an accuracy of $(10-30)\,\%$ at low hadronic scale below 1 GeV.

Turning to TMDs, we recall that in models without gluon degrees of freedom certain relations among TMDs hold, the so-called quark-model Lorentz-invariance relations (qLIRs) [2, 31].[2] Initially thought to be exact [2, 31], qLIRs were shown to be invalid in models with gluons [80, 81] and in QCD [82]. They originate from decomposing the (completely

[2]Notice that the qLIRs of [2, 31] are valid only in quark models with no gluons and should not be confused with the LIRs of [52], which are exact relations in QCD, see Sec. 3.1. In the literature, both are often simply referred to as LIRs. This ambiguity is unfortunate.

unintegrated) quark correlator in terms of Lorentz-invariant amplitudes, and TMDs are certain integrals over those amplitudes. When gluons are absent, the correlator consists of 12 amplitudes [2, 31], i.e., fewer amplitudes than TMDs which implies relations: the qLIRs. In QCD the correct Lorentz decomposition requires the consideration of gauge links, which introduces further amplitudes. As a result one has as many amplitudes as TMDs and no relations exist [82]. However, qLIRs "hold" in QCD in the WW-type approximation [29]. In models without gluon degrees of freedom they are exact [29, 30, 75, 76].

The bag, spectator and light-cone constituent quark models support the approximations (3.6a, 3.6b) within an accuracy of $(10-30)\,\%$ [75, 76, 78, 79]. The spectator and bag model support WW-type approximations within $(10-30)\,\%$ [75]. As they are defined in terms of quark bilinear expressions (2.11) it is possible to evaluate twist-3 functions in quark models [16]. The tilde-terms arise due to the different model interactions, and it is important to discuss critically how realistically they describe the $\bar{q}gq$–terms of QCD [83, 84].

In the covariant parton model with intrinsic 3D-symmetric parton orbital motion [85] quarks are free, $\bar{q}gq$ correlations absent, and all WW and WW-type relations exact [86, 87]. The phenomenological success of this approach [85] may hint at a general smallness of $\bar{q}gq$ terms, although many of the predictions from this model have yet to be tested [86].

Noteworthy is the result from the chiral quark soliton model where the WW-type approximation (3.3b) happens to be exact: $xf^{\perp q}(x,k_\perp^2) = f_1^q(x,k_\perp^2)$ for quarks and antiquarks [83]. The degrees of freedom in this model are quarks, antiquarks and Goldstone bosons which are strongly coupled (the coupling constant is ~ 4) and has to be solved using nonperturbative techniques (expansion in $1/N_c$ where N_c is the number of colors) with the nucleon described as a chiral soliton. In general, the model predicts non-zero tilde-terms, for instance $\tilde{e}^a(x) \neq 0$ [88–90]. However, despite strong interactions in this effective theory, the tilde term $\tilde{f}^{\perp q}(x,k_\perp^2)$ vanishes exactly in this model [83] and the WW-type approximation (3.3b) becomes exact at the low initial scale of this model of $\mu_0 \sim 0.6\,\mathrm{GeV}$.

Let us finally discuss quark-target models, where gluon degrees of freedom are included and WW(-type) approximations badly violated [80, 81, 91, 92]. This is natural in this class of models for two reasons. First, quark-mass terms are of $\mathcal{O}(m_q/M_N)$ and negligible in the nucleon case, but of $\mathcal{O}(100\,\%)$ in a quark target where m_q plays also the role of M_N. Second, even if one refrains from mass terms the approximations are spoiled by gluon radiation, see for instance [93] in the context of (3.2a). This means that perturbative QCD does not support the WW-approximations: they certainly are not preserved by evolution. However, scaling violations *per se* do not need to be large. What is crucial in this context are dynamical reasons for the smallness of the *matrix elements* of $\bar{q}gq$–operators. This requires the consideration of chiral symmetry breaking effects reflected in the hadronic spectrum, as considered in the instanton vacuum model [18, 19] but out of scope in quark-target models.

We are not aware of systematic tests of WW-type approximations for FFs. One information worth mentioning in this context is that in spectator models [76] tilde-contributions to FFs are proportional to the offshellness of partons [83, 84]. This natural feature may indicate that in the region dominated by effects of small $P_\perp$ tilde-terms might be small. On the other hand, quarks have sizable constituent masses of the order of few hundred MeV in spectator models and the mass-terms are not small. The applicability of WW-type approximations to FFs remains the least tested point in our approach.

3.7 Basis functions for the WW-type approximations

The leading–twist 6 TMDs f_1^a, $f_{1T}^{\perp a}$, g_1^a, h_1^a, $h_1^{\perp a}$, $h_{1T}^{\perp a}$ and 2 FFs D_1^a, $H_1^{\perp a}$ provide a basis in the sense that in WW-type approximation all other TMDs and FFs can either be expressed in terms of these basis functions or vanish. Below we shall see that, under the assumption of the validity of WW-type approximations, it is possible to express all SIDIS structure functions in terms of the basis functions. Notice that SIDIS alone is of course not sufficient to determine the basis functions uniquely: the 8 basis functions appear in 6 SIDIS structure functions. It is crucial to take advantage of other processes: Drell–Yan for PDFs and TMDs and hadron production in e^+e^- annihilation for FFs. Other processes play also important roles.

These basis functions allow us to describe, in WW-type approximation, all other TMDs. The experiment will tell us how well the approximations work. In some cases, however, we know in advance that the WW-type approximations have limitations, see next Section.

3.8 Limitation of WW-type approximation

The approximation may work in the case when the TMD or FF $= \langle \bar{q}q \rangle + \langle \bar{q}gq \rangle \approx \langle \bar{q}q \rangle \neq 0$ with a "controlled approximation" in the spirit of Eq. (3.1). We know cases where this works, see Secs. 3.3, 3.4, but it has to be checked case by case whether $|\langle \bar{q}gq \rangle| \ll |\langle \bar{q}q \rangle|$ for a given operator. At least in such cases the approximation has a chance to work.

However, it may happen that after applying the QCD equations of motion one ends up in the situation that a given function $= \langle \bar{q}q \rangle + \langle \bar{q}gq \rangle$ with $\langle \bar{q}q \rangle = 0$. This happens for the T-even TMD e^a in Eqs. (3.2c, 3.3a), for the T-odd TMDs e_L^q, e_T^q, $e_T^{\perp q}$, $f_L^{\perp q}$, $g^{\perp q}$ in Eqs. (3.4a–3.4e), and for the FFs E^q, $G^{\perp q}$ in Eqs. (3.7a, 3.7b) (actually, all twist-3 FFs are affected, we will discuss this in detail below). In this situation the "leading term" is absent, so neglecting the "subleading (pure twist-3) term" actually constitutes an error of 100 % even if the neglected matrix element $\langle \bar{q}gq \rangle$ is very small. Notice that this type occurs for all subleading-twist FFs, which enter SIDIS structure functions only in the shape of tilde-FFs, see Sec. 2 and Eqs. (2.19). We shall see that some structure functions are potentially more and others potentially less affected by this generic limitation. In any case, phenomenological work has to be carried out to find out whether or not the approximation works.

For both FFs and TMDs there are also limitations which go beyond this generic issue. To illustrate this for FFs we recall that both $H_1^{\perp(1)q}$ and $\tilde{H}_1^q$ are related to integrals of an underlying function $H_{FU}^{q,\Im}(z, z_1)$ as pointed out in Ref. [52]. Therefore, if one literally assumed $\tilde{H}^q(z)$ to be zero, this would imply that also $H_1^{\perp(1)q}$ would vanish, indicating that the WW-type approximation has to be used with care in the chiral-odd FF sector.

Similar limitations exist also for TMDs. This is manifest in particular for those twist-3 T-odd TMDs that appear in the decomposition of the correlator (2.11) with no prefactor of $k_\perp$. There are three cases: $f_T^a(x, k_\perp)$, $h^a(x, k_\perp)$, $e_L^a(x, k_\perp)$. Such TMDs in principle survive integration of the correlator over $k_\perp$ and would have PDF counterparts if there were not the sum rules in Eq. (2.14). These sum rules arise because hypothetical PDF versions of T-odd

TMDs vanish: they have a simple straight gauge link along the lightcone, and such objects vanish due to parity and time-reversal symmetry of strong interactions. This argument does not apply to other T-odd TMDs because they drop out from the $k_\perp$–integrated correlator due to explicit factors of, e.g., $k_\perp^j$ in the case of the Sivers function.

Let us first discuss the case of $f_T^a(x,k_\perp)$. Taking the WW-type approximation (3.4g) literally means $x\int d^2k_\perp\, f_T^a(x,k_\perp) \stackrel{!?}{=} -f_{1T}^{\perp(1)a}(x) \neq 0$ at variance with the sum rule (2.14). We have $xf_T^a(x,k_\perp) = x\tilde{f}_T^a(x,k_\perp) - f_{1T}^{\perp(1)a}(x,k_\perp)$ from QCD equations of motion [5], which yields (3.4g). The point is that in this case it is essential to keep the tilde-function. The situation for the chirally and T-odd twist-3 TMD $h^a(x,k_\perp)$ is analogous. The third function in (2.14) causes no issues since $e_L^a(x,k_\perp) = \tilde{e}_L^a(x,k_\perp) \approx 0$ in WW-type approximation.

Does it mean WW-type approximations fail for $f_T^a(x,k_\perp)$ and $h^a(x,k_\perp)$? Not necessarily! The approximations may work in some but not all regions of $k_\perp$, but the sum rules (2.14) include integration over all $k_\perp$. Notice also that, e.g., $f_{1T}^{\perp(1),q}(x)$ is related to the soft-gluon-pole matrix element $F_{FT}(x,x)$ [94, 95], which is a $\bar{q}gq$-term that one would naturally neglect in WW-type approximation. In this sense (3.4g) could be consistent. Thus, issues with the sum rules (2.14) do not need to exclude the possibility that the WW-type approximations for $f_T^a(x,k_\perp)$ and $h^a(x,k_\perp)$ in (3.4g, 3.4h) may work at small $k_\perp$ where we use them in our TMD approach. This would mean the UV region is essential to realize the sum rules (2.14). Alternatively, one could also envision the sum rules (2.14) to be sensitive to the IR region through gluonic or fermionic pole contributions manifest in tilde-terms.

Presently too little is known in the theory of subleading-twist TMDs. Below in Sec. 7.6 and 7.8 we will present a pragmatic solution for how to deal with the TMDs $f_T^a(x,k_\perp)$ and $h^a(x,k_\perp)$ phenomenologically. For now let us keep in mind that one has to keep a vigilant eye on all WW-type approximations, and especially on those for $f_T^a(x,k_\perp)$ and $h^a(x,k_\perp)$.

4 SIDIS in the WW-type approximation and Gaussian model

In this section, we consequently apply the WW and WW-type approximation to SIDIS, and describe our procedure to evaluate the structure functions in this approximation and the Gaussian Ansatz which we use to model the $k_\perp$ dependence of TMDs.

4.1 Leading structure functions amenable to WW-type approximations

The WW and WW-type approximations are useful for the following two leading-twist structure functions:

$$F_{LT}^{\cos(\phi_h-\phi_S)} \stackrel{\rm WW}{=} \mathcal{C}\left[\omega_{\rm B}^{\{1\}}\, g_{1T}^{\perp} D_1\right]\Bigg|_{\substack{g_{1T}^{\perp a}\,\to\, g_1^a \\ \text{Eq. (3.6a)}}}\,, \tag{4.1a}$$

$$F_{UL}^{\sin 2\phi_h} \stackrel{\rm WW}{=} \mathcal{C}\left[\omega_{\rm AB}^{\{2\}}\, h_{1L}^{\perp} H_1^{\perp}\right]\Bigg|_{\substack{h_{1L}^{\perp a}\,\to\, h_1^a \\ \text{Eq. (3.6b)}}}\,. \tag{4.1b}$$

4.2 Subleading structure functions in WW-type approximations

In the case of the subleading-twist structure functions the WW-type approximations in Eqs. (3.3a–3.4h) lead to considerable simplifications. We obtain the approximations

$$F_{LU}^{\sin\phi_h} \stackrel{\text{WW}}{=} 0\,, \tag{4.2a}$$

$$F_{LT}^{\cos\phi_S} \stackrel{\text{WW}}{=} \frac{2M_N}{Q}\,\mathcal{C}\Big[-\omega^{\{0\}}\,x\,g_T D_1\Big]\bigg|_{\substack{g_T^a \to g_1^a \\ \text{Eq. (3.2a)}}} \tag{4.2b}$$

$$F_{LL}^{\cos\phi_h} \stackrel{\text{WW}}{=} \frac{2M_N}{Q}\,\mathcal{C}\Big[-\omega_{\text{B}}^{\{1\}}\,x g_L^\perp D_1\Big]\bigg|_{\substack{g_L^{\perp a} \to g_1^a \\ \text{Eq. (3.3c)}}} \tag{4.2c}$$

$$F_{LT}^{\cos(2\phi_h-\phi_S)} \stackrel{\text{WW}}{=} \frac{2M_N}{Q}\,\mathcal{C}\Big[-\omega_{\text{C}}^{\{2\}}\,x g_T^\perp D_1\Big]\bigg|_{\substack{g_T^{\perp a} \to g_1^a \\ \text{Eqs. (3.3d, 3.6a)}}} \tag{4.2d}$$

$$F_{UL}^{\sin\phi_h} \stackrel{\text{WW}}{=} \frac{2M_N}{Q}\,\mathcal{C}\Big[\;\omega_{\text{A}}^{\{1\}}\,x\,h_L H_1^\perp\Big]\bigg|_{\substack{h_L^a \to h_{1L}^{\perp a} \\ \text{with Eq. (3.3f)}}} \tag{4.2e}$$

$$F_{UU}^{\cos\phi_h} \stackrel{\text{WW}}{=} \frac{2M_N}{Q}\,\mathcal{C}\Big[\;\omega_{\text{A}}^{\{1\}}\,x\,h\,H_1^\perp - \omega_{\text{B}}^{\{1\}}\,x\,f^\perp D_1\Big]\bigg|_{\substack{f^{\perp a} \to f_1^a,\; h^a \to h_1^{\perp a} \\ \text{with Eqs. (3.3b, 3.4h)}}} \tag{4.2f}$$

$$F_{UT}^{\sin\phi_S} \stackrel{\text{WW}}{=} \frac{2M_N}{Q}\,\mathcal{C}\Big[\;\omega^{\{0\}}\,x\,f_T D_1 - \frac{\omega_{\text{B}}^{\{2\}}}{2}\,(xh_T - xh_T^\perp)\,H_1^\perp\Big]\bigg|_{\substack{f_T^a \to f_{1T}^{\perp a}, \\ h_T^a - h_T^{\perp a} \to h_1^a \\ (3.4\text{g, } 3.3\text{g, } 3.3\text{h})}} \tag{4.2g}$$

$$F_{UT}^{\sin(2\phi_h-\phi_S)} \stackrel{\text{WW}}{=} \frac{2M_N}{Q}\,\mathcal{C}\Big[\omega_{\text{C}}^{\{2\}}\,x\,f_T^\perp D_1 + \frac{\omega_{\text{AB}}^{\{2\}}}{2} x(h_T + h_T^\perp)H_1^\perp\Big]\bigg|_{\substack{f_T^{\perp a} \to f_{1T}^{\perp a}, \\ (h_T^a + h_T^{\perp a}) \to h_{1T}^{\perp a} \\ \text{with } (3.4\text{f, } 3.3\text{g, } 3.3\text{h})}} . \tag{4.2h}$$

4.3 Gaussian Ansatz for TMDs and FFs

In this work we will use the so-called Gaussian Ansatz for the TMDs and FFs. This Ansatz, which for a generic TMD or FF is given by

$$f(x,k_\perp^2) = f(x)\,\frac{e^{-k_\perp^2/\langle k_\perp^2\rangle}}{\pi\langle k_\perp^2\rangle}\,, \quad D(z,P_\perp^2) = D(z)\,\frac{e^{-P_\perp^2/\langle P_\perp^2\rangle}}{\pi\langle P_\perp^2\rangle}\,, \tag{4.3}$$

is popular not only because it considerably simplifies the calculations. In fact, all convolution integrals of the type (2.17) can be solved analytically with this Ansatz. Far more important is the fact that it works phenomenologically with a good accuracy in many practical applications [96–101]. Of course this Ansatz is only a rough approximation. For instance, it is not consistent with general matching expectations for large $k_\perp$ [102].

Nevertheless, if one limits oneself to work in a regime where the transverse momenta (of hadrons produced in SIDIS, dileptons produced in the Drell–Yan process, etc) are small compared to the hard scale in the process, then the Ansatz works quantitatively very well. The most recent and detailed tests were reported in [99], where the Gaussian Ansatz was shown to describe the most recent SIDIS data: no deviations were observed within the error bars of the data provided one takes into account the broadening of the Gaussian widths with increasing energy [99] according with expectations from QCD [41]. The Gaussian Ansatz is approximately compatible with the $k_\perp$–shapes obtained from evolution [41] or fits to high-energy Tevatron data on weak-boson production [103]. Effective models at low [75, 78, 79] and high [87] renormalization scales support this Ansatz as a good approximation.

4.4 Evaluation of structure functions in WW-type & Gaussian approximation

The Gaussian Ansatz is compatible with many WW-type approximations, but not all. The trivial approximations (3.3a) and (3.4a–3.4e) cause no issue. The Gaussian Ansatz can also be applied to the nontrivial approximations in Eqs. (3.3b–3.3d) and (3.4f), provided the corresponding Gaussian widths are defined to be equal to each other: for example, in the WW-type approximation (3.3b), $xf^{\perp q}(x, k_\perp^2) \approx f_1^q(x, k_\perp^2)$, one may assume Gaussian $k_\perp$–dependence for $f^{\perp q}(x, k_\perp^2)$ and for $f_1^q(x, k_\perp^2)$ as long as the Gaussian widths of these two TMDs are assumed to be equal.

In the case of the approximations (3.3e–3.3h) the situation is different because here twist-3 TMDs are related to transverse moments of twist-2 TMDs. In such cases the Gaussian Ansatz is not compatible with the WW-type approximations: for instance, the approximation (3.3e) relates $xg_T^q(x, k_\perp^2) \approx \frac{k_\perp^2}{2M_N^2}\, g_{1T}^q(x, k_\perp^2)$, i.e., if $g_{1T}^q(x, k_\perp^2)$ was exactly Gaussian then $g_T^q(x, k_\perp^2)$ certainly could not be Gaussian. If one wanted to take the Gaussian Ansatz and WW-type approximations literally, one clearly would deal with an incompatibility. However, we of course must keep in mind that both are approximations.

Some comments are in order to understand how the usage of the Gaussian Ansatz and the WW-type approximations can be reconciled. First, let us remark that the individual TMDs, say $g_T^q(x, k_\perp^2)$ and $g_{1T}^q(x, k_\perp^2)$ in our example, may each by itself be assumed to be approximately Gaussian in $k_\perp$ which is supported by quark model calculations [75]. Second, we actually do not need the unintegrated WW-type approximations. For phenomenological applications we can use the WW-type approximations in "integrated form."

Let us stress that if one took an unintegrated WW-type approximation of the type $xg_T^q(x, k_\perp^2) \approx \frac{k_\perp^2}{2M_N^2}\, g_{1T}^q(x, k_\perp^2)$ literally and assumed both TMDs to be exactly Gaussian, one would find "incompatibilities:" perhaps most strikingly in the limit $k_\perp \to 0$ where the left-hand side is finite while the right-hand side vanishes. However, such incompatibilities are washed out and not apparent after the convolution integrals defining the structure functions are solved. Notice that the failure of the WW-type approximations (3.3e–3.3h) in the limit $k_\perp \to 0$ is not specific to the Gaussian model, but a general feature caused by neglecting tilde-terms. This indicates a practical scheme how to use responsibly the WW-type approximations in Eqs. (3.3e–3.3h).

Our procedure is as follows. In a first step we assume that all TMDs and FFs are (approximately) Gaussian, and solve the convolution integrals. In the second step we use the integrated WW-type approximations to simplify the results for the structure functions.

Notice that in some cases (when T-even TMDs are involved) one could choose a different order of the steps: first apply WW-type approximations and then solve convolution integrals with Gaussian Ansatz. In general, this would yield different (and bulkier) analytical expressions, but we convinced ourselves that the differences are numerically within the accuracy expected for this approach. However, for the structure functions discussed in Secs. 7.6 and 7.8, such an "alternative scheme" would give results at variance with the sum rules for the twist-3 T-odd TMDs in Eq. (2.14), as discussed in Sec. 3.8. The scheme presented here will allow us to implement those sum rules in a convenient and consistent way. We will follow up on this in more detail in Secs. 7.6 and 7.8.

To summarize, our procedure is to solve first the convolution integrals in Gaussian Ansatz, and use then WW-type approximations. When implementing this procedure we will see that the results for the structure functions can be conveniently expressed in terms of the basis TMDs or their adequate transverse moments.

4.5 Phenomenological information on basis functions

We have seen that the following 6 TMDs and 2 FFs provide a basis (Sec. 3) and allow us to express all SIDIS structure functions (Sec. 4) in WW-type approximation:

$$\text{basis:} \quad f_1^a,\; f_{1T}^{\perp a},\; g_1^a,\; h_1^a,\; h_1^{\perp a},\; h_{1T}^{\perp a};\; D_1^a,\; H_1^{\perp a}\,. \tag{4.4}$$

Phenomenological information is available for all basis functions at least to some extent. In Fig. 3 we present plots of the basis functions, and refer to App. A for details. The four

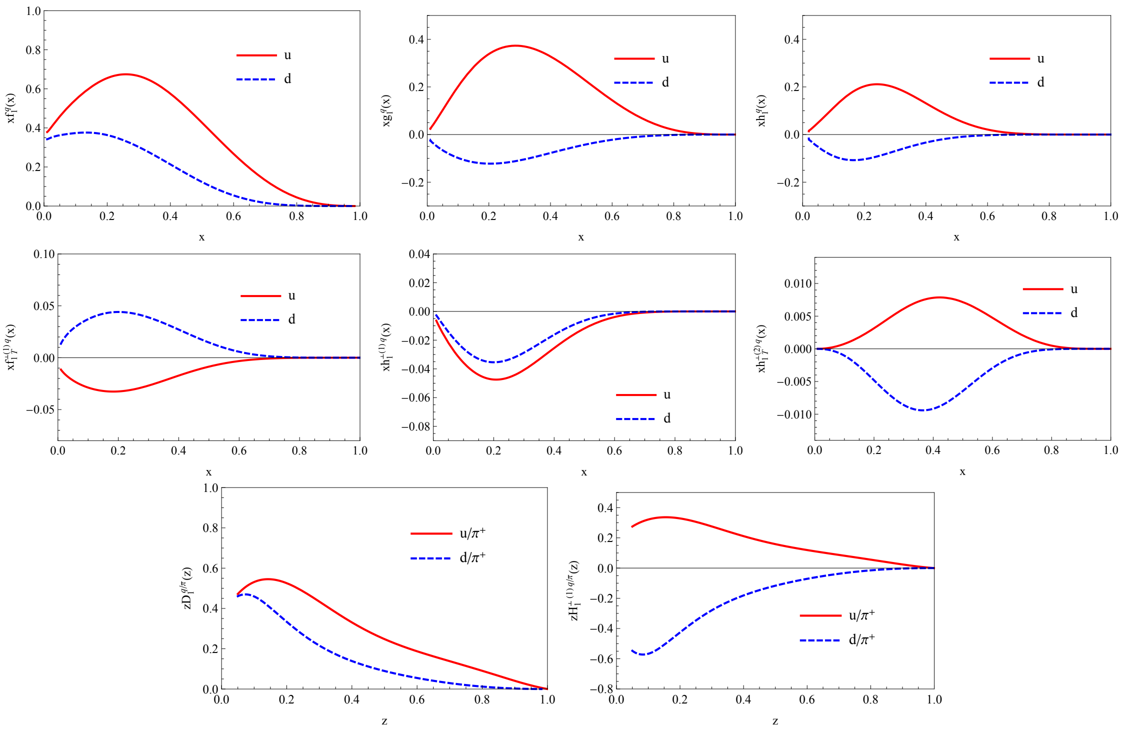

Figure 3. The basis functions f_1^a, g_1^a, h_1^a, $f_{1T}^{\perp a}$, $h_1^{\perp a}$, $h_{1T}^{\perp a}$; D_1^a, $H_1^{\perp a}$. For details see App. A.

functions f_1^a, g_1^a, h_1^a, D_1^a are related to twist-2 collinear functions. All collinear functions are calculated at $Q^2 = 2.4$ GeV^2. Collinear $f_1^a(x)$ are from Ref. [104], $g_1^a(x)$ are from Ref. [57], and D_1^a are from Ref. [105]. The other four TMDs have no collinear counterparts. For $f_{1T}^{\perp a}$, $h_1^{\perp a}$, $H_1^{\perp a}$ it is convenient to consider their (1)-moments, for $h_{1T}^{\perp a}$ the (2)-moment, see Eq. (B.8) for definitions. This has two important advantages. First, this step simplifies the Gaussian model expressions, and the Gaussian width parameters are largely absorbed in the definitions of the transverse moments. Second, the $k_\perp$–moments of these TMDs have in principle simple definitions in QCD (whereas, e.g., the function $f_{1T}^{\perp q}(x)$ can be computed in models but is very cumbersome to define in QCD). The parametrizations for the basis functions read

$$f_1^a(x, k_\perp^2) = f_1^a(x) \, \frac{1}{\pi \langle k_\perp^2 \rangle_{f_1}} \, e^{-k_\perp^2/\langle k_\perp^2 \rangle_{f_1}} \, , \tag{4.5a}$$

$$D_1^a(z, P_\perp^2) = D_1^a(z) \, \frac{1}{\pi \langle P_\perp^2 \rangle_{D_1}} \, e^{-P_\perp^2/\langle P_\perp^2 \rangle_{D_1}} \, , \tag{4.5b}$$

$$g_1^a(x, k_\perp^2) = g_1^a(x) \, \frac{1}{\pi \langle k_\perp^2 \rangle_{g_1}} \, e^{-k_\perp^2/\langle k_\perp^2 \rangle_{g_1}} \, , \tag{4.5c}$$

$$h_1^q(x, k_\perp^2) = h_1^q(x) \, \frac{1}{\pi \langle k_\perp^2 \rangle_{h_1}} \, e^{-k_\perp^2/\langle k_\perp^2 \rangle_{h_1}} \, , \tag{4.5d}$$

$$H_1^\perp(z, P_\perp^2) = H_1^{\perp(1)}(z) \, \frac{2 z^2 m_h^2}{\pi \langle P_\perp^2 \rangle_{H_1^\perp}^2} \, e^{-P_\perp^2/\langle P_\perp^2 \rangle_{H_1^\perp}} \, , \tag{4.5e}$$

$$f_{1T}^{\perp q}(x, k_\perp^2) = f_{1T}^{\perp(1)q}(x) \, \frac{2M^2}{\pi \langle k_\perp^2 \rangle_{f_{1T}^\perp}^2} \, e^{-k_\perp^2/\langle k_\perp^2 \rangle_{f_{1T}^\perp}} \, , \tag{4.5f}$$

$$h_1^{\perp q}(x, k_\perp^2) = h_1^{\perp(1)q}(x) \, \frac{2M^2}{\pi \langle k_\perp^2 \rangle_{h_1^\perp}^2} \, e^{-k_\perp^2/\langle k_\perp^2 \rangle_{h_1^\perp}} \, , \tag{4.5g}$$

$$h_{1T}^{\perp q}(x, k_\perp^2) = h_{1T}^{\perp(2)q}(x) \, \frac{2M^4}{\pi \langle k_\perp^2 \rangle_{h_{1T}^\perp}^3} \, e^{-k_\perp^2/\langle k_\perp^2 \rangle_{h_{1T}^\perp}} \, . \tag{4.5h}$$

The parametrizations of the basis functions and the Gaussian model parameters are described in detail in App. A.

5 Leading-twist asymmetries and basis functions

In this section we review how the basis functions describe available SIDIS data. This is of importance to assess the reliability of the predictions presented in the next sections.

5.1 Leading-twist F_{UU} and Gaussian Ansatz

As explained in Sec. 4.3 the Gaussian Ansatz is chosen not only because it considerably simplifies the calculations, but more importantly because it works phenomenologically with a good accuracy in many processes including SIDIS [96–101].

The Gaussian Ansatz for the unpolarized TMD and FF is given by Eqs. (4.5a, 4.5b). The parameters $\langle k_\perp^2 \rangle_{f_1}$ and $\langle P_\perp^2 \rangle_{D_1}$ can be assumed to be flavor- and x– or z–independent, as present data hardly allow us to constrain too many parameters, see App. A.1 for a review.

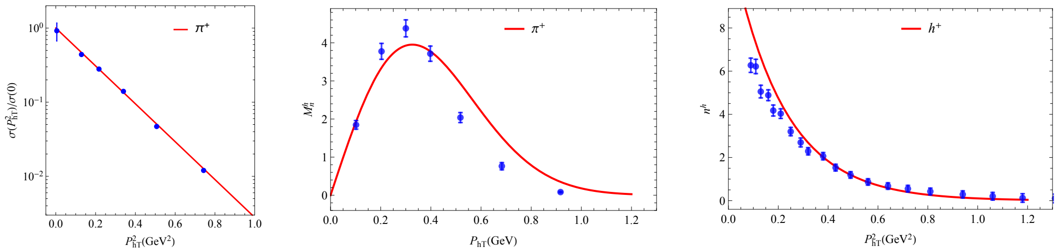

Figure 4. Left panel: $F_{UU}(P_{hT}^2)/F_{UU}(0)$ for π^+ production at Jefferson Lab with 5.75 GeV beam [108]. Middle panel: HERMES multiplicity (5.3) at $\langle Q^2\rangle = 2.87\,\text{GeV}^2$, $\langle x\rangle = 0.15$, $\langle z\rangle = 0.22$ [109]. Right panel: COMPASS multiplicity (5.4) at $\langle Q^2\rangle = 20\,\text{GeV}^2$, $\langle x\rangle = 0.15$, $\langle z\rangle = 0.2$ [110].

This assumption can be relaxed, e.g., theoretical studies in chiral effective theories predict a strong flavor-dependence in the $k_\perp$–behavior of sea and valence quark TMDs [106].

The structure function F_{UU} needed for our analysis reads

$$F_{UU}(x,z,P_{hT}) = x\sum_q e_q^2\, f_1^q(x)\, D_1^q(z)\, \mathcal{G}(P_{hT})\,, \tag{5.1a}$$

$$F_{UU}(x,z) = x\sum_q e_q^2\, f_1^q(x)\, D_1^q(z)\,, \tag{5.1b}$$

where we introduce the notation $\mathcal{G}(P_{hT})$, which is defined as

$$\mathcal{G}(P_{hT}) = \frac{\exp(-P_{hT}^2/\lambda)}{\pi\,\lambda}\,, \quad \lambda = z^2\,\langle k_\perp^2\rangle_{f_1} + \langle P_\perp^2\rangle_{D_1}\,, \tag{5.2}$$

with the understanding that the convenient abbreviation λ is expressed in terms of the Gaussian widths of the *preceding* TMD and FF. Notice that $\mathcal{G}(P_{hT}) \equiv \mathcal{G}(x,z,P_{hT})$ and that in general $\mathcal{G}(P_{hT})$ appears under the flavor sum due to a possible flavor-dependence of the involved Gaussian widths. The normalization $\int d^2P_{hT}\,\mathcal{G}(P_{hT}) = 1$ correctly connects the structure function $F_{UU}(x,z,P_{hT})$ in (5.1a) with its P_{hT}–integrated counterpart (5.1b). In our effective description this step is trivial. In QCD the connection of TMDs to PDFs is subtle [107]. Figure 4 illustrates how the Gaussian Ansatz describes selected SIDIS data.

Let us begin with Jefferson Lab where, in the pre-12 GeV era, electron beams from CEBAF with energies in the range 4.3 to 5.7 GeV were scattered off proton or deuterium targets in the typical kinematics $1\,\text{GeV}^2 < Q^2 < 4.5\,\text{GeV}^2$, $W > 2\,\text{GeV}$, $0.1 < x < 0.6$, $y < 0.85$, $0.5 < z < 0.8$. The left panel of Fig. 4 shows basically the SIDIS structure function $F_{UU}(P_{hT}^2)$ normalized with respect to its value at zero transverse hadron momentum[3] for π^+ production from a proton target measured in the CLAS experiment with a 5.75 GeV beam for the kinematics $\langle Q^2\rangle = 2.37\,\text{GeV}^2$, $\langle x\rangle = 0.24$, $\langle z\rangle = 0.30$ [108]. Clearly, the Gaussian model works for the entire region of P_{hT} covered in this experiment, in which the structure function F_{UU} falls down by 2 orders of magnitude [99].

Next we discuss a representative plot from the HERMES experiment where pions or kaons were measured in the scattering of 27.6 GeV positrons from the HERA polarized

[3]Strictly speaking in [108] data for the normalized SIDIS cross section was presented. But these data correspond to $F_{UU}(P_{hT}^2)/F_{UU}(0) \equiv F_{UU}(\langle x\rangle,\langle z\rangle,P_{hT}^2)/F_{UU}(\langle x\rangle,\langle z\rangle,0)$ up to $1/Q^2$-suppressed terms.

positron storage ring at DESY off proton and deuteron targets in the SIDIS kinematics $Q^2 > 1\,\mathrm{GeV}^2$, $W^2 > 10\,\mathrm{GeV}^2$, $0.023 < x < 0.4$, $y < 0.85$, $0.2 < z < 0.7$. The middle panel of Fig. 4 displays the HERMES multiplicity [109]

$$M_n^h(x,z,P_{hT}) \equiv \frac{d\sigma_{\rm SIDIS}(x,z,P_{hT})/dx\,dz\,dP_{hT}}{d\sigma_{\rm DIS}(x)/dx} = 2\pi P_{hT}\frac{F_{UU}(x,z,P_{hT})}{x\sum_q e_q^2\,f_1^q(x)} \tag{5.3}$$

at $\langle Q^2\rangle = 2.87\,\mathrm{GeV}^2$, $\langle x\rangle = 0.15$, $\langle z\rangle = 0.22$ for π^+ production on the proton target [109].

Finally we show also a representative plot from the COMPASS experiment where charged pions, kaons, or hadrons were measured with 160 GeV longitudinally polarized muons scattered off proton and deuteron targets in the typical SIDIS kinematics $Q^2 > 1\,\mathrm{GeV}^2$, $W > 5\,\mathrm{GeV}$, $0.003 < x < 0.7$, $0.1 < y < 0.9$, $0.2 < z < 1$. The right panel of Fig. 4 shows the COMPASS multiplicity [110]

$$n^h(x,z,P_{hT}^2) \equiv \frac{d\sigma_{\rm SIDIS}(x,z,P_{hT}^2)/dx\,dz\,dP_{hT}^2}{d\sigma_{\rm DIS}(x)/dx} = \pi\frac{F_{UU}(x,z,P_{hT}^2)}{x\sum_q e_q^2\,f_1^q(x)} \tag{5.4}$$

at $\langle Q^2\rangle = 20\,\mathrm{GeV}^2$, $\langle x\rangle = 0.15$, $\langle z\rangle = 0.2$ for h^+ production on the deuterium target [110].

To streamline the presentation we refer to the comprehensive Appendix on the used parametrizations (App. A), and for technical details on the Gaussian Ansatz (App. B).

The description of the HERMES and COMPASS multiplicities in Fig. 4 is good and sufficient for our purposes, but it is not perfect. The descriptions of the COMPASS data in the region of small P_{hT}^2 and that of the HERMES data for $P_{hT} \gtrsim 0.3\,\mathrm{GeV}$ are not ideal. However, notice that in our description we use the Gaussian widths as fitted and employed in the original extractions of the TMDs. These values were not optimized to fit the HERMES or COMPASS multiplicities. Keeping this in mind, the description in Fig. 4 can be considered as satisfactory. We also remark that we do not take into account $k_\perp$-broadening effects between HERMES and COMPASS energies and that the HERMES data actually represent multiplicities integrated (separately for numerator and denominator) over the kinematic ranges of each bin while the curve is plotted for a fixed set of kinematics. Through dedicated fits to the HERMES, COMPASS (and other) data and consideration of $k_\perp$-evolution effects it is possible to obtain a better description than in Fig. 4, see [111].

5.2 Leading-twist A_{LL} and first test of Gaussian Ansatz in polarized scattering

The Gaussian Ansatz is useful in unpolarized case [96–101], but nothing is known about its applicability to spin asymmetries. The Jefferson Lab data [112] on $A_{LL}(P_{hT})$ put us in the position to conduct a first "test" for polarized partons. We assume Gaussian form for $g_1^a(x,k_\perp^2)$, Eq. (4.5c), and use lattice QCD results [62] to estimate the width $\langle k_\perp^2\rangle_{g_1}$, see App. A.2. With $\lambda = z^2\langle k_\perp^2\rangle_{g_1} + \langle P_\perp^2\rangle_{D_1}$ implicit in $\mathcal{G}(P_{hT})$, the structure function F_{LL} reads

$$F_{LL}(x,z,P_{hT}) = x\sum_q e_q^2\,g_1^q(x)\,D_1^q(z)\,\mathcal{G}(P_{hT})\,, \tag{5.5a}$$

$$F_{LL}(x,z) = x\sum_q e_q^2\,g_1^q(x)\,D_1^q(z)\,. \tag{5.5b}$$

The definition of the asymmetry in the Jefferson Lab experiment [112] was

$$A_{LL,\langle y\rangle}(x,z,P_{hT}) = \langle p_2\, A_{LL}(x,z,P_{hT})\rangle \;=\; \frac{\langle y(2-y)\; F_{LL}(x,z,P_{hT})\rangle}{\langle(1+(1-y)^2)\; F_{UU}(x,z,P_{hT})\rangle} \tag{5.6}$$

where $p_2 = y(2-y)/(1+(1-y)^2)$ and averaging (separately in numerator and denominator) over the kinematics of [112] is implied. We use the lattice data [62] to constrain the Gaussian width $\langle k_\perp^2\rangle_{g1}$ as described in App. A.2. All other ingredients in (5.6) are known and tested through other observables in Sec. 5.1. Therefore the comparison of our results to the Jefferson Lab data [112] shown in Fig. 5 provides several important tests. First, the Jefferson Lab data [112] are compatible with the Gaussian Ansatz within uncertainties. Second, the lattice results—in the way we use them in App. A.2—give an appropriate description of the data. (Another important test was already presented in [112]: the P_{hT}–integrated ("collinear") asymmetry (5.5b) is compatible with data from other experiments and theoretical results obtained from parametrizations of $f_1^a(x)$, $g_1^a(x)$, $D_1^a(z)$. This shows that even at the moderate beam energies of the pre-12 GeV era one was, to a good approximation, indeed probing DIS at Jefferson Lab [112].)

Encouraged by these findings we will use lattice predictions from Ref. [62] below also for the Gaussian widths of $g_{1T}^{\perp(1)a}$ and $h_{1L}^{\perp(1)a}$. Of course, at this point one could argue that the WW and WW-type approximations (3.6a, 3.6b) also dictate that $g_{1T}^{\perp}$ and $h_{1L}^{\perp}$ have the same Gaussian widths as g_1 and h_1. In fact, the lattice results for the respective widths are numerically similar, which can be interpreted as yet another argument in favor of the

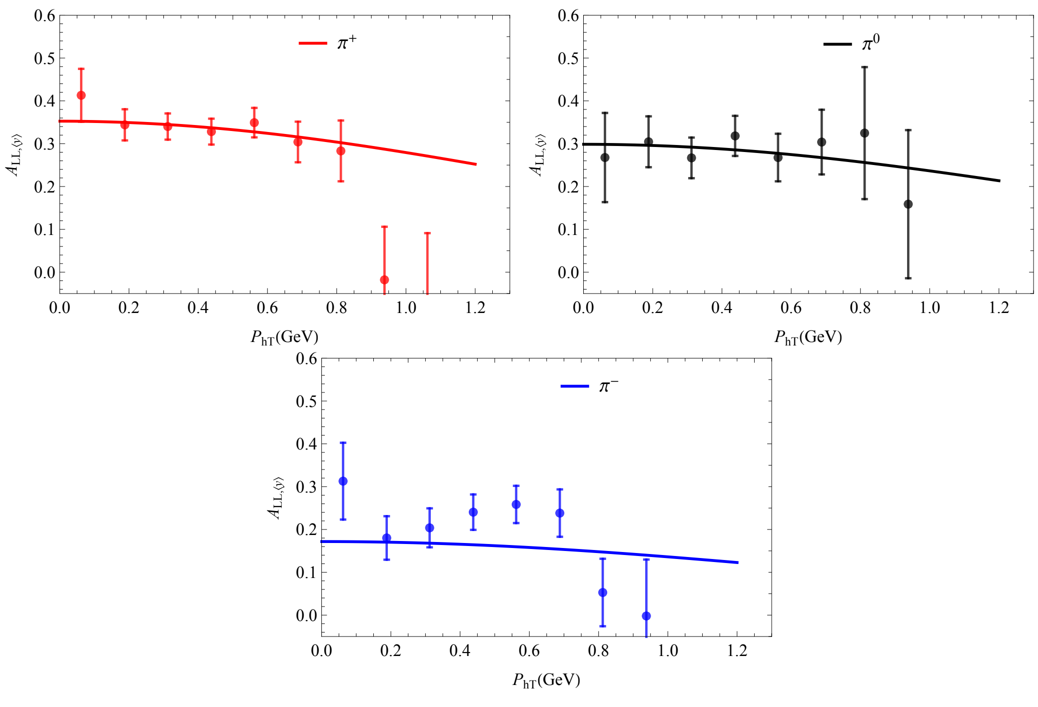

Figure 5. $A_{LL,\langle y\rangle}$ as function of P_{hT} vs JLab data [112] for π^+, π^0, π^-. The solid lines are our results for the mean values of kinematical variables $\langle x\rangle = 0.25$, $\langle z\rangle = 0.5$, $\langle Q^2\rangle = 1.67$ GeV^2.

usefulness of the approximations. The practical predictions depend only weakly on the choice of parameters.

5.3 Leading-twist $A_{UT}^{\sin(\phi_h-\phi_S)}$ Sivers asymmetry

The $F_{UT}^{\sin(\phi_h-\phi_S)}$ structure function is related to the Sivers function [113], which describes the distribution of unpolarized quarks inside a transversely polarized proton. It has so far received the widest attention, from both phenomenological and experimental points of view.

The Sivers function $f_{1T}^{\perp}$ is related to initial and final-state interactions of the struck quark and the rest of the nucleon and could not exist without the contribution of the orbital angular momentum of partons to the spin of the nucleon. As such it encodes the correlation between the partonic intrinsic motion and the transverse spin of the nucleon, and it generates a dipole deformation in momentum space. The Sivers function has been extracted from SIDIS data by several groups, with consistent results [43, 97, 114–119].

The structure function $F_{UT}^{\sin(\phi_h-\phi_S)}$ reads

$$F_{UT}^{\sin(\phi_h-\phi_S)}(x,z,P_{hT}) = -x\sum_q e_q^2\, f_{1T}^{\perp(1)q}(x)\, D_1^q(z)\, b_{\rm B}^{(1)}\left(\frac{zP_{hT}}{\lambda}\right)\mathcal{G}(P_{hT})\,, \tag{5.7a}$$

$$F_{UT}^{\sin(\phi_h-\phi_S)}(x,z,\langle P_{hT}\rangle) = -x\sum_q e_q^2\, f_{1T}^{\perp(1)q}(x)\, D_1^q(z)\, c_{\rm B}^{(1)}\left(\frac{z}{\lambda^{1/2}}\right), \tag{5.7b}$$

where $\lambda = z^2\langle k_\perp^2\rangle_{f_{1T}^\perp} + \langle P_\perp^2\rangle_{D_1}$ and $b_{\rm B}^{(1)} = 2M_N$ and $c_{\rm B}^{(1)} = \sqrt{\pi}\,M_N$, see App. B.5 for details.

Notice that integrating structure functions over P_{hT} is different from integrating the cross section over P_{hT} where azimuthal hadron modulations drop out. Only if the relevant weight is $\omega^{\{0\}}$ we obtain "collinear structure functions:" $F_{UU}(x,z)$, $F_{LL}(x,z)$ in Secs. 5.1, 5.2 and below in Secs. 7.2, 7.6. In all other cases, despite integration over P_{hT}, we end up always with true convoluted TMDs (here within Gaussian model). We stress this important point by displaying the dependence of the structure functions on the mean transverse hadron momenta, for instance $F_{UT}^{\sin(\phi_h-\phi_S)}(x,z,\langle P_{hT}\rangle) = \int d^2P_{hT}F_{UT}^{\sin(\phi_h-\phi_S)}(x,z,P_{hT})$ in (5.7b).

The asymmetries $A_{UT}^{\sin(\phi_h-\phi_S)} = F_{UT}^{\sin(\phi_h-\phi_S)}/F_{UU}$ obtained from the fit [120] are plotted in Fig. 6 as functions of x in comparison to HERMES [121] and COMPASS [122] data

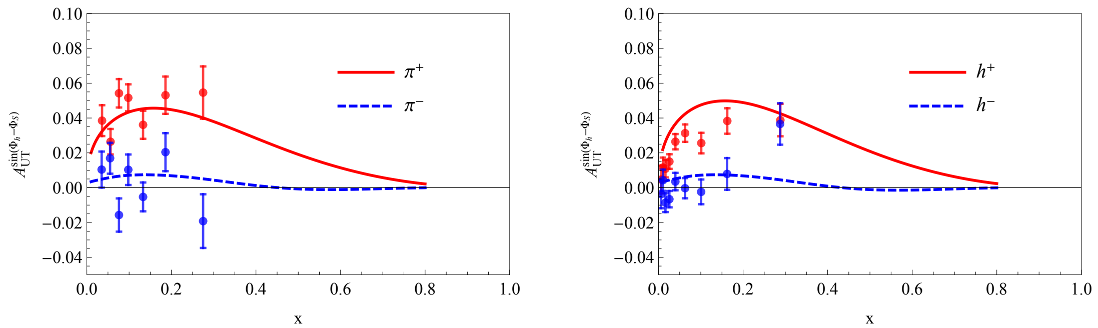

Figure 6. Sivers asymmetry $A_{UT}^{\sin(\phi_h-\phi_S)}$ from proton target as function of x based on the fit [120] in comparison to (left panel) HERMES [121] and (right panel) COMPASS data [122].

on respectively charged pion and hadron production from a proton target. The P_{hT}–dependences of the data are equally well described, which confirms that the Gaussian model works also in this case.

5.4 Leading-twist $A_{UT}^{\sin(\phi_h+\phi_S)}$ Collins asymmetry

The $F_{UT}^{\sin(\phi_h+\phi_S)}$ modulation of the SIDIS cross section is due to the convolution of the transversity distribution h_1 and the Collins FF $H_1^\perp$. Transversity can in principle be accessed also as a PDF in Drell–Yan or in dihadron production [123–128]. It describes the distribution of transversely polarized quarks in a transversely polarized nucleon, and is the only source of information on the tensor charge of the nucleon. The Collins FF $H_1^\perp$ decodes the fundamental correlation between the transverse spin of a fragmenting quark and the transverse momentum of the final produced hadron [129].

There are many extractions of h_1 and $H_1^\perp$ from a combined fit of SIDIS and e^+e^- data, for instance those of Refs. [130–132]. In this work we will use the extractions of h_1 and $H_1^\perp$ from Ref. [130].

The structure function $F_{UT}^{\sin(\phi_h+\phi_S)}$ reads

$$F_{UT}^{\sin(\phi_h+\phi_S)}(x,z,P_{hT}) = x\sum_q e_q^2\, h_1^q(x)\, H_1^{\perp(1)q}(z)\, b_{\rm A}^{(1)}\left(\frac{zP_{hT}}{\lambda}\right)\mathcal{G}(P_{hT})\,, \qquad (5.8a)$$

$$F_{UT}^{\sin(\phi_h+\phi_S)}(x,z,\langle P_{hT}\rangle) = x\sum_q e_q^2\, h_1^q(x)\, H_1^{\perp(1)q}(z)\, c_{\rm A}^{(1)}\left(\frac{z}{\lambda^{1/2}}\right), \qquad (5.8b)$$

where $\lambda = z^2\langle k_\perp^2\rangle_{h_1} + \langle P_\perp^2\rangle_{H_1^\perp}$ and $b_{\rm A}^{(1)} = 2m_h$ and $c_{\rm A}^{(1)} = \sqrt{\pi}\, m_h$, see App. B.5 for details.

The asymmetries $A_{UT,\langle y\rangle}^{\sin(\phi_h+\phi_S)} = (1-y)F_{UT}^{\sin(\phi_h+\phi_S)}/((1-y+y^2/2)F_{UU})$ are plotted in Fig. 7 as functions of x in comparison to HERMES [133] and $A_{UT}^{\sin(\phi_h+\phi_S)} = F_{UT}^{\sin(\phi_h+\phi_S)}/F_{UU}$ for COMPASS [134] data on charged pion production from proton targets. We remark that the description of the P_{hT}–dependencies of this azimuthal spin asymmetry is equally satisfactory by the fit of Ref. [130], which implies that the data are compatible with the Gaussian Ansatz also in this case.

5.5 Leading-twist $A_{UU}^{\cos(2\phi_h)}$ Boer–Mulders asymmetry

The structure function $F_{UU}^{\cos(2\phi_h)}$ arises from a convolution of the Collins fragmention function and the TMD $h_1^{\perp q}$ which describes the distribution of transversely polarized partons inside an unpolarized target. The expression of this structure function is given by

$$F_{UU}^{\cos(2\phi_h)}(x,z,P_{hT}) = x\sum_q e_q^2\, h_1^{\perp(1)q}(x)\, H_1^{\perp(1)q}(z)\, b_{\rm AB}^{(2)}\left(\frac{zP_{hT}}{\lambda}\right)^2\mathcal{G}(P_{hT})\,, \qquad (5.9a)$$

$$F_{UU}^{\cos 2\phi_h}(x,z,\langle P_{hT}\rangle) = x\sum_q e_q^2\, h_1^{\perp(1)q}(x)\, H_1^{\perp(1)q}(z)\, c_{\rm AB}^{(2)}\left(\frac{z}{\lambda^{1/2}}\right)^2, \qquad (5.9b)$$

where $\lambda = z^2\langle k_\perp^2\rangle_{h_1^\perp} + \langle P_\perp^2\rangle_{H_1^\perp}$ and $b_{\rm AB}^{(2)} = 4M_N m_h$ and $c_{\rm AB}^{(2)} = 4M_N m_h$, see App. B.5.

Asymmetries for $A_{UU,\langle y\rangle}^{\cos(2\phi_h)} = (1-y)F_{UU}^{\cos(2\phi_h)}/((1-y+y^2/2)F_{UU})$ HERMES [136] and $A_{UU}^{\cos(2\phi_h)} = F_{UU}^{\cos(2\phi_h)}/F_{UU}$ COMPASS [137] are plotted in Fig. 8, where we only considered the Boer–Mulders contribution to $A_{UU}^{\cos(2\phi_h)}$, which does not describe the data accurately. In fact, it is suspected that this observable receives a significant contribution from the Cahn effect [138], a term of higher-twist character of the type $\langle P_{hT}^2\rangle/Q^2$ which is not negligible in fixed-target experiments [99]. This contribution was estimated and corrected for in the phenomenological works [135, 139, 140], which was of importance to obtain a picture of the Boer–Mulders function undistorted from Cahn effect. The point is that this substantial twist-4 contamination can be estimated phenomenologically, even though there is no rigorous theoretical basis for the description of such power-suppressed terms. In this work we consistently neglect power-suppressed contributions of order $1/Q^2$, and do so also in Fig. 8. Nevertheless, we of course use the parametrizations of [135, 139, 140] offering the best currently available parametrizations for $h_1^\perp$, which were corrected for the Cahn effect as good as it is possible at the current state of art. It is unknown whether other asymmetries could be similarly effected by such type of power-corrections. This is an important point to be kept in mind as the lesson from Fig. 8 shows.

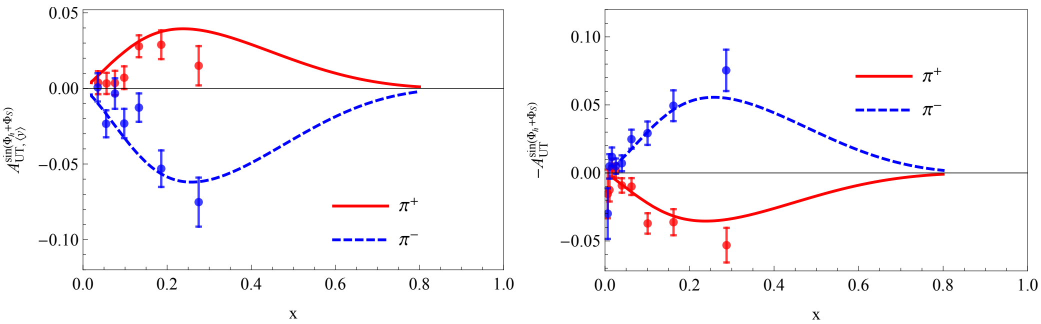

Figure 7. Collins asymmetry $A_{UT,\langle y\rangle}^{\sin(\phi_h+\phi_S)}$ from proton target as function of x based on the fit [130] in comparison to (left panel) HERMES [133] and (right panel) COMPASS data [134] (where $(-1)A_{UT}^{\sin(\phi_h+\phi_S)}$ is shown since for historical reasons the COMPASS collaboration likes to analyze their data with an opposite sign convention.)

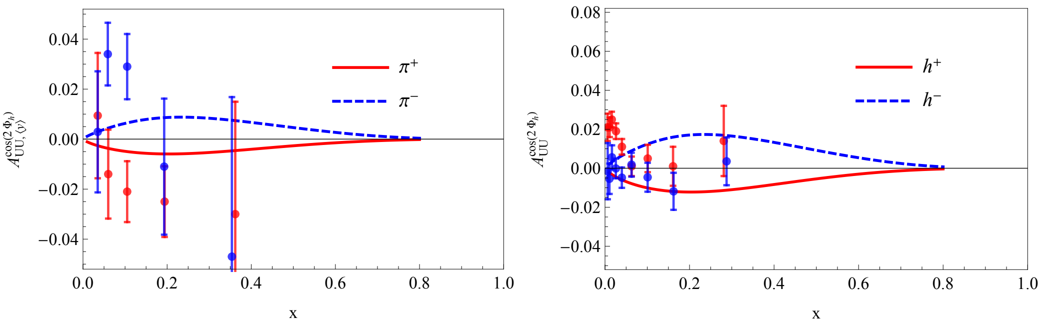

Figure 8. The asymmetry $A_{UU,\langle y\rangle}^{\cos(2\phi_h)}$ from proton target as function of x based on the fit [135] in comparison to (left panel) HERMES [136] and $A_{UU}^{\cos(2\phi_h)}$ (right panel) COMPASS data [137].

5.6 Leading-twist $A_{UT}^{\sin(3\phi_h-\phi_S)}$ asymmetry

The pretzelosity TMD $h_{1T}^{\perp q}$ is the least known of the basis functions. It is of interest as it allows one to measure the deviation of the nucleon spin density from spherical shape [11], as it is related to the only leading-twist SIDIS structure function where the small-P_{hT} description in terms of TMDs and the large-P_{hT} expansion in perturbative QCD mismatch [102], and as it is the only TMD where a clear relation to quark orbital angular momentum could be established (albeit only within quark models) [75, 141–143].

The structure function $F_{UT}^{\sin(3\phi_h-\phi_S)}$ reads

$$F_{UT}^{\sin(3\phi_h-\phi_S)}(x,z,P_{hT}) = x\sum_q e_q^2\, h_{1T}^{\perp(2)q}(x)\, H_1^{\perp(1)q}(z)\, b^{(3)} \left(\frac{zP_{hT}}{\lambda}\right)^3 \mathcal{G}(P_{hT})\,, \quad (5.10a)$$

$$F_{UT}^{\sin(3\phi_h-\phi_S)}(x,z,\langle P_{hT}\rangle) = x\sum_q e_q^2\, h_{1T}^{\perp(2)q}(x)\, H_1^{\perp(1)q}(z)\, c^{(3)} \left(\frac{z}{\lambda^{1/2}}\right)^3, \quad (5.10b)$$

where $\lambda = z^2\langle k_\perp^2\rangle_{h_{1T}^\perp} + \langle P_\perp^2\rangle_{H_1^\perp}$ and $b^{(3)} = 2M_N^2 m_h$ and $c^{(3)} = 3/2\sqrt{\pi}\, M_N^2 m_h$, see App. B.5. In Eq. (5.10a) we see that this structure function suffers a cubic suppression for small transverse hadron momenta. This is the strongest P_{hT}-suppression of all SIDIS structure functions through leading and subleading twist, making it challenging to measure.

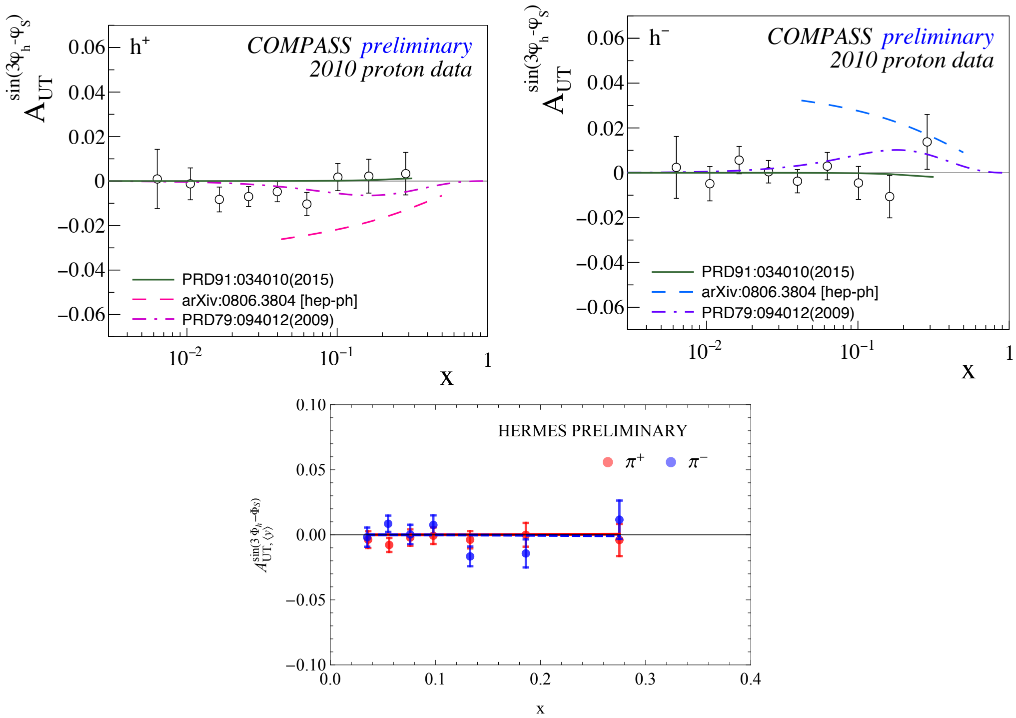

Figure 9. $A_{UT}^{\sin(3\phi_h-\phi_S)}$ as a function of x from preliminary COMPASS [144] and $A_{UT,\langle y\rangle}^{\sin(3\phi_h-\phi_S)}$ HERMES [145] in comparison to the best fit (whose 1-σ uncertainty band is compatible with zero) from [146]. For comparison the COMPASS plots show the model results [147, 148].

The preliminary COMPASS data [144] for $A_{UT}^{\sin(3\phi_h-\phi_S)} = F_{UT}^{\sin(3\phi_h-\phi_S)}/F_{UU}$ and the preliminary HERMES data [145] for $A_{UT,\langle y\rangle}^{\sin(3\phi_h-\phi_S)} = (1-y)F_{UT}^{\sin(3\phi_h-\phi_S)}/((1-y+y^2/2)F_{UU})$ are plotted in Fig. 9. Clearly, the pretzelosity TMD is the least known of the basis TMDs. Nevertheless it is of fundamental importance, as it provides one of the basis functions in our approach. It is so difficult to access it experimentally, because its contribution to the SIDIS cross section is proportional to P_{hT}^3, the TMD approach requires us to necessarily operate at $P_{hT} \ll Q$, and so far only moderate values of Q could be achieved in the fixed target experiments. A notable exception is COMPASS where the largest x–bins (where Q^2 is largest) bear the best hints on this TMD, see Fig. 9. Future high luminosity data from JLab 12 are expected to significantly improve our knowledge of this TMD.

5.7 Statistical and systematic uncertainties of basis functions

Even the well-known collinear functions $f_1^a(x)$, $g_1^a(x)$ have statistical uncertainties and systematic uncertainties (the latter introduced by choosing a certain fit Ansatz which however can be avoided through neural network techniques [149]). These uncertainties as well as those of $D_1^a(z)$ can safely be neglected for our purposes. For TMDs the situation is different. Already the transverse momentum descriptions of $f_1^a(x, k_\perp)$ and $D_1^a(z, P_\perp)$ are associated with non-negligible statistical uncertainties, which are reviewed in App. A, and with systematic uncertainties that are very difficult to assess as they are related to model bias (because of Gaussian model and its limitations). The statistical and systematic uncertainties are significant when we deal with the basis functions $f_{1T}^{\perp q}$, h_1^q, $H_1^{\perp q}$. The least well-controlled uncertainties are associated with the Boer–Mulders function $h_1^{\perp q}$ and pretzelosity $h_{1T}^{\perp q}$.

In this work we are not interested in these uncertainties, which future data will allow us to diminish, even though in practice they may be sizable. Rather in this work we are interested in making projections based on the WW-type approximation. To avoid cumbersome and difficult to interpret figures we will therefore refrain from indicating the uncertainties associated with our current knowledge of the basis functions. In the following we will only display the estimated systematic uncertainty associated with the WW-type approximations *assuming* it works within a relative accuracy of $\pm 40\%$. We stress that this is only to simplify the presentation. The actual uncertainty of the predictions may be larger.

6 Leading-twist asymmetries in WW-type approximation

Two out of the 8 leading–twist structure functions can be described in WW-type approximation thanks to Eqs. (3.6a, 3.6b) which relate $g_{1T}^{\perp(1)q}(x)$ and $h_{1L}^{\perp(1)q}(x)$ to the basis functions $g_1^q(x)$ and $h_1^a(x)$, see Fig. 10. These TMDs are sometimes referred to as "gear worms:" $g_{1T}^{\perp q}$ describes the distributions of longitudinally polarized quarks inside a transversely polarized nucleon, $h_{1L}^{\perp q}$ the opposite configuration, namely transversely polarized quarks inside a longitudinally polarized nucleon. It is interesting that both cases can be expressed in the WW-type approximation in terms of the basis functions. In this section we discuss the associated asymmetries.

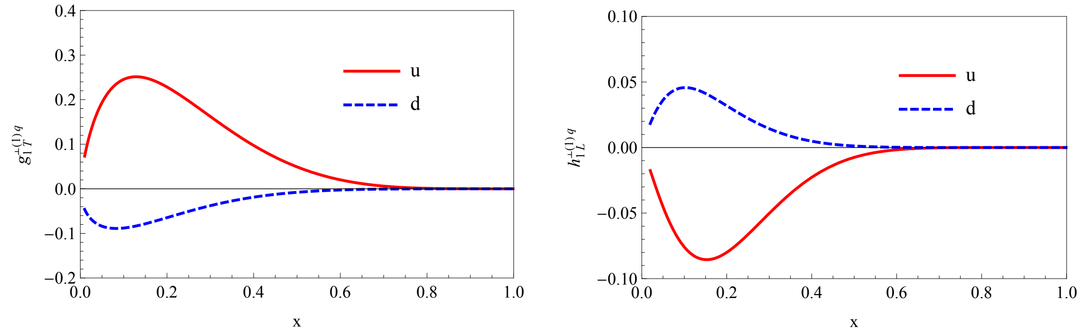

Figure 10. $g_{1T}^{\perp(1)q}(x)$ (left panel) and $h_{1L}^{\perp(1)q}(x)$ distributions (right panel) for $u-$ and d–flavor as predicted by the WW-type approximations in Eqs. (3.6a, 3.6b).

6.1 Leading-twist $A_{LT}^{\cos(\phi_h-\phi_S)}$

We assume for $g_{1T}^{\perp}$ the Gaussian Ansatz as shown in Eq. (B.9a) of App. B.3, see also [27], and evaluate $g_{1T}^{\perp(1)q}(x)$ using Eq. (3.6a), which yields the result shown in Fig. 10. For our numerical estimates we use $\langle k_\perp^2\rangle_{g_{1T}^\perp} = \langle k_\perp^2\rangle_{g_1}$ which is supported by lattice results [62].

In the Gaussian Ansatz the structure function $F_{LT}^{\cos(\phi_h-\phi_S)}$ has the form

$$F_{LT}^{\cos(\phi_h-\phi_S)}(x,z,P_{hT}) = x\sum_q e_q^2\, g_{1T}^{\perp(1)q}(x)\, D_1^q(z)\, b_{\rm B}^{(1)}\left(\frac{zP_{hT}}{\lambda}\right)\mathcal{G}(P_{hT}) \tag{6.1a}$$

$$F_{LT}^{\cos(\phi_h-\phi_S)}(x,z,\langle P_{hT}\rangle) = x\sum_q e_q^2\, g_{1T}^{\perp(1)q}(x)\, D_1^q(z)\, c_{\rm B}^{(1)}\left(\frac{z}{\lambda^{1/2}}\right) \tag{6.1b}$$

where $\lambda = z^2\langle k_\perp^2\rangle_{g_{1T}^\perp} + \langle P_\perp^2\rangle_{D_1}$, $b_{\rm B}^{(1)} = 2M_N$, $c_{\rm B}^{(1)} = \sqrt{\pi}\,M_N$, see App. B.5 for details.

This asymmetry was measured at Jefferson Lab [151], COMPASS [150] and HERMES [152, 153] (for the latter two experiments only preliminary results are available so far). Fig. 11 shows the preliminary results from the 2010 COMPASS data [150]. We approximate the charged hadrons (90 % of which are $\pi^\pm$ at COMPASS) by charged pions, see App. A.1. Our results are shown as a shaded area, which indicates a rough estimate of the uncertainty of the WW-type approximation. We observe that the WW-type approximation describes the data within their experimental uncertainties. For comparison also results from the theoretical works [27, 147, 148] are shown. Our results are also compatible with the Jefferson Lab data, which was taken with a neutron (^{3}He) target [151] and has larger statistical uncertainty than the preliminary COMPASS data.

6.2 Leading-twist $A_{UL}^{\sin 2\phi_h}$ Kotzinian–Mulders asymmetry

We use the Gaussian form for the Kotzinian–Mulders function $h_{1L}^{\perp a}$, Eq. (B.9b) in App. B.3, with $\langle k_\perp^2\rangle_{h_{1L}^\perp} = \langle k_\perp^2\rangle_{h_1}$ as supported by lattice data [62]. From (3.6b) we obtain the WW-type estimate for $h_{1L}^{\perp(1)a}(x)$ shown in Fig. 10. The structure function $F_{UL}^{\sin(2\phi_h)}$ reads

$$F_{UL}^{\sin(2\phi_h)}(x,z,P_{hT}) = x\sum_q e_q^2\, h_{1L}^{\perp(1)q}(x)\, H_1^{\perp(1)q/h}(z)\left(\frac{zP_{hT}}{\lambda}\right)^2 b_{\rm AB}^{(2)}\,\mathcal{G}(P_{hT})\,, \tag{6.2a}$$

$$F_{UL}^{\sin(2\phi_h)}(x,z,\langle P_{hT}\rangle) = x \sum_q e_q^2\, h_{1L}^{\perp(1)q}(x)\, H_1^{\perp(1)q/h}(z) \left(\frac{z}{\lambda^{1/2}}\right)^2 c_{\rm AB}^{(2)}\,, \tag{6.2b}$$

where $\lambda = z^2\langle k_\perp^2\rangle_{h_{1L}^\perp} + \langle P_\perp^2\rangle_{H_1^\perp}$ and $b_{\rm AB}^{(2)} = c_{\rm AB}^{(2)} = 4M_N m_h$, see App. B.5 for details.

The asymmetry $A_{UL}^{\sin(2\phi_h)} = F_{UL}^{\sin(2\phi_h)}/F_{UU}$ was studied at HERMES [154, 156], COMPASS [150], and Jefferson Lab [112, 155]. In Fig. 12 proton data are shown for $\pi^\pm$ in the HERMES experiment which were measured with the 27.6 GeV positron beam from the HERA polarized positron storage ring at DESY for $1\,\text{GeV}^2 < Q^2 < 15\,\text{GeV}^2$, $W > 2\,\text{GeV}$, $0.023 < x < 0.4$ and $y < 0.85$. The COMPASS data were taken with a 160 GeV muon

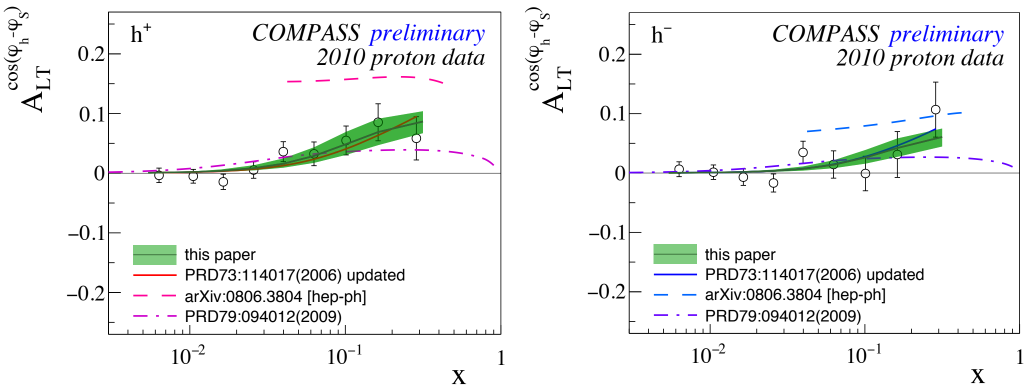

Figure 11. Leading-twist $A_{LT}^{\cos(\phi_h-\phi_S)}$ in comparison to the preliminary COMPASS data [150].

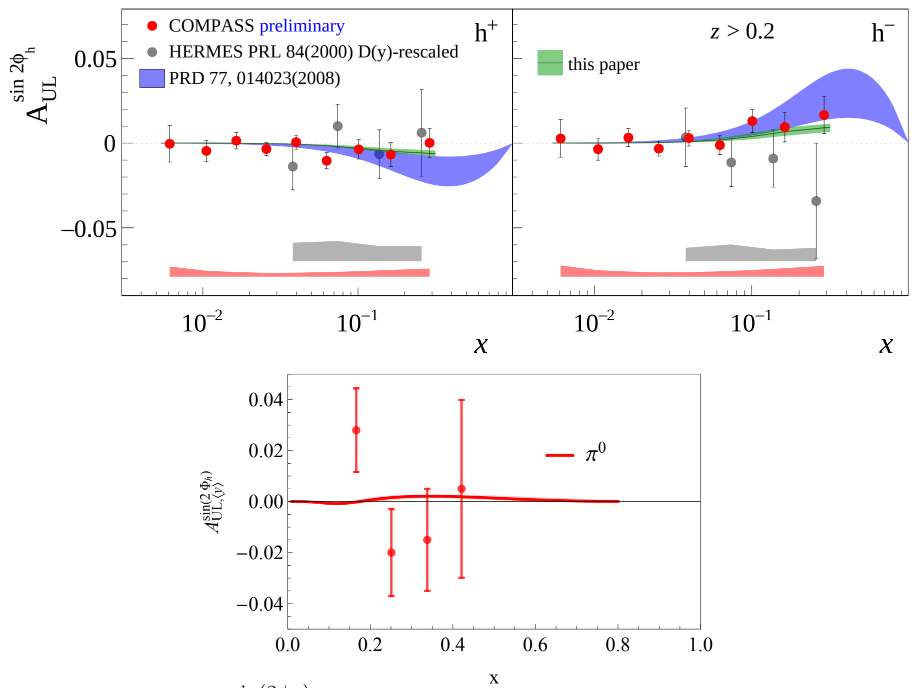

Figure 12. Leading twist $A_{UL}^{\sin(2\phi_h)}$ vs x from the WW-type approximation in comparison to data from HERMES [154], and $A_{UL}^{\sin(2\phi_h)}$ COMPASS [150] (left panel), and $A_{UL,\langle y\rangle}^{\sin(2\phi_h)}$ Jefferson Lab [155] (right panel). Results from [28] are also shown.

beam and show the asymmetry for charged hadrons (in practice mainly pions). Since y–dependent prefactors were included in the analyses (see Sec. 2.1), the HERMES data is adequately ("$D(y)$–")rescaled. The CLAS π^0 data in the right panel were measured using 6 GeV longitudinally polarized electrons scattering off longitudinally polarized protons in a cryogenic $^{14}NH_3$ target in the kinematics $1.0\,\mathrm{GeV}^2 < Q^2 < 3.2\,\mathrm{GeV}^2$, $0.12 < x < 0.48$ and $0.4 < z < 0.7$ [155].

$A_{UL}^{\sin(2\phi_h)}$ can be expected to be smaller than $A_{LT}^{\cos(\phi_h-\phi_S)}$ discussed in the previous section, even though both are leading twist. This is because $F_{UL}^{\sin(2\phi_h)}$ is quadratic in the hadron transverse momenta $P_{hT} \ll Q$, while $F_{LT}^{\cos(\phi_h-\phi_S)}$ is linear. In addition, the former is proportional to the Collins function which is smaller than $D_1^q(z)$, and the WW-type approximation predicts the magnitude of $h_{1L}^{\perp(1)q}(x)$ to be about half of the size of $g_{1T}^{\perp(1)q}(x)$. The data support these expectations. HERMES and Jefferson Lab data are compatible with zero for this asymmetry. So are the preliminary COMPASS data except for the region $x > 0.1$ for negative hadrons, where the trend of the data provides a first encouraging confirmation for our results. The current data are compatible with the WW-type approximation for $h_{1L}^{\perp(1)q}(x)$.

6.3 Inequalities and a cross check

We discussed WW-type approximations for the twist-2 TMDs $g_{1T}^{\perp q}$ and $h_{1L}^{\perp q}$ in Secs. 6.1, 6.2. Before proceeding with twist-3 let us pause and revisit positivity bounds [14].

The Kotzinian–Mulders function $h_{1L}^{\perp q}$ in conjunction with the Boer–Mulders function, and the TMD $g_{1T}^{\perp q}$ in conjunction with the Sivers function obey the positivity bounds [14]

$$\frac{k_\perp^2}{4M_N^2}\,\big((f_1^q(x,k_\perp^2))^2-(g_1^q(x,k_\perp^2))^2\big)-(h_{1L}^{\perp(1)q}(x,k_\perp^2))^2-(h_1^{\perp(1)q}(x,k_\perp^2))^2 \geq 0\,, \quad (6.3a)$$

$$\frac{k_\perp^2}{4M_N^2}\,\big((f_1^q(x,k_\perp^2))^2-(g_1^q(x,k_\perp^2))^2\big)-(f_{1T}^{\perp(1)q}(x,k_\perp^2))^2-(g_{1T}^{\perp(1)q}(x,k_\perp^2))^2 \geq 0\,, \quad (6.3b)$$

where $f^{(1)}(x,k_\perp^2) \equiv \frac{k_\perp^2}{2M_N^2} f(x,k_\perp^2)$. The inequalities provide a non-trivial test of our approach. The inequalities (6.3a, 6.3b) must be strictly satisfied by the *exact* leading-order QCD expressions for the TMDs. (For PDFs it is known that positivity can be preserved in some schemes and violated in others. For TMDs not much is known about positivity conditions beyond leading order.) However, here we do not deal with exact TMDs but (i) we invoked strong model assumptions (WW-type approximations for $g_{1T}^{\perp q}$ and $h_{1L}^{\perp q}$ and Gaussian Ansatz for all TMDs), and (ii) we deal with first extractions which have sizable uncertainties including poorly controlled systematic uncertainties. Therefore, considering that we deal with approximations (WW-type, Gauss) and considering the current state of TMD extractions, the inequalities (6.3a, 6.3b) constitute a challenging test for the approach.

To conduct a test we use the Gaussian Anśatze (4.5a, 4.5d, 4.5f, 4.5g, B.9a, B.9b) for the TMDs and integrate over $k_\perp$. The results are shown in Fig. 13 where we plot the "normalized inequalities" defined as follows: given an inequality $a - b - \ldots \geq 0$, the normalized inequality is defined as: $0 \leq (a-b-\ldots)/(|a|+|b|+\ldots) \leq 1$.

Fig. 13 shows that the results of our approach for the "normalized inequalities" for both TMDs lie between zero and one, as it is dictated by positivity constraints. This is an important consistency cross-check for our approach.

7 Subleading-twist asymmetries in WW-type approximation

WW-type approximations can be applied to all 8 subleading–twist asymmetries, see Sec. 4.2. In this section we discuss all of them, starting with less complex cases and proceeding then to those structure functions whose description in WW-type approximation is more involved.

7.1 Subleading-twist $A_{LU}^{\sin\phi_h}$

We start our discussion with the structure function $F_{LU}^{\sin\phi_h}$, Eq. (2.19b), containing 4 terms: 2 term are proportional to pure twist-3 fragmentation functions $\tilde{G}^{\perp a}$ and $\tilde{E}^a$ and neglected; the other 2 terms are proportional to the twist-3 TMDs e^a and $g^{\perp a}$, which also turn out to be given in terms of pure twist-3 terms upon the inspection of Eqs. (3.3a, 3.4d). Hence, after consequently applying the WW-type approximation, we are left with no term. Our approximation predicts this structure function to be zero.

In this asymmetry we encounter the generic limitation of the WW-type approximation in most extreme form. As discussed in Sec. 3.8, if we have a function $= \langle\bar{q}q\rangle + \langle\bar{q}gq\rangle$ the necessary condition for the approximation to work is that $\langle\bar{q}q\rangle \neq 0$ and the sufficient condition would be $|\langle\bar{q}q\rangle| \gg |\langle\bar{q}gq\rangle|$. Remarkably, none of the twist-3 TMDs or FFs entering this structure function satisfy even the necessary condition. In this situation we do not expect the WW-type approximation to be applicable.

Indeed, data from Jefferson Lab, HERMES and COMPASS show a clearly non-zero asymmetry $A_{LU}^{\sin\phi_h} = F_{LU}^{\sin\phi_h}/F_{UU}$ of the order of 2 % [137, 157–161]. On the one hand this is interesting: this observable provides a unique opportunity to learn about the physics of $\bar{q}gq$-terms. On the other hand, this observable is beyond the applicability of the WW-type approximation and we cannot make a non-trivial prediction for this asymmetry.

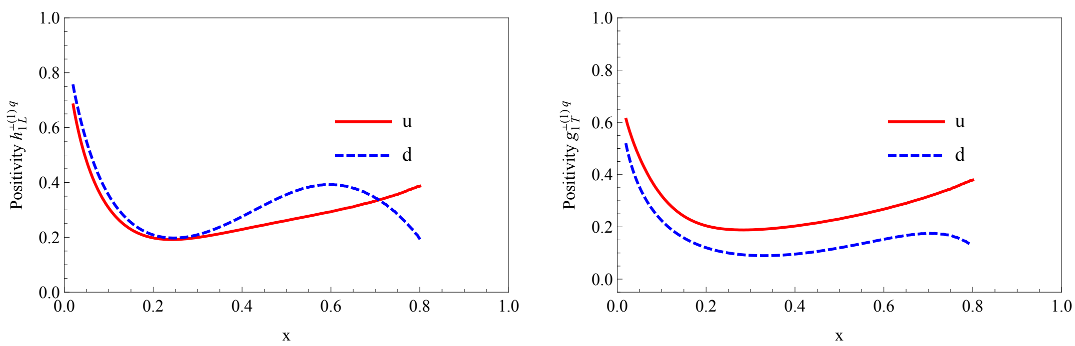

Figure 13. The normalized inequalities for $g_{1T}^{\perp(1)q}(x)$ and $h_{1L}^{\perp(1)q}(x)$ vs x which are obtained by integrating (6.3a) and (6.3b) over $k_\perp$, and normalizing with respect to the sum of the absolute values of the individual terms. The result must be positive and smaller than unity *if* the WW-type approximations and the application of the Gaussian model are compatible with positivity, see text. Clearly, our approach respects this test of the positivity conditions.

With the numerator of the asymmetry proportional to $\bar{q}gq$–terms and the denominator given in terms of $\bar{q}q$–terms, one could be tempted to interpret this observation as

$$A_{LU}^{\sin\phi_h} \;\propto\; \frac{\langle\bar{q}gq\rangle}{\langle\bar{q}q\rangle} \;\stackrel{\rm exp}{\sim}\; \mathcal{O}(2\,\%)\,. \tag{7.1}$$

Thus, in some sense the observed effect hints at the smallness of the involved $\bar{q}gq$–terms. While in principle a correct observation, one should keep in mind several reservations. First, the experimental result (7.1) contains kinematic prefactors which help to reduce the value. Second, the denominator contains f_1^a and D_1^a which are the largest TMD and FF because of positivity constraints. Third, the numerator is a sum of 4 terms, so its overall smallness could result from cancellation of different terms, rather than indicating that each single $\bar{q}gq$–term is small. Fourth, some asymmetries predicted to be non-zero in WW-approximation are not much larger and in some cases even smaller than the result in (7.1).

To conclude, the WW-type approximation predicts $A_{LU}^{\sin\phi} \approx 0$ in contradiction to experiment. The size of the observed effect seems in line with the WW-type approximation, as $A_{LU}^{\sin\phi_h} \sim \langle\bar{q}gq\rangle/\langle\bar{q}q\rangle \sim \mathcal{O}(2\,\%)$ is not large, although this interpretation has reservations. $F_{LU}^{\sin\phi}$ is the only twist-3 SIDIS structure function not "contaminated" by leading twist. Attempts to describe this observable and relevant model studies have been reported [47, 50, 83, 88–90, 162–170]. But more phenomenological work and dedicated studies on the basis of models of $\bar{q}gq$ terms are needed to fully understand this asymmetry.

7.2 Subleading-twist $A_{LT}^{\cos\phi_S}$

In WW-type approximation the structure function $F_{LT}^{\cos\phi_S}$ arises from $g_T^a(x, k_\perp)$ and $D_1^a(z, P_\perp)$ whose collinear counterparts are more or less known, see Secs. 3.4 and 5.1. We assume the Gaussian Ansatz for $g_T^a(x, k_\perp)$ shown in Eq. (B.9c) of App. B.3 with $\langle k_\perp^2\rangle_{g_T} = \langle k_\perp^2\rangle_{g_1}$. We then determine $g_T^q(x)$ according to Eq. (3.2a), which is a well-tested approximation in DIS, see Sec. 3.4. In this way we obtain for $F_{LT}^{\cos\phi_S}$ the result

$$F_{LT}^{\cos\phi_S}(x, z, P_{hT}) = -\frac{2M_N}{Q}\,x^2\sum_q e_q^2\,g_T^q(x)\,D_1^q(z)\,\mathcal{G}(P_{hT})\,, \tag{7.2a}$$

$$F_{LT}^{\cos\phi_S}(x, z) = -\frac{2M_N}{Q}\,x^2\sum_q e_q^2\,g_T^q(x)\,D_1^q(z)\,, \tag{7.2b}$$

with the width $\lambda = z^2\langle k_\perp^2\rangle_{g_T} + \langle P_\perp^2\rangle_{D_1}$ in the Gaussian $\mathcal{G}(P_{hT})$.

Notice that we followed here the scheme explained in Sec. 4.4: first assume Gaussian Ansatz, then apply WW-type approximation. For some structure functions the order of these steps is not relevant, but here it is. It is instructive to discuss what the opposite order of these steps yields. One may first plug in the WW-type approximation (3.3e) in the convolution integral (3.2a) and then solve the convolution integral with Gaussian Ansatz. The result is an analytical expression which is bulkier than (7.2a) though it yields a numerically similar result. But there are 2 critical issues with that. First, the WW-type approximation (3.3e) relates $g_T^q(x, k_\perp^2)$ to $g_{1T}^{\perp(1)q}(x, k_\perp^2)$ which (due to the weight $k_\perp^2/(2M_N^2)$ in the (1)-moment) implies a kinematical zero in $k_\perp$ as $g_T^q(x, 0) = 0$, which is not supported by model calculations [75]. Second, the more economic (because less bulky) expression in (7.2a) automatically yields (7.2b) which is the correct collinear result for this SIDIS function in Eq. (2.21c) in WW-type approximation. This technical remark confirms the consistency of the scheme suggested in Sec. 4.4.

Fig. 14 shows our predictions for $A_{LT}^{\cos\phi_S}$ are shown in comparison to preliminary COMPASS data from Ref. [150]. The predicted asymmetry is small and compatible with the COMPASS data within uncertainties. Preliminary HERMES data [153] confirm a small asymmetry. More precise data are necessary to judge how well the WW-type approximation works in this case. Such data could come from JLab12 experiments.

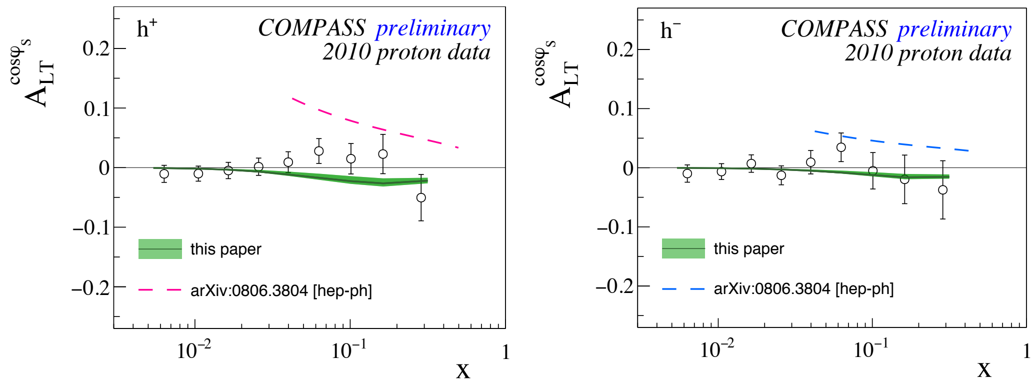

Figure 14. Subleading-twist $A_{LT}^{\cos\phi_S}$ as functions of x from scattering of 160 GeV longitudinally polarized muons off a transversely polarized proton target [150].

7.3 Subleading-twist $A_{LT}^{\cos(2\phi_h-\phi_S)}$

In the WW-type approximation this asymmetry is expressed in terms of $g_T^{\perp a}(x,k_\perp)$, for which we assume a Gaussian Ansatz according to Eq. (B.9d) in App. B.3, and use the WW-type approximation (3.3d) as

$$x g_T^{\perp(2)q}(x) = \frac{\langle k_\perp^2\rangle_{g_{1T}^\perp}}{M_N^2}\, g_{1T}^{\perp(1)q}(x)\,, \tag{7.3}$$

where we finally express $g_{1T}^{\perp(1)q}(x)$ in terms of $g_1^q(x)$ according to Eq. (3.6a). For the Gaussian widths we assume $\langle k_\perp^2\rangle_{g_T^\perp} = \langle k_\perp^2\rangle_{g_{1T}^\perp} = \langle k_\perp^2\rangle_{g_1}$. This yields for the structure function

$$F_{LT}^{\cos(2\phi_h-\phi_S)}(x,z,P_{hT}) = -\frac{2M_N}{Q}x\sum_q e_q^2\, x\, g_T^{\perp(2)q}(x)\, D_1^q(z)\, b_C^{(2)}\left(\frac{zP_{hT}}{\lambda}\right)^2 \mathcal{G}(P_{hT}) \tag{7.4a}$$

$$F_{LT}^{\cos(2\phi_h-\phi_S)}(x,z,\langle P_{hT}\rangle) = -\frac{2M_N}{Q}x\sum_q e_q^2\, x\, g_T^{\perp(2)q}(x)\, D_1^q(z)\, c_C^{(2)}\left(\frac{z}{\lambda^{1/2}}\right)^2 \tag{7.4b}$$

where $\lambda = z^2\langle k_\perp^2\rangle_{g_T^\perp} + \langle P_\perp^2\rangle_{D_1}$ and $b_{\rm C}^{(2)} = c_{\rm C}^{(2)} = M_N^2$, see App. B.5 for details.

Our predictions for the asymmetry $A_{LT}^{\cos(2\phi_h-\phi_S)} = F_{LT}^{\cos(2\phi_h-\phi_S)}/F_{UU}$ as function of x are displayed in Fig. 15 in comparison to preliminary COMPASS data from Ref. [150].

The asymmetry is very small, so at the current stage one may conclude that the WW-type approximation for the asymmetry $A_{LT}^{\cos(2\phi_h-\phi_S)}$ is compatible with available data. In view of the smallness of the effect, cf. Fig. 15, it might be difficult to obtain more quantitative insights in near future.

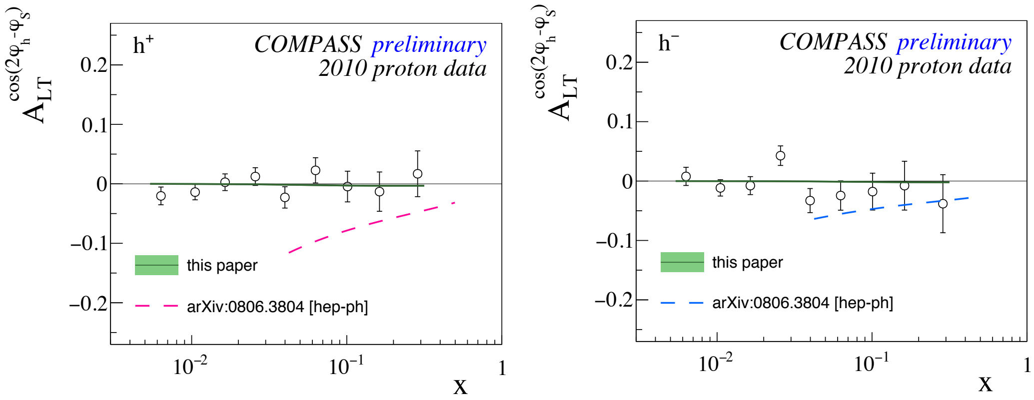

Figure 15. $A_{LT}^{\cos(2\phi_h-\phi_S)}$ as a function of x from a proton target in comparison to the preliminary COMPASS data [150]. The smallness of this asymmetry has two natural reasons. First, being twist-3 it is M_N/Q suppressed. Second, it is proportional to P_{hT}^2 with $P_{hT} \ll Q$ in TMD approach.

7.4 Subleading-twist $A_{LL}^{\cos\phi_h}$

In WW-type approximation the only contribution to $F_{LL}^{\cos\phi_h}$ is due to $g_L^{\perp q}(x,k_\perp)$, which we assume to have a Gaussian $k_\perp$–behavior according to Eq. (B.9e) in App. B.3 with the Gaussian width $\langle k_\perp^2\rangle_{g_L^\perp} = \langle k_\perp^2\rangle_{g_1}$. The structure function $F_{UL}^{\cos\phi_h}$ reads

$$F_{LL}^{\cos\phi_h}(x,z,P_{hT}) = -\frac{2M_N}{Q}\,x\sum_q e_q^2\,x\,g_L^{\perp(1)q}(x)\,D_1^q(z)\,b_{\rm B}^{(1)}\left(\frac{zP_{hT}}{\lambda}\right)\mathcal{G}(P_{hT})\,, \quad (7.5a)$$

$$F_{LL}^{\cos\phi_h}(x,z,\langle P_{hT}\rangle) = -\frac{2M_N}{Q}\,x\sum_q e_q^2\,x\,g_L^{\perp(1)q}(x)\,D_1^q(z)\,c_{\rm B}^{(1)}\left(\frac{z}{\lambda^{1/2}}\right), \quad (7.5b)$$

where $\lambda = z^2\langle k_\perp^2\rangle_{g_L^\perp} + \langle P_\perp^2\rangle_{D_1}$, $b_{\rm B}^{(1)} = 2M_N$, $c_{\rm B}^{(1)} = \sqrt{\pi}\,M_N$, see App. B.5. Finally we explore the WW-type approximation (3.3c) to relate $x\,g_L^{\perp(1)a}(x) = \frac{\langle k_\perp^2\rangle_{g_1}}{2M_N^2}\,g_1^a(x)$.

The asymmetry $A_{LL}^{\cos\phi_h} = F_{LL}^{\cos\phi_h}/F_{UU}$ predicted by the WW-type approximation in this case is small and compatible with presently available data, see Fig. 16. We remark that previously this asymmetry was studied in [171] and more recently in [172].

7.5 Subleading-twist $A_{UL}^{\sin\phi_h}$

In WW-type approximation $A_{UL}^{\sin\phi_h}$ is described by $h_L^q(x,k_\perp)$, for which we assume the Gaussian Ansatz (B.9f) in App. B.3 with $\langle k_\perp^2\rangle_{h_L} = \langle k_\perp^2\rangle_{h_1}$. We explore (3.3f) to estimate $x\,h_L^q(x) = -2h_{1L}^{\perp(1)q}(x)$ and express $h_{1L}^{\perp(1)q}(x)$ through $h_1^a(x)$ according to (3.6b). This yields

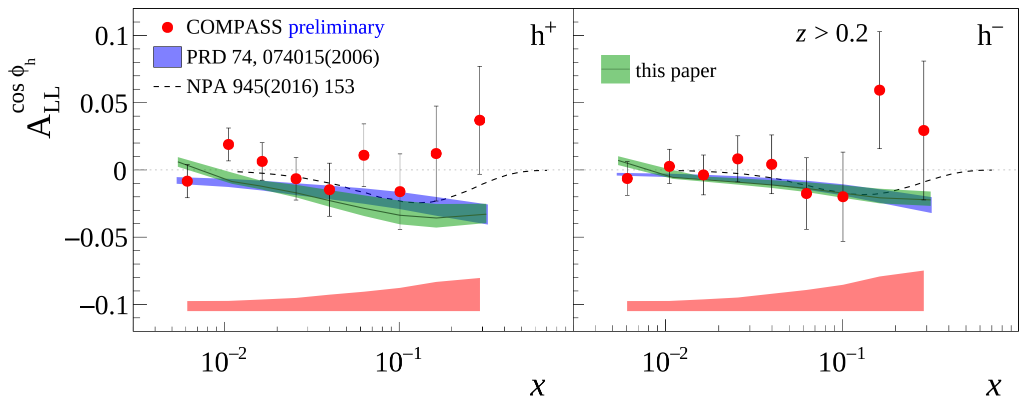

Figure 16. $A_{LL}^{\cos(\phi_h)}$ as a function of x from the WW-type approximation in comparison to the preliminary COMPASS data [150].

$$F_{UL}^{\sin\phi_h}(x,z,P_{hT}) = \frac{2M_N}{Q}\, x \sum_q e_q^2\, x\, h_L^q(x)\, H_1^{\perp(1)q}(z)\, b_{\rm A}^{(1)} \left(\frac{zP_{hT}}{\lambda}\right) \mathcal{G}(P_{hT})\,, \quad (7.6a)$$

$$F_{UL}^{\sin\phi_h}(x,z,\langle P_{hT}\rangle) = \frac{2M_N}{Q}\, x \sum_q e_q^2\, x\, h_L^q(x)\, H_1^{\perp(1)q}(z)\, c_{\rm A}^{(1)} \left(\frac{z}{\lambda^{1/2}}\right) \quad (7.6b)$$

where $\lambda = z^2\langle k_\perp^2\rangle_{h_L} + \langle P_\perp^2\rangle_{H_1^\perp}$ and $b_{\rm A}^{(1)} = 2m_h$ and $c_{\rm A}^{(1)} = \sqrt{\pi}\, m_h$, see App. B.5 for details.

The asymmetries $A_{UL}^{\sin\phi_h} = F_{UL}^{\sin\phi_h}/F_{UU}$ are compared to HERMES, Jefferson Lab, and preliminary COMPASS data in Fig. 17. The WW-type approximation reproduces the positive sign of the asymmetry seen consistently at HERMES and COMPASS for π^+ and positive hadrons but underestimates its magnitude. The results for negative pions and hadrons at HERMES and COMPASS are compatible. An important test for this asymmetry is provided by neutral pions where in WW-type approximation the contributions of Collins fragmentation function largely cancel. The WW-type approximation is not able to explain the large effect observed at HERMES and Jefferson Lab for π^0 in the large–x region $0.1 < x < 0.5$ in Fig. 17. Overall, the WW-type approximation is not adequate to catch the flavor dependence of this asymmetry. This indicates that here the tilde-terms are not negligible, and have a characteristic flavor dependence that is distinct from that of the Collins effect.

7.6 Subleading-twist $A_{UT}^{\sin\phi_S}$

In this structure function some interesting new features occur. The first feature is that after applying the WW-type approximation, not one but three terms are left, cf. Eqs. (2.19e, 4.2g): two terms proportional to $h_T^{\perp q}(x,k_\perp)$, $h_T^q(x,k_\perp)$, and one term proportional to $f_T^q(x,k_\perp)$, which is associated with the second interesting feature. This T-odd TMD must satisfy the sum rule $\int d^2k_\perp\, f_T^q(x,k_\perp) = 0$, see Eq. (2.14) and Sec. 3.8. This could be implemented in two ways: one could describe it with a superposition of Gaussians, see App. B.4. But at this point we have no guidance from phenomenology or theory to fix additional parameters.

So we choose an alternative and pragmatic solution, namely to neglect the contribution of $f_T^q(x,k_\perp)$.[4] Assuming Gaussian Ans´atze (B.9g, B.9h) for $h_T^{\perp q}(x,k_\perp)$, $h_T^q(x,k_\perp)$ in App. B.3 and relating them to transversity via the WW-type approximations (3.3g, 3.3h), the expression for $F_{UT}^{\sin\phi_S}$ is given in terms of a single term

$$F_{UT}^{\sin\phi_S}(x,z,P_{hT}) = \frac{2M_N}{Q}\, x \sum_q e_q^2\, h_1^{(1)q}(x)\, H_1^{\perp(1)q}(z)\, \frac{4z^2 m_h\, M_N}{\lambda}\left(1-\frac{P_{hT}^2}{\lambda}\right)\mathcal{G}(P_{hT}) \tag{7.7a}$$

$$F_{UT}^{\sin\phi_S}(x,z) = 0\,. \tag{7.7b}$$

with $\lambda = z^2\langle k_\perp^2\rangle_{h_T^\perp} + \langle P_\perp^2\rangle_{H_1^\perp}$ and $\langle k_\perp^2\rangle_{h_T^\perp} = \langle k_\perp^2\rangle_{h_T} = \langle k_\perp^2\rangle_{h_1}$. The third interesting feature is the occurrence of a term that drops out upon integrating the structure function over P_{hT}, cf. Eq. (7.7a) vs. (7.7b). This is a property of the weight $\omega_{\rm B}^{\{2\}}$, see Eq. (2.20) and App. B (which appears also in $F_{LT}^{\cos\phi_S}$, Eq. (2.19f), where it drops out in WW-type approximation). This property can help to discriminate experimentally the terms associated with this weight.

The final result in Eq. (7.7b) is the consistent result for the structure function $F_{UT}^{\sin\phi_S}(x,z)$ in WW-type approximation, see Eq. (2.21d). Our prediction is therefore $A_{UT}^{\sin\phi_S}(x) = 0$.

[4] This corresponds to using a "single Gaussian" as $f_T^q(x,k_\perp) = f_T^q(x)\,\frac{\exp(-k_\perp^2/\langle k_\perp^2\rangle_{f_T})}{\pi\langle k_\perp^2\rangle_{f_T}}$ with the "coefficient" $f_T^q(x) = 0$ as dictated by the sum rule (2.14).

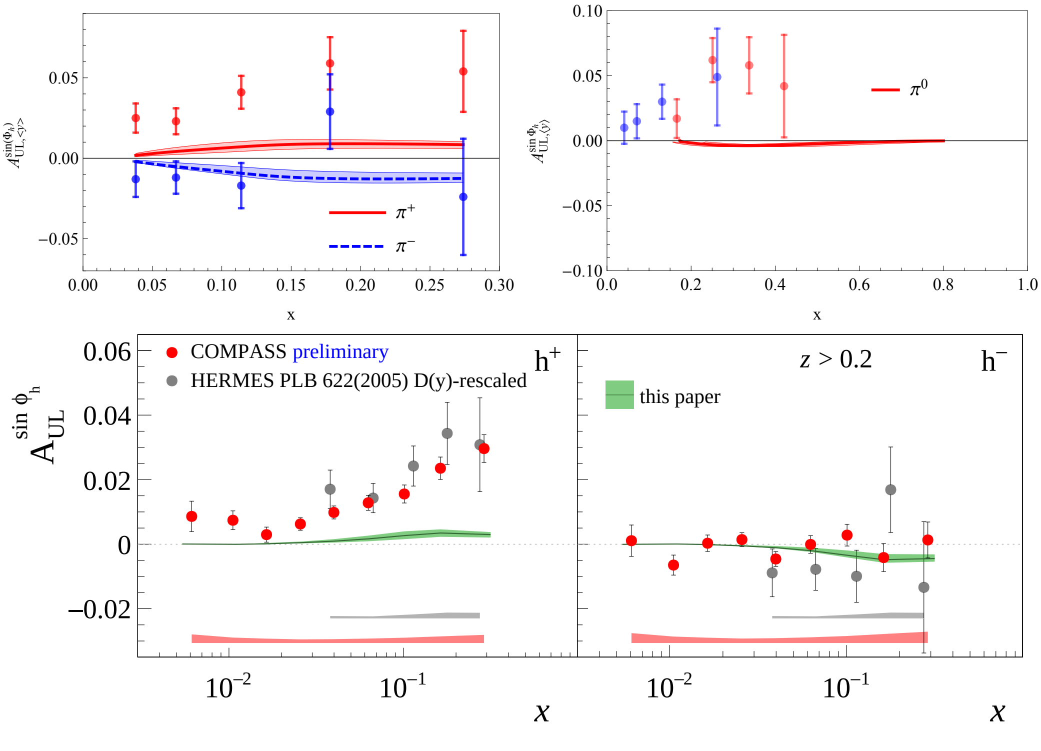

Figure 17. $A_{UL}^{\sin\phi_h}$ for proton target vs x from WW-type approximation in comparison to data for the following hadrons. Upper panel left: $\pi^\pm$ from HERMES [173]. Upper panel right: π^0 from HERMES (blue) [174] and JLab (red) [155]. Lower panel: preliminary $h^\pm$ COMPASS data [150].

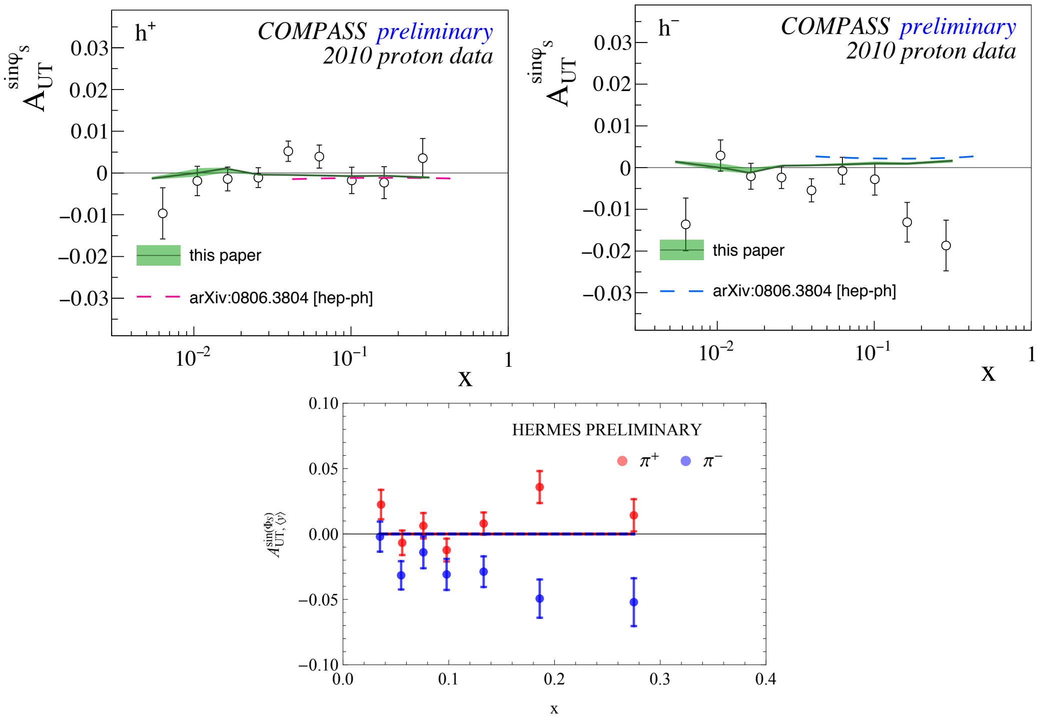

Figure 18. Subleading-twist asymmetry $A_{UT}^{\sin\phi_S}(x)$, which is predicted to vanish in the WW-type approximation, in comparison to preliminary COMPASS [150] and HERMES data [145].

Preliminary HERMES [145] (Fig. 18) and COMPASS [150] (Fig. 18) data indicate that at $x \gtrsim 0.1$ the signal is clearly non-zero and thus inconsistent with this WW-type prediction.

7.7 Subleading-twist $A_{UT}^{\sin(2\phi_h-\phi_S)}$

Also in this asymmetry we end up with more than one surviving contribution in our treatment. We assume Gaussian Ans´atze for $f_T^{\perp q}(x,k_\perp)$, $h_T^{\perp q}(x,k_\perp)$, $h_T^q(x,k_\perp)$ according to Eqs. (B.9g, B.9h, B.9i) in App. B.3 with $\langle k_\perp^2\rangle_{h_T^\perp} = \langle k_\perp^2\rangle_{h_T} = \langle k_\perp^2\rangle_{h_{1T}^\perp}$ and $\langle k_\perp^2\rangle_{f_T^\perp} = \langle k_\perp^2\rangle_{f_{1T}^\perp}$ and obtain

$$F_{UT}^{\sin(2\phi_h-\phi_S)}(x,z,P_{hT}) = \frac{2M_N}{Q}\, x\sum_q e_q^2 \Bigg[x\, f_T^{\perp(2)q}(x)\; D_1(z)\; b_{\rm C}^{(2)}\,\left(\frac{zP_{hT}}{\lambda}\right)^2 \mathcal{G}(P_{hT}) + \frac{x}{2}\left(h_T^{(1)q}(x)+h_T^{\perp(1)q}(x)\right) H_1^{\perp(1)q}(z)\, b_{\rm AB}^{(2)}\left(\frac{zP_{hT}}{\lambda}\right)^2 \mathcal{G}(P_{hT})\Bigg] \tag{7.8a}$$

$$F_{UT}^{\sin(2\phi_h-\phi_S)}(x,z,\langle P_{hT}\rangle) = \frac{2M_N}{Q}\, x\sum_q e_q^2 \Bigg[x\; f_T^{\perp(2)q}(x)\; D_1(z)\; c_{\rm C}^{(2)}\,\left(\frac{z}{\lambda^{1/2}}\right)^2 + \frac{x}{2}\left(h_T^{(1)q}(x)+h_T^{\perp(1)q}(x)\right) H_1^{\perp(1)q}(z)\, c_{\rm AB}^{(2)}\left(\frac{z}{\lambda^{1/2}}\right)^2\Bigg] \tag{7.8b}$$

with respectively $\lambda = z^2\langle k_\perp^2\rangle_{f_T^\perp} + \langle P_\perp^2\rangle_{D_1}$ in the first, and $\lambda = z^2\langle k_\perp^2\rangle_{h_T^\perp} + \langle P_\perp^2\rangle_{H_1^\perp}$ in the second terms in Eqs. (7.8a, 7.8b). The coefficients $b_i^{(2)}$ and $c_i^{(2)}$ are defined in App. B.5. In the next step we explore the WW-type approximations (3.3g, 3.3h, 3.4f) to relate $x\, f_T^{\perp(2)q}(x) = \frac{\langle k_\perp^2\rangle_{f_{1T}^\perp}}{M_N^2}\, f_{1T}^{\perp(1)q}(x)$ and $-\frac{1}{2}\, x\, \Big(h_T^{(1)q}(x) + h_T^{\perp(1)q}(x)\Big) = h_{1T}^{\perp(2)q}(x)$.

The asymmetries $A_{UT}^{\sin(2\phi_h-\phi_S)} = F_{UT}^{\sin(2\phi_h-\phi_S)}/F_{UU}$ are plotted in Fig. 19 in comparison to preliminary COMPASS [150] and HERMES [145] data. The predicted asymmetry is small and compatible with the data that are consistent with a zero effect within uncertainties.

7.8 Subleading-twist $A_{UU}^{\cos\phi_h}$

Historically this was the earliest azimuthal SIDIS asymmetry to be discussed in literature: the first prediction for this asymmetry from intrinsic $k_\perp$ was made in [138, 175], a first measurement was reported in [176].[5] This structure function contains after the WW-type approximation initially two contributions, proportional to $f^\perp(x, P_\perp)$ and $h^q(x, k_\perp)$. The latter is T-odd and obeys the sum rule (2.14). We treat $h^q(x, k_\perp)$ exactly as $f_T^q(x, k_\perp)$ in

[5] First hints [177] of azimuthal modulations in SIDIS date back to the early 1970s, i.e., 10 years before the CERN measurements, but (unfortunately) were discarded by the authors.

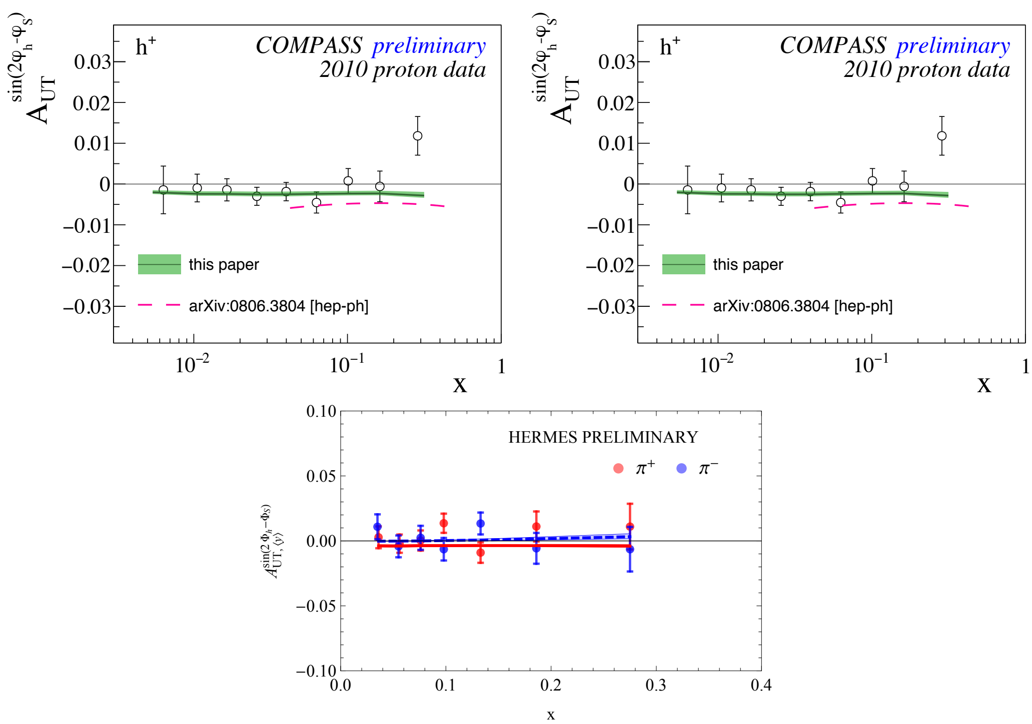

Figure 19. Subleading–twist $A_{UT}^{\sin(2\phi_h-\phi_S)}(x)$ in comparison with preliminary COMPASS data [150], and subleading–twist $A_{UT,\langle y\rangle}^{\sin(2\phi_h-\phi_S)}(x)$ in comparison to the preliminary HERMES data [145].

Sec. 7.6. Using the Gaussian Ansatz for $f^\perp(x,k_\perp)$ in Eq. (B.9j) of App. B.3 we obtain

$$F_{UU}^{\cos\phi_h}(x,z,P_{hT}) = \frac{2M_N}{Q}\, x \sum_q e_q^2 \left[-x\, f^{\perp(1)q}(x)\, D_1^q(z)\, b_{\rm B}^{(1)} \left(\frac{zP_{hT}}{\lambda}\right) \mathcal{G}(P_{hT}) \right] \tag{7.9a}$$

$$F_{UU}^{\cos\phi_h}(x,z,\langle P_{hT}\rangle) = \frac{2M_N}{Q}\, x \sum_q e_q^2 \left[-x\, f^{\perp(1)q}(x)\, D_1^q(z)\, c_{\rm B}^{(1)} \left(\frac{z}{\lambda^{1/2}}\right) \right] \tag{7.9b}$$

with $\lambda = z^2\langle k_\perp^2\rangle_{f^\perp} + \langle P_\perp^2\rangle_{D_1}$. The coefficients $b_i^{(1)}$ and $c_i^{(1)}$ are defined in App. B.5. Note that Eq. (7.9a) is valid in the "scheme" of footnote 4, but Eq. (7.9a) holds independently how one implements the sum rule (2.14) (as in footnote 4 or App. B.4).

For $f^{\perp(1)}(x)$ we explore Eq. (3.3b) as $xf^{\perp(1)q}(x) = \frac{\langle k_\perp^2\rangle_{f_1}}{2M_N^2} f_1^q(x)$ and assume for its Gaussian width $\langle k_\perp^2\rangle_{f^\perp} = \langle k_\perp^2\rangle_{f_1}$. The latter means the Gaussian factors of $F_{UU}^{\cos\phi_h}$ and F_{UU} cancel out, i.e. at some point for $P_{hT} \gtrsim 1\,\text{GeV}$ we would obtain from (7.9a) an asymmetry $A_{UU}^{\cos\phi_h} = F_{UU}^{\cos\phi_h}/F_{UU}$ exceeding 100 % and violating unitarity. This is of course an artifact of our approximations, and reminds us that Gaussian and WW-type approximations as well as the entire TMD formalism must be applied to small $P_{hT} \ll Q$.

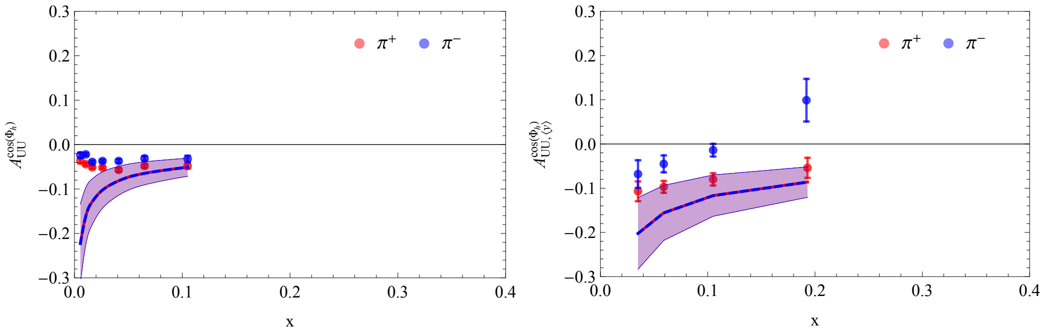

Figure 20. Left panel: asymmetry $A_{UU}^{\cos\phi_h}$ for positive and negative hadrons at COMPASS for a proton target [137]. Right panel: the same asymmetry $A_{UU,\langle y\rangle}^{\cos\phi_h}$ for $\pi^\pm$ from HERMES [136].

The asymmetries $A_{UU}^{\cos\phi_h}$ were measured by EMC [176], at Jefferson Lab [108, 178], HERMES [136], and COMPASS [137]. In Fig. 20 we compare our predictions to the HERMES and COMPASS data. The WW-type approximation tends to overstimate the data at COMPASS especially in the small-x region. It is also not compatible with the flavor dependence seen at HERMES. However, both experiments seem not to agree for instance on the shape of the asymmetry for negative pions or hadrons. More experimental and theoretical work is need to clarify whether this could be due to power corrections.

8 Conclusions

In this work a comprehensive and complete treatment of SIDIS spin and azimuthal asymmetries was presented. The theoretical and phenomenological understanding of most of the leading-twist SIDIS structure functions for the production of unpolarized hadrons is relatively advanced: factorization is proven, and each structure functions is unambiguously expressed in terms of one of 8 twist-2 TMDs convoluted with one of 2 twist-2 FFs. For subleading-twist SIDIS structure functions the situation is far more complex for two reasons. First, factorization is not proven and must be assumed. Second, each of the subleading-twist structure functions receives 4 or 6 contributions from various TMDs and FFs one of which is twist-2 and the other twist-3. Clearly, to make predictions for new experiments or interpret early data, an organizing theoretical guideline is needed.

In this work we have explored the so-called WW-type approximation as a candidate guideline for the description of SIDIS structure functions. This approximation consists of a systematic neglect of $\bar{q}gq$-terms in the correlators defining the TMDs and FFs. We have shown that in such an approach all twist-2 and twist-3 structure functions can be described in terms of 8 basis functions: 6 TMDs and 2 FFs, which are each twist-2. All other TMDs and FFs, assuming this approximation, are either related to the basis functions or vanish. We remark that the generalized parton model approach of Ref. [179] provides a description that is largely equivalent to ours.

To make this work self-contained we included a review of the available phenomenological information on the basis functions which is given in terms of 6 SIDIS structure functions. (Of course, one cannot extract 8 basis functions from 6 observables: the extraction of 2 basis functions, the unpolarized TMD and FF $f_1^q(x, k_\perp)$ and $D_1^q(x, P_\perp)$, makes also use of other experiments, most notably Drell–Yan and hadron production in e^+e^- annihilations.)

The WW-type approximation for TMDs and FFs is inspired by the observation that the classical WW-approximation for the twist-3 SIDIS structure function $g_2(x)$ (or PDF $g_T^q(x)$) works well. This was predicted in theoretical studies in the instanton model of the QCD vacuum, and confirmed by data and lattice QCD studies. The classic WW approximation for $g_2(x)$ works with a relative accuracy of $\pm 40\,\%$ or better. This is remarkable. The instanton vacuum model predicts an analogous WW approximation for the chirally odd twist-3 PDF $h_L^q(x)$ to work similarly well. This prediction remains to be tested in experiment.

In each case, $g_T^q(x)$ and $h_L^q(x)$, we deal with nucleon matrix elements of different $\bar{q}gq$ correlators, which are assumed to be small. Can one generalize these approximations to TMDs? This is a key question, which has been addressed in the past in literature in selected cases. This work is the first systematic investigation of this question. As in the unintegrated correlators one deals with different classes of operators, we prefer to speak of the WW-type approximation to distinguish from the collinear case.

We have studied in detail all SIDIS structure function in this approximation. This includes a review of results from lattice QCD calculations, effective theories and models. We found that from theoretical point of view the WW-type approximations receive certain support, though there is less evidence than in the collinear case. Most importantly, we have conducted systematic tests of WW approximations with available published or preliminary (and soon to be published) SIDIS data from HERMES, COMPASS, and Jefferson Lab.

We found the following results. The two leading-twist structure functions amenable to WW-type approximations, $F_{LT}^{\cos(\phi_h-\phi_S)}$ and $F_{UL}^{\sin(2\phi_h)}$, are well-described (the former) or at least compatible (the latter) with the data in this approximation. For $F_{UL}^{\sin(2\phi_h)}$ more precise data are needed, but also in this case the trend is encouraging especially thanks to the recent preliminary COMPASS data. We have also shown that our approach satisfies positivity inequalities, which is a non-trivial consistency check considering the crude approximations (WW-type, Gaussian Ansatz for TMDs) in our approach.

At subleading twist the WW-type approximation for the structure functions $F_{LT}^{\cos\phi_S}$, $F_{LT}^{\cos(2\phi_h-\phi_S)}$, $F_{LL}^{\cos\phi_h}$, $F_{UT}^{\sin(2\phi_h-\phi_S)}$ is compatible with data, too. Some of these asymmetries are predicted to be very small in the WW-type approximation, sometimes smaller than a fraction of a percent. This is compatible with the available data in the sense that the data are consistent with zero within their statistical accuracies. This cannot be considered a thorough evidence for the applicability of the WW-type approximations, but on the positive site we also observe no alarming hints that the WW-type approximations fail in these cases.

In the case of the three subleading-twist structure functions $F_{UU}^{\cos\phi_h}$, $F_{UL}^{\sin\phi_h}$, $F_{LU}^{\sin\phi_h}$, and $F_{UT}^{\sin\phi_S}$ the situation is clearer and indicates that here the WW-type approximations do not work. Incidently, these asymmetries include the very first non-zero azimuthal asymmetry measured in unpolarized SIDIS ($F_{UU}^{\cos\phi_h}$), the very first non-zero target single-spin asymmetry measured in SIDIS ($F_{UL}^{\sin\phi_h}$), and the very first non-zero beam single-spin asymmetry measured in SIDIS ($F_{LU}^{\sin\phi_h}$). The WW-type prediction for $F_{UU}^{\cos(\phi_h)}$ tends to overshoot the data. In the case of $F_{UL}^{\sin\phi_h}$ the WW-type approximation undershoots data by a factor of 2 or so. Most interestingly, in the case of $F_{LU}^{\sin\phi_h}$ the WW-type approximation predicts exactly a zero asymmetry, but experiments see small but non-zero effect.

The non-applicability of the WW–type approximation in these three cases should not be too surprising. After all it is a crude method to model TMDs and FFs and an uncontrollable "expansion" (in nuclear physics the concept of 2–body, 3–body, etc operators is well-justified and an effective expansion can be conducted; in the case of TMDs, however, it is less appropriate to speak about a systematic expansion in terms of $\bar{q}q$, $\bar{q}gq$, etc correlators). It will be very interesting to learn whether, e.g., in $F_{UL}^{\sin\phi_h}$ or $F_{LU}^{\sin\phi_h}$ a single $\bar{q}gq$–term is anomalously large, or whether it is a accumulative effect of several small terms $\bar{q}gq$–terms adding up to the observed asymmetry.

Among all SIDIS structure functions $F_{LU}^{\sin\phi_h}$ emerges as a particularly interesting case: this asymmetry is due to $\bar{q}gq$ only, without "contamination" from $\bar{q}q$ terms. Thus $F_{LU}^{\sin\phi_h}$ offers a unique view on the physics of $\bar{q}gq$ correlators, worth exploring for its own sake.

The results presented in this work are of importance for several reasons. To the best of our knowledge, it is the first complete study of all SIDIS structure functions up to twist-3 in a unique approach. The results are useful for experiments prepared in the near term (JLab 12) or proposed in the long term (Electron Ion Collider), and provide helpful input for Monte Carlo event generators [32]. Our predictions will help to pave the way towards a better understanding of the quark-gluon structure of the nucleon beyond leading twist.

9 Acknowledgments

First and foremost, the authors would like to thank their families for patience and constant support throughout writing this paper. The authors would like to thank Werner Vogelsang for many useful discussions. This work was partially supported by the U.S. Department of

Energy under Contract No. DE-AC05-06OR23177 (A.P.) and within the TMD Collaboration framework, and by the National Science Foundation under Contract No. PHY-1623454 (A.P.) and Contract No. PHY-1406298 (P.S.), and the Wilhelm Schuler Stiftung (P.S.).

A The "minimal basis" of TMDs and FFs

This Appendix describes the technical details of the parametrizations used in this work.

A.1 Unpolarized functions $f_1^a(x, k_\perp^2)$ and $D_1^a(z, P_\perp^2)$

In this work we use the leading-order parametrizations from [104] for the unpolarized PDF $f_1^a(x)$ and from [105] for the unpolarized FF $D_1^a(z)$. If not otherwise stated the parametrizations are taken at the scale $Q^2 = 2.4\,\mathrm{GeV}^2$ typical for many currently available SIDIS data. These parametrizations were used in [96] and other works whose extractions we adopt.

To describe the transverse momentum dependence of $f_1^a(x, k_\perp^2)$ and $D_1(z, P_\perp^2)$ we use the Gaussian Ansatz in Eqs. (4.5a, 4.5b). All early [96–99] and some recent [100] analyses employed flavor and x– or z–independent widths $\langle k_\perp^2\rangle$ and $\langle P_\perp^2\rangle$. In the analysis [101] of HERMES multiplicities flavor-independence of the widths was assumed. On long run one may anticipate that new precision data will require to relax these assumptions. However, one may also expect that the Gaussian Ansatz will remain a useful *approximation* as long as one is interested in describing data on transverse hadron momenta $P_{hT} \ll Q$.

The parameters resulting from calculations or extractions are presented in Table 1. As most extractions of TMDs that we will use are done with the choice of $\langle k_\perp^2\rangle_{f_1} = 0.25$ GeV^2, $\langle P_\perp^2\rangle_{D_1} = 0.2$ GeV^2, for our numerical estimates in this work we will use these fixed widths.

Some comments are in order. In [96] no attempt was made to assign an uncertainty of the best fit result. The uncertainty of the numbers from [99] includes only the statistical uncertainty, but no systematic uncertainty. For comparison lattice results from [62] are included whose range indicates flavor-dependence (first number u–flavor, second number d–flavor). Notice that this is the contribution of the flavor averaged over contributions from the respective quarks and antiquarks. Chiral theories predict significant differences in the $k_\perp$–behavior of sea and valence quarks [106]. We will comment more on the lattice results

study	$\langle Q^2\rangle$, $\langle x\rangle$, $\langle z\rangle$ [GeV^2]	$\langle k_\perp^2\rangle_{f_1}$ [GeV^2]	$\langle P_\perp^2\rangle_{D_1}$ [GeV^2]	$\langle k_\perp^2\rangle_{g_1}$ [GeV^2]
fit of [96]	5.0, 0.1, 0.3	~ 0.25	~ 0.2	–
fit of [99]	2.5, 0.1, 0.4	0.38 ± 0.06	0.16 ± 0.01	–
fit of [101]	2.4, 0.1, 0.3	0.57 ± 0.08	0.12 ± 0.01	–
fit of [100]	2.4, 0.1, 0.5	~ 0.3	~ 0.18	–
lattice [62]	4.0, – , –	0.14–0.15	–	0.11-0.15

Table 1. Gaussian model parameters for $f_1^a(x, k_\perp)$, $D_1^a(z, P_\perp)$, $g_1^a(x, k_\perp)$ from phenomenological and lattice QCD studies. The kinematics to which the phenomenological results and the renormalization scale of the lattice results are indicated. The range of lattice values indicates flavor dependence (first number refers to u–flavor, second number to d–flavor).

in the next section. In view of the large (and partly underestimated) uncertainties and the fact that those parameters are anti-correlated the numbers from the different approaches quoted in Table 1 can be considered to be in good agreement.

A.2 Helicity distribution $g_1^a(x, k_\perp^2)$

For the helicity PDF $g_1^a(x) = \int d^2k_\perp\, g_1^a(x, k_\perp^2) \equiv \int d^2k_\perp\, g_{1L}^a(x, k_\perp^2)$ we use in this work the leading-order parametrizations from [57]. If not otherwise stated the parametrizations are taken at the scale $Q^2 = 2.4\,\text{GeV}^2$.

In lack of phenomenological information on the $k_\perp$–dependence of $g_1^a(x, k_\perp^2)$ we explore lattice QCD results from [62] to constrain the Gaussian width in Eq. (4.5c). On a lattice with pion and nucleon masses $m_\pi \approx 500\,\text{MeV}$ and $M_N = 1.291(23)\,\text{GeV}$ and with an axial coupling constant $g_A^{(3)} = 1.209(36)$ reasonably close to its physical value 1.2695(29) the following results were obtained for the mean square transverse parton momenta [62]. For the unpolarized TMDs it was found $\langle k_\perp^2\rangle_{f_1^u} = (0.3741\,\text{GeV})^2$ and $\langle k_\perp^2\rangle_{f_1^d} = (0.3839\,\text{GeV})^2$. For the helicity TMDs it was found $\langle k_\perp^2\rangle_{g_1^u} = (0.327\,\text{GeV})^2$ and $\langle k_\perp^2\rangle_{g_1^d} = (0.385\,\text{GeV})^2$. These values are quoted in Table 1.

The lattice values for $\langle k_\perp^2\rangle_{f_1}$ consistently underestimate the phenomenological numbers, see Table 1. The exact reasons for that are unknown, but it is natural to think it might be related to the fact that the lattice predictions [62] do not refer to TMDs entering in SIDIS (or Drell–Yan or other process) because a different gauge link was chosen, see Sec. 3.5. Still one may expect these results to bear considerable information on QCD dynamics.[6] To make use of this information we shall assume that the lattice results [62] provide robust predictions for the *ratios* $\langle k_\perp^2\rangle_{g_1^u}/\langle k_\perp^2\rangle_{f_1^u} \approx 0.76$. With the phenomenological value $\langle k_\perp^2\rangle_{f_1} = 0.25\ \text{GeV}^2$ we then obtain the estimate for the width of the helicity TMD $\langle k_\perp^2\rangle_{g_1} = 0.19\ \text{GeV}^2$. In our phenomenological study we use this value for u–quarks and for simplicity also for d–quarks. Even though the lattice values indicate an interesting flavor dependence, see Table 1, for a proton target this is a very good approximation due to u–quark dominance. When precision data for deuterium and especially for ^{3}He from JLab become available, it will be interesting to re-investigate this point in detail.

A.3 Sivers function $f_{1T}^{\perp q}(x, k_\perp)$

Sivers distribution function was studied in Refs. [42, 43, 118–120, 179–183]. We will use parametrizations from Refs. [118, 120, 179]:

$$\langle k_\perp^2\rangle_{f_{1T}^\perp} \equiv \frac{\langle k_\perp^2\rangle M_1^2}{\langle k_\perp^2\rangle + M_1^2} \tag{A.1}$$

$$f_{1T}^\perp(x, k_\perp^2) = -\frac{M}{M_1}\sqrt{2e}\,\mathcal{N}_q(x)\, f_{q/p}(x, Q)\, \frac{e^{-k_\perp^2/\langle k_\perp^2\rangle_{f_{1T}^\perp}}}{\pi\langle k_\perp^2\rangle}, \tag{A.2}$$

where M_1 is a mass parameter, M the proton mass and

$$\mathcal{N}_q(x) = N_q\, x^\alpha (1-x)^\beta\, \frac{(\alpha+\beta)^{(\alpha+\beta)}}{\alpha^\alpha \beta^\beta} \tag{A.3}$$

[6] The results [62] refer also to pion masses above the physical value. This caveat is presumably less critical and will be overcome as lattice QCD simulations are becoming feasible at physical pion masses.

$N_u = 0.40$	$\alpha_u = 0.35$	$\beta_u = 2.6$	
$N_d = -0.97$	$\alpha_d = 0.44$	$\beta_d = 0.90$	$M_1^2 = 0.19$ (GeV^2)

Table 2. Best values of the fit of the Sivers functions. Table from Ref. [120]

The first moment of Sivers function is:

$$f_{1T}^{\perp(1)q}(x) = -\frac{\sqrt{\frac{e}{2}}\,\langle k_\perp^2\rangle M_1^3}{M(\langle k_\perp^2\rangle + M_1^2)^2}\,\mathcal{N}_q(x) f_q(x,Q) = -\sqrt{\frac{e}{2}}\frac{1}{MM_1}\frac{\langle k_\perp^2\rangle^2_{f_{1T}^\perp}}{\langle k_\perp^2\rangle}\,\mathcal{N}_q(x) f_q(x,Q) \quad \text{(A.4)}$$

We can rewrite parametrizations of Sivers functions as

$$f_{1T}^{\perp q}(x,k_\perp^2) = f_{1T}^{\perp(1)q}(x)\frac{2M^2}{\pi\langle k_\perp^2\rangle^2_{f_{1T}^\perp}} e^{-k_\perp^2/\langle k_\perp^2\rangle_{f_{1T}^\perp}}\,. \quad \text{(A.5)}$$

The fit the HERMES proton and COMPASS deuteron data from including only Sivers functions for u and d quarks was done in Ref. [120], corresponding to seven free parameters, and parameters are shown in Table 2.

A.4 Transversity $h_1^q(x,k_\perp)$ and Collins function $H_1^{\perp q}(x,P_\perp)$

These functions were studied in Refs. [46, 59, 60, 130–132]. The following shape was assumed for parametrizations in Refs. [59, 60, 130]:

$$h_1^q(x,k_\perp^2) = h_1^q(x)\frac{e^{-k_\perp^2/\langle k_\perp^2\rangle_{h_1}}}{\pi\langle k_\perp^2\rangle_{h_1}}\,, \quad \text{(A.6)}$$

$$h_1^q(x) = \frac{1}{2}\mathcal{N}_q^T(x)\,[f_1(x) + g_1(x)]\,, \quad \text{(A.7)}$$

$$H_{1h/q}^{\perp}(z,P_\perp^2) = \frac{zm_h}{2P_\perp}\Delta^N D_{h/q^\uparrow}(z,P_\perp^2) = \frac{zm_h}{M_C}e^{-p_\perp^2/M_C^2}\sqrt{2e}H_{1h/q}^{\perp}(z)\,\frac{e^{-P_\perp^2/\langle P_\perp^2\rangle}}{\pi\langle P_\perp^2\rangle}\,, \quad \text{(A.8)}$$

with m_h the mass of the produced hadron and

$$\mathcal{N}_q^T(x) = N_q^T\, x^\alpha(1-x)^\beta\,\frac{(\alpha+\beta)^{(\alpha+\beta)}}{\alpha^\alpha\beta^\beta}\,, \quad \text{(A.9)}$$

$$H_{1h/q}^{\perp}(z) = \mathcal{N}_q^C(z) D_{h/q}(z)\,, \quad \text{(A.10)}$$

$$\mathcal{N}_q^C(z) = N_q^C\, z^\gamma(1-z)^\delta\,\frac{(\gamma+\delta)^{(\gamma+\delta)}}{\gamma^\gamma\delta^\delta}\,, \quad \text{(A.11)}$$

and $-1 \le N_q^T \le 1$, $-1 \le N_q^C \le 1$. The helicity distributions $g_1(x)$ are taken from Ref. [184], parton distribution and fragmentation functions are the GRV98LO PDF set [57] and the DSS fragmentation function set [105]. Notice that with these choices both the transversity and the Collins function automatically obey their proper positivity bounds. Note that as in Ref. [130] we use two Collins fragmentation functions, *favored* and *disfavored* ones, see Ref. [130] for details on implementation, and corresponding parameters N_a^C are then N_{fav}^C and N_{dis}^C. For numerical estimates we use parameters extracted in Ref. [130], see Table 3.

$N_u^T = 0.46^{+0.20}_{-0.14}$	$N_d^T = -1.00^{+1.17}_{-0.00}$	
$\alpha = 1.11^{+0.89}_{-0.66}$	$\beta = 3.64^{+5.80}_{-3.37}$	$\langle k_\perp^2\rangle_{h_1} = 0.25$ (GeV^2)
$N_{\rm fav}^C = 0.49^{+0.20}_{-0.18}$	$N_{\rm dis}^C = -1.00^{+0.38}_{-0.00}$	
$\gamma = 1.06^{+0.45}_{-0.32}$	$\delta = 0.07^{+0.42}_{-0.07}$	$M_C^2 = 1.50^{+2.00}_{-1.12}$ (GeV^2)

Table 3. Best values of the 9 free parameters fixing the u and d quark transversity distribution functions and favored and disfavored Collins fragmentation functions. The table is from Ref. [130].

According to Eq. (B.8) we obtain the following expression for the first moment of Collins fragmentation function:

$$H_{1h/q}^{\perp(1)}(z) = \frac{H_{1h/q}^{\perp}(z)\sqrt{e/2}\langle P_\perp^2\rangle M_C^3}{zm_h(M_C^2+\langle P_\perp^2\rangle)^2} \; . \tag{A.12}$$

We also define the following variable:

$$\langle P_\perp^2\rangle_{H_1^\perp} = \frac{\langle P_\perp^2\rangle M_C^2}{\langle P_\perp^2\rangle + M_C^2}. \tag{A.13}$$

We can rewrite the parametrizations of Collins FF as

$$H_1^\perp(z,P_\perp^2) = H_1^{\perp(1)}(z)\frac{2z^2m_h^2}{\pi\langle P_\perp^2\rangle^2_{H_1^\perp}}e^{-P_\perp^2/\langle P_\perp^2\rangle_{H_1^\perp}} \; . \tag{A.14}$$

A.5 Boer-Mulders function $h_1^{\perp q}(x,k_\perp)$

The Boer-Mulders function $h_1^\perp$ [3] measures the transverse polarization asymmetry of quarks inside an unpolarized nucleon. The Boer-Mulders functions were studied phenomenologically in Refs. [135, 139, 140]

Ref. [139] used the parametrization in which Boer-Mulders function is proportional to the Sivers functions, such that:

$$\langle k_\perp^2\rangle_{h_1^\perp} = \frac{\langle k_\perp^2\rangle\, M_{BM}^2}{\langle k_\perp^2\rangle + M_{BM}^2}\,, \tag{A.15}$$

$$h_1^\perp(x,k_\perp^2) = -\frac{M}{M_{BM}}\sqrt{2e}\; N_{BM}^q \mathcal{N}_q(x)\, f_{q/p}(x,Q)\frac{e^{-k_\perp^2/\langle k_\perp^2\rangle_{h_1^\perp}}}{\pi\langle k_\perp^2\rangle}, \tag{A.16}$$

where

$$\mathcal{N}_q(x) = N_q\, x^\alpha(1-x)^\beta\,\frac{(\alpha+\beta)^{(\alpha+\beta)}}{\alpha^\alpha\beta^\beta} \; . \tag{A.17}$$

The first moment of Boer-Mulders function is:

$$h_1^{\perp(1)q}(x) = -\frac{\sqrt{\frac{e}{2}}\,\langle k_\perp^2\rangle M_{BM}^3}{M(\langle k_\perp^2\rangle + M_{BM}^2)^2}\; N_q f_q(x,Q) = -\sqrt{\frac{e}{2}}\frac{1}{MM_{BM}}\frac{\langle k_\perp^2\rangle^2_{h_1^\perp}}{\langle k_\perp^2\rangle}\; N_q f_q(x,Q) \tag{A.18}$$

$N^u_{BM} = 2.1 \pm 0.1$	$N^d_{BM} =$	-1.111 ± 0.001	
Fixed	parameters:		
$N_u = 0.35$	$\alpha_u = 0.73$	$\beta_u = 3.46$	
$N_d = -0.9$	$\alpha_d = 1.08$	$\beta_d = 3.46$	$M^2_{BM} = 0.34$ (GeV^2)

Table 4. Fitted parameters of Boer-Mulders quark distributions. Values are from Ref. [135].

We can rewrite parametrizations of Boer-Mulders functions as

$$h_1^{\perp q}(x, k_\perp^2) = h_1^{\perp(1)q}(x) \frac{2M^2}{\pi \langle k_\perp^2 \rangle^2_{h_1^\perp}} e^{-k_\perp^2/\langle k_\perp^2 \rangle_{h_1^\perp}} \; . \tag{A.19}$$

A.6 Pretzelosity distribution $h_{1T}^{\perp q}(x, k_\perp)$

Pretzelosity distribution function $h_{1T}^\perp$ [146] describes transversely polarized quarks inside a transversely polarized nucleon. We use the following form of $h_{1T}^{\perp a}$ [146]:

$$h_{1T}^{\perp a}(x, k_\perp^2) = \frac{M^2}{M_{TT}^2} e^{-k_\perp^2/M_{TT}^2} h_{1T}^{\perp a}(x) \frac{e^{-k_\perp^2/\langle k_\perp^2 \rangle}}{\pi \langle k_\perp^2 \rangle} = \frac{M^2}{M_T^2} h_{1T}^{\perp a}(x) \frac{e^{-k_\perp^2/\langle k_\perp^2 \rangle_{h_{1T}^\perp}}}{\pi \langle k_\perp^2 \rangle} \; , \tag{A.20}$$

where

$$h_{1T}^{\perp a}(x) = e\, \mathcal{N}^a(x)(f_1^a(x, Q) - g_1^a(x, Q)), \tag{A.21}$$

$$\mathcal{N}^a(x) = N^a x^\alpha (1-x)^\beta \frac{(\alpha+\beta)^{\alpha+\beta}}{\alpha^\alpha \beta^\beta} \; , \tag{A.22}$$

$$\langle k_\perp^2 \rangle_{h_{1T}^\perp} = \frac{\langle k_\perp^2 \rangle M_{TT}^2}{\langle k_\perp^2 \rangle + M_{TT}^2} \; , \tag{A.23}$$

where N^a, α, β, and M_T are parameters fitted to data that can be found in Table 5.

We use Eq. (B.8) to calculate the second moment of $h_{1T}^{\perp a}(x, k_\perp^2)$ of Eq. (A.20) and obtain:

$$h_{1T}^{\perp(2)a}(x) = \frac{h_{1T}^{\perp a}(x) \langle k_\perp^2 \rangle^3_{h_{1T}^\perp}}{2M^2 M_{TT}^2 \langle k_\perp^2 \rangle} \; . \tag{A.24}$$

We can rewrite parametrization of pretzelosity functions as

$$h_{1T}^{\perp q}(x, k_\perp^2) = h_{1T}^{\perp(2)q}(x) \frac{2M^4}{\pi \langle k_\perp^2 \rangle^3_{h_{1T}^\perp}} e^{-k_\perp^2/\langle k_\perp^2 \rangle_{h_{1T}^\perp}} \; . \tag{A.25}$$

α	$=$	2.5 ± 1.5	β	$=$	2 fixed	
N_u	$=$	1 ± 1.4	N_d	$=$	-1 ± 1.3	$M_{TT}^2 = 0.18 \pm 0.7$ GeV^2

Table 5. Fitted parameters of the pretzelosity quark distributions. Table from Ref. [146]

B Convolution integrals and expressions in Gaussian Ansatz

In this Appendix we explain the notation for convolution integrals of TMDs and FFs and give the explicit results obtained assuming the Gaussian Ansatz.

B.1 Notation for convolution integrals

Structure functions are expressed as convolutions of TMDs and FFs in the Bjorken limit at tree level. For reference we quote the convolution integrals in "Amsterdam notation" [5]

$$\mathcal{C}[w\,f\,D] = x\sum_a e_a^2 \int d^2\boldsymbol{p}_T\, d^2\boldsymbol{k}_T\, \delta^{(2)}(\boldsymbol{p}_T - \boldsymbol{k}_T - \boldsymbol{P}_{h\perp}/z)\, w(\boldsymbol{p}_T, \boldsymbol{k}_T)\, f^a(x, p_T^2)\, D^a(z, z^2 k_T^2), \tag{B.1}$$

where all transverse momenta refer to the virtual photon-proton center-of-mass frame and $\hat{\boldsymbol{h}} = \boldsymbol{P}_{h\perp}/P_{h\perp}$. Hereby $\boldsymbol{p}_T$ is the transverse momentum of quark with respect to nucleon, $\boldsymbol{k}_T$ is the transverse momentum of the fragmenting quark with respect to produced hadron. The notation is not unique. The one chosen in this work, in comparison to other works, is

$$\text{transverse momentum in TMD:}\quad [\boldsymbol{k}_\perp]_{\text{our}} = [\boldsymbol{k}_\perp]_{\text{Ref.[179]}} = [\boldsymbol{p}_T]_{\text{Ref.[5]}}\,, \tag{B.2}$$

$$\text{transverse momentum in FF:}\quad [\boldsymbol{P}_\perp]_{\text{our}} = [\boldsymbol{p}_\perp]_{\text{Ref.[179]}} = -z\,[\boldsymbol{k}_T]_{\text{Ref.[5]}}\,, \tag{B.3}$$

$$\text{transverse hadron momenta:}\quad [\boldsymbol{P}_{hT}]_{\text{our}} = [\boldsymbol{P}_T]_{\text{Ref.[179]}} = [\boldsymbol{P}_{h\perp}]_{\text{Ref.[5]}}\,. \tag{B.4}$$

Notice that $[\boldsymbol{P}_\perp]_{\text{our}} = -z\,[\boldsymbol{k}_T]_{\text{Ref.[5]}}$ is the transverse momentum the hadron acquires in the fragmentation process. The normalization for unpolarized fragmentation functions is

$$D_1^a(z) = \left[\int d^2\boldsymbol{P}_\perp D_1^a(z, P_\perp^2)\right]_{\text{our}} = \left[z^2\int d^2\boldsymbol{k}_T D_1^a(z, z^2 k_T^2)\right]_{\text{Ref. [5]}}. \tag{B.5}$$

The "Amsterdam" convolution integral (B.1) reads in our notation

$$\mathcal{C}[w\,f\,D] = x\sum_a e_a^2 \int d^2\boldsymbol{k}_\perp\, d^2\boldsymbol{P}_\perp\, \delta^{(2)}(z\boldsymbol{k}_\perp + \boldsymbol{P}_\perp - \boldsymbol{P}_{hT})\, w\left(\boldsymbol{k}_\perp, -\frac{\boldsymbol{P}_\perp}{z}\right) f^a(x, k_\perp^2)\, D^a(z, P_\perp^2). \tag{B.6}$$

B.2 Gaussian Ansatz

For a generic TMD and FF the Gaussian Ansatz is given by

$$f^a(x, k_\perp^2) = f^a(x)\,\frac{\exp(-k_\perp^2/\langle k_\perp^2\rangle)}{\pi\langle k_\perp^2\rangle}\,, \quad D^a(z, P_\perp^2) = D^a(z)\,\frac{\exp(-P_\perp^2/\langle P_\perp^2\rangle)}{\pi\langle P_\perp^2\rangle} \tag{B.7}$$

where $\langle k_\perp^2\rangle$ could be x–dependent, and $\langle P_\perp^2\rangle$ z–dependent. Both could be flavor-dependent. The variable $P_\perp$ is convenient because phenomenological experience shows that $P_\perp$ in $D_1^{q/h}(z, P_\perp^2)$ exhibits a Gaussian distribution with weakly z–dependent Gaussian width. The distribution of transverse momenta in $\left[D^a(z, z^2k_T^2)\right]_{\text{Ref.[5]}}$ would require a strongly z–dependent Gaussian width. It is a matter of taste which one prefers to use.

It is convenient to work with transverse moments of TMDs and FFs which are defined, and in the Gaussian model given by

$$
\begin{aligned}
f^{(n)}(x) = & \int d^2\boldsymbol{k}_\perp \left(\frac{k_\perp^2}{2M^2}\right)^n f(x,k_\perp^2) \overset{\text{Gauss}}{=} \frac{n!\,\langle k_\perp^2\rangle^n}{2^n\,M_N^{2n}}\, f(x), \\
D^{(n)}(z) = & \int d^2\boldsymbol{P}_\perp \left(\frac{P_\perp^2}{2z^2m_h^2}\right)^n D(z,P_\perp^2) \overset{\text{Gauss}}{=} \frac{n!\,\langle P_\perp^2\rangle^n}{2^n z^{2n}\,m_h^{2n}} D(z)\,.
\end{aligned}
\tag{B.8}
$$

It is important to keep in mind that these objects are well-defined in the Gaussian model. However, in QCD and even in simple models [75, 106] one faces issues with UV divergences and has to carefully define how to deal with them.

In Eqs. (B.8) the Gaussian dependence is factorized from x or z dependence and parametrizations are made with respect to either $f(x)$ or $D(z)$. As we saw in Appendix A some TMD functions are parametrized with higher moments directly as operator product expansion of TMDs may start from higher twist matrix element instead of the usual twist-2 one. In those cases equivalent formulas to Eqs. (B.8) can be easily derived.

B.3 Gaussian Ans´atze for the derived TMDs used in this work

Having discussed the Gaussian Ans´atze for the 8 basis functions in Eqs. (4.5a–4.5h) of Sec. 4.4 and in App. A, we list here the Ans´atze for the following derived TMDs:

$$g_{1T}^{\perp q}(x,k_\perp^2) = g_{1T}^{\perp(1)q}(x)\,\frac{2M_N^2}{\pi\langle k_\perp^2\rangle_{g_{1T}^\perp}^2}\,e^{-k_\perp^2/\langle k_\perp^2\rangle_{g_{1T}^\perp}}\,, \qquad \text{cf. Sec. 6.1,} \tag{B.9a}$$

$$h_{1L}^{\perp a}(x,k_\perp^2) = h_{1L}^{\perp(1)a}(x)\,\frac{2M_N^2}{\pi\langle k_\perp^2\rangle_{h_{1L}^\perp}^2}\,e^{-k_\perp^2/\langle k_\perp^2\rangle_{h_{1L}^\perp}^2} \qquad \text{cf. Sec. 6.2,} \tag{B.9b}$$

$$g_T^q(x,k_\perp^2) = g_T^q(x)\,\frac{1}{\pi\langle k_\perp^2\rangle_{g_T}}\,e^{-k_\perp^2/\langle k_\perp^2\rangle_{g_T}}\,, \qquad \text{cf. Sec. 7.2,} \tag{B.9c}$$

$$g_T^{\perp q}(x,k_\perp^2) = g_T^{\perp(2)q}(x)\,\frac{2M^4}{\pi\langle k_\perp^2\rangle_{g_T^\perp}^3}\,e^{-k_\perp^2/\langle k_\perp^2\rangle_{g_T^\perp}}\,, \qquad \text{cf. Sec. 7.3,} \tag{B.9d}$$

$$g_L^{\perp q}(x,k_\perp^2) = g_L^{\perp(1)q}(x)\,\frac{2M_N^2}{\pi\langle k_\perp^2\rangle_{g_L^\perp}^2}\,e^{-k_\perp^2/\langle k_\perp^2\rangle_{g_L^\perp}}\,, \qquad \text{cf. Sec. 7.4,} \tag{B.9e}$$

$$h_L^q(x,k_\perp^2) = h_L^q(x)\,\frac{1}{\pi\langle k_\perp^2\rangle_{h_L}}\,e^{-k_\perp^2/\langle k_\perp^2\rangle_{h_L}}\,, \qquad \text{cf. Sec. 7.5,} \tag{B.9f}$$

$$h_T^{\perp q}(x,k_\perp^2) = h_T^{\perp(1)q}(x)\,\frac{2M^2}{\pi\langle k_\perp^2\rangle_{h_T^\perp}^2}\,e^{-k_\perp^2/\langle k_\perp^2\rangle_{h_T^\perp}}\,, \qquad \text{cf. Sec. 7.6,} \tag{B.9g}$$

$$h_T^q(x,k_\perp^2) = h_T^{(1)q}(x)\,\frac{2M^2}{\pi\langle k_\perp^2\rangle_{h_T}^2}\,e^{-k_\perp^2/\langle k_\perp^2\rangle_{h_T}}\,, \qquad \text{cf. Sec. 7.6,} \tag{B.9h}$$

$$f_T^{\perp q}(x,k_\perp^2) = f_T^{\perp(2)q}(x)\,\frac{2M^4}{\pi\langle k_\perp^2\rangle_{f_T^\perp}^3}\,e^{-k_\perp^2/\langle k_\perp^2\rangle_{f_T^\perp}}\,, \qquad \text{cf. Sec. 7.7,} \tag{B.9i}$$

$$f^{\perp q}(x,k_\perp^2) = f^{\perp(1)q}(x)\,\frac{2M^2}{\pi\langle k_\perp^2\rangle_{f^\perp}^2}\,e^{-k_\perp^2/\langle k_\perp^2\rangle_{f^\perp}}\,, \qquad \text{cf. Sec. 7.8,} \tag{B.9j}$$

B.4 Comment on TMDs subject to the sum rules (2.14)

In this section we comment on the twist-3 TMDs $f_T^q(x,k_\perp)$, $h^q(x,k_\perp)$, $e_L^q(x,k_\perp)$, which are T-odd, appear in the decompositions of the correlator with no explicit $k_\perp^j$–prefactors, and would have collinear PDF counterparts. But T-odd PDFs are forbidden by time-reversal and parity invariance of strong interactions, which dictate the sum rules (2.14), see Sec. 3.8. Such TMDs could be described by functions with a node in $k_\perp$[7] such that they can integrate to zero in Eq. (2.14). A single Gaussian has no node and is not adequate for that. However, one could work with a superposition of Gaussians with different widths,

$$
\begin{aligned}
x\, f_T^q(x,k_\perp) = -\, f_{1T}^{\perp(1)q}(x)\, &\sum_{i=1}^n a_i\, \frac{\exp(-k_\perp^2/\langle k_\perp^2\rangle_i)}{\pi\langle k_\perp^2\rangle_i}\,, \\
&\sum_{i=1}^n a_i = 0\,,\ \ \langle k_\perp^2\rangle_i \neq \langle k_\perp^2\rangle_j\ \ \forall\, i\neq j,\ 1\le i,\, j\le n,\ n\ge 2.
\end{aligned}
\tag{B.10}
$$

Notice that in (B.10) we cannot write "$f_T^q(x)$" which would be zero according to (2.14) and we explore here the WW-type approximation (3.4g). The minimal choice would be $n=2$ with $a_1=-a_2=1$ and $\langle k_\perp^2\rangle_1 = \langle k_\perp^2\rangle_{f_{1T}^\perp}$ to make use of the theoretical guidance provided by the WW-type approximation (3.4g). The second Gaussian width $\langle k_\perp^2\rangle_2$ could be chosen very large $\langle k_\perp^2\rangle_2 \gg \langle k_\perp^2\rangle_{f_1^\perp}$ to model the Gaussian description of $f_T^q(x,k_\perp)$ similar to that of $f_{1T}^{\perp(1)q}(x,k_\perp^2)$ at intermediate $k_\perp$. A very large parameter $\langle k_\perp^2\rangle_2$ could be thought of as a relict which enters in the sum rule (2.14) where the $k_\perp$–integration formally extends up to infinity where the TMD description does not apply. The theoretical understanding of higher–twist TMDs is too limited at the present stage, but in principle this could be a pragmatic way of modeling the TMD $f_T^q(x,k_\perp)$ and analogously $h^q(x,k_\perp)$, $e_L^q(x,k_\perp)$.

B.5 Convolution integrals in Gaussian Ansatz

Solving the convolution integrals relevant for SIDIS in the Gaussian Ansatz yields

$$\mathcal{C}[\,\omega^{\{0\}}\, f\, D] = \quad u\,\mathcal{G}(P_{hT}) \tag{B.11a}$$

$$\mathcal{C}[\omega_{\rm A}^{\{1\}}\, f\, D] = \quad u\,\mathcal{G}(P_{hT})\left(\frac{zP_{hT}}{m_h}\right)\frac{\langle P_\perp^2\rangle}{z^2\lambda} \tag{B.11b}$$

$$\mathcal{C}[\omega_{\rm B}^{\{1\}}\, f\, D] = -\,u\,\mathcal{G}(P_{hT})\left(\frac{zP_{hT}}{M_N}\right)\frac{\langle k_\perp^2\rangle}{\lambda} \tag{B.11c}$$

$$\mathcal{C}[\omega_{\rm A}^{\{2\}}\, f\, D] = \quad u\,\mathcal{G}(P_{hT})\,\frac{\langle k_\perp^2\rangle\langle P_\perp^2\rangle}{\lambda M_N m_h}\left(-1+\frac{2P_{hT}^2}{\lambda}\right) \tag{B.11d}$$

$$\mathcal{C}[\omega_{\rm B}^{\{2\}}\, f\, D] = \quad u\,\mathcal{G}(P_{hT})\,\frac{\langle k_\perp^2\rangle\langle P_\perp^2\rangle}{\lambda M_N m_h}\left(1-\frac{P_{hT}^2}{\lambda}\right) \tag{B.11e}$$

$$\mathcal{C}[\,\omega_{\rm AB}^{\{2\}}\, f\, D] = \quad u\,\mathcal{G}(P_{hT})\left(\frac{zP_{hT}}{M_N}\right)\left(\frac{zP_{hT}}{M_h}\right)\frac{\langle k_\perp^2\rangle}{\lambda}\,\frac{\langle P_\perp^2\rangle}{z^2\lambda} \tag{B.11f}$$

[7] The possibility of TMDs with nodes is not unrealistic. For instance in the covariant parton model the helicity TMDs exhibit nodes for the u– and d–flavor [86]. We will have to revise our description of $g_1^q(x,k_\perp)$ in Eq. (4.5c) and App. A.2 to something of the type (B.10), if that prediction is confirmed experimentally.

$$\mathcal{C}[\,\omega_{\rm C}^{\{2\}}\, f\,D] = \quad \frac{u}{2}\,\mathcal{G}(P_{hT})\,\left(\frac{zP_{hT}}{M_N}\right)\!\left(\frac{zP_{hT}}{M_N}\right)\,\frac{\langle k_\perp^2\rangle}{\lambda}\,\frac{\langle k_\perp^2\rangle}{\lambda} \tag{B.11g}$$

$$\mathcal{C}[\,\omega^{\{3\}}\, f\,D] = \quad \frac{u}{2}\,\mathcal{G}(P_{hT})\,\left(\frac{zP_{hT}}{M_N}\right)\!\left(\frac{zP_{hT}}{M_N}\right)\!\left(\frac{zP_{hT}}{m_h}\right)\,\frac{\langle k_\perp^2\rangle}{\lambda}\,\frac{\langle k_\perp^2\rangle}{\lambda}\,\frac{\langle P_\perp^2\rangle}{z^2\lambda} \tag{B.11h}$$

with the $\omega_i^{\{n\}}$ as defined in Eq. (2.20), and we introduced the abbreviations

$$u = x\sum_a e_a^2 f^a(x) D^a(z)\,, \quad \mathcal{G}(P_{hT}) = \frac{\exp(-P_{hT}^2/\lambda)}{\pi\lambda}\,, \quad \lambda = z^2\langle k_\perp^2\rangle + \langle P_\perp^2\rangle\,, \tag{B.12}$$

with the normalization $\int d^2P_{hT}\,\mathcal{G}(P_{hT}) = 1$. It is important to keep in mind that strictly speaking $\mathcal{G}(P_{hT}) = \mathcal{G}(P_{hT},x,z)$ *also* depends on x and z. The "non-compact" notation in Eqs. (B.11) was chosen to display the pattern. The masses M_N or m_h in the denominators of the P_{hT} indicate the "origins" of the contributions: due to intrinsic $k_\perp$ from target, due to transverse momenta $P_\perp$ acquired during fragmentation, or both. The weight $\omega_{\rm B}^{\{2\}}$ is the only which enters cross sections and does not have a homogeneous scaling in P_{hT}.

For practical application it is convenient to absorb as many (Gaussian model) parameters as possible into expressions that can be more easily fitted to data. One way to achieve this is to make use of the transverse moments (B.8). We introduce the following abbreviations

$$u_{\rm A}^{\{1\}} = \quad x\sum_a e_a^2 f^a(x) D^{(1)a}(z)\,, \qquad u_{\rm B}^{\{1\}} = x\sum_a e_a^2 f^{(1)a}(x) D^a(z)\,, \tag{B.13}$$

$$u_{\rm AB}^{\{2\}} = x\sum_a e_a^2 f^{(1)a}(x) D^{(1)a}(z)\,, \qquad u_{\rm C}^{\{2\}} = x\sum_a e_a^2 f^{(2)a}(x) D^a(z)\,, \tag{B.14}$$

$$u_{\rm C}^{\{3\}} = x\sum_a e_a^2 f^{(2)a}(x) D^{(1)a}(z)\,. \tag{B.15}$$

In this notation the results in Eqs. (B.11) read

$$\mathcal{C}[\omega_{\rm A}^{\{1\}}\, f\,D] = \quad u_{\rm A}^{(1)}\,\mathcal{G}(P_{hT})\,\left(\frac{zP_{hT}}{m_h}\right)\,\frac{2m_h^2}{\lambda} \tag{B.16a}$$

$$\mathcal{C}[\omega_{\rm B}^{\{1\}}\, f\,D] = -\,u_{\rm B}^{(1)}\,\mathcal{G}(P_{hT})\,\left(\frac{zP_{hT}}{M_N}\right)\,\frac{2M_N^2}{\lambda} \tag{B.16b}$$

$$\mathcal{C}[\omega_{\rm B}^{\{2\}}\, f\,D] = \quad u_{\rm B}^{(2)}\,\mathcal{G}(P_{hT})\,\frac{4z^2 m_h\,M_N}{\lambda}\,\left(1-\frac{P_{hT}^2}{\lambda}\right) \tag{B.16c}$$

$$\mathcal{C}[\,\omega_{\rm AB}^{\{2\}}\, f\,D] = \quad u_{\rm AB}^{(2)}\,\mathcal{G}(P_{hT})\,\left(\frac{zP_{hT}}{M_N}\right)\!\left(\frac{zP_{hT}}{M_h}\right)\,\frac{2M_N^2}{\lambda}\,\frac{2m_h^2}{\lambda} \tag{B.16d}$$

$$\mathcal{C}[\,\omega_{\rm C}^{\{2\}}\, f\,D] = \quad \frac{u_{\rm C}^{(2)}}{2}\,\mathcal{G}(P_{hT})\,\left(\frac{zP_{hT}}{M_N}\right)\!\left(\frac{zP_{hT}}{M_N}\right)\,\frac{2M_N^2}{\lambda}\,\frac{2M_N^2}{\lambda} \tag{B.16e}$$

$$\mathcal{C}[\,\omega^{\{3\}}\, f\,D] = \quad \frac{u^{(3)}}{2}\,\mathcal{G}(P_{hT})\,\left(\frac{zP_{hT}}{M_N}\right)\!\left(\frac{zP_{hT}}{M_N}\right)\!\left(\frac{zP_{hT}}{m_h}\right)\,\frac{2M_N^2}{\lambda}\,\frac{2M_N^2}{\lambda}\,\frac{2m_h^2}{\lambda} \tag{B.16f}$$

In this notation the results in Eqs. (B.11) read

$$\mathcal{C}[\omega_i^{\{n\}}\, f\,D] = u_i^{(n)}\,\mathcal{G}(P_{hT})\;\times\left[\delta_{n2}\,\delta_{i\rm B}\,a_B^{(2)} + b_i^{(n)}\left(\frac{zP_{hT}}{\lambda}\right)^n\,\right] \tag{B.17}$$

with

$$
\begin{aligned}
&b^{(0)} = 1\,, && && (B.18)\\
&b^{(1)}_{\rm A} = 2m_h\,, && b^{(1)}_{\rm B} = 2M_N\,, && (B.19)\\
&a^{(2)}_{\rm B} = 4M_N m_h \lambda^{-1}\, z^2\,, && b^{(2)}_{\rm AB} = -\,b^{(2)}_{\rm B} = 4M_N m_h\,, \quad b^{(2)}_{\rm C} = M_N^2\,, && (B.20)\\
&b^{(3)} = 2M_N^2 m_h\,. && && (B.21)
\end{aligned}
$$

Finally, integrating out transverse hadron momenta yields

$$
\int d^2P_{hT}\, \mathcal{C}[\,\omega_i^{\{n\}}\, f\, D] = u_i^{(n)}\; c_i^{(n)} \left(\frac{z}{\lambda^{1/2}}\right)^n \tag{B.22}
$$

with

$$
\begin{aligned}
&c^{(0)} = 1\,, && && (B.23)\\
&c^{(1)}_{\rm A} = \sqrt{\pi}\, m_h\,, && c^{(1)}_{\rm B} = \sqrt{\pi}\, M_N\,, && (B.24)\\
&c^{(2)}_{\rm AB} = 4M_N m_h\,, && c^{(2)}_{\rm C} = M_N^2\,, \quad c^{(2)}_{\rm B} = 0\,, && (B.25)\\
&c^{(3)} = \tfrac{3}{2}\sqrt{\pi}\, M_N^2 m_h\,. && && (B.26)
\end{aligned}
$$

C Mathematica package

A package available to a wide physics community is needed for several reasons. First of all it is intended to facilitate visualization, reproduction, and verification of our results presented in this paper. Second, the package may prove useful for experimentalists in need of estimates of measured quantities for certain kinematics of a particular experiment. Third, the phenomenological workers in the community will have an easy access to our results for comparison and/or use in phenomenological or theoretical papers. The authors believe that the open source access to the codes used in a project is the right way of handling scientific information in the 21^{st} century. For example, collinear parton distribution functions are well tabulated in the `LHAPDF` project [185], but collinear fragmentation function still need a dedicated repository. There exist already several databases which are being developed for extensions of collinear one-dimensional picture of the nucleon structure. Generalized Parton Distributions are present in the framework called `PARTONS` [186], several extractions of Transverse Momentum Dependent distributions are tabulated in `TMDlib` project [187].

If you use this package, please, cite this paper and the link to the repository. Please, acknowledge using any of the extracted TMDs presented in this package. The corresponding `bibitem` codes are included in the description of each TMD function.

The source code of the project can be downloaded or cloned from the open source repository: `https://github.com/prokudin/WW-SIDIS`. Using `Mathematica` run the file named `example.nb`, you will see an example of usage of the code, code description and several visualizations of functions, asymmetries, and SIDIS cross-sections. Please note that, for now, the package can compute the aforementioned observables for a proton target, detected charged pions and beam helicities ± 1 or 0 (with the latter denoting an unpolarized beam).

Make sure that you do not move `example.nb` to another directory as it uses grids for TMDs, PDFs, and FFs.

SIDIS cross section examples are presented in Fig. 21 .

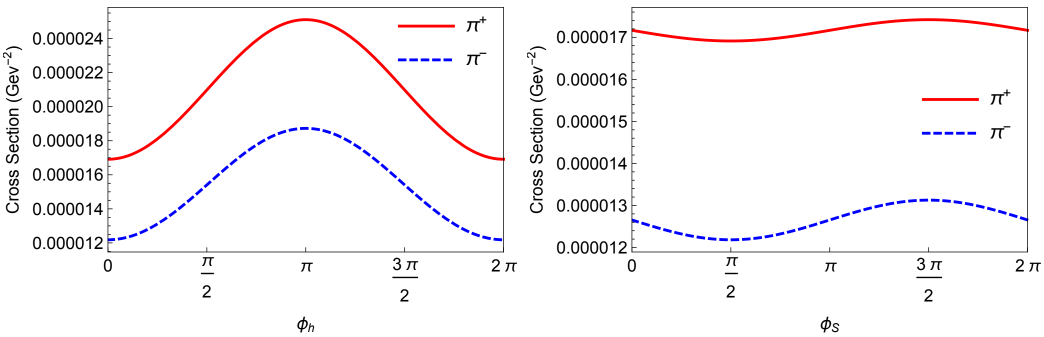

Figure 21. Left panel: ϕ_h dependence of the SIDIS cross section at $\phi_S = \pi/2$. Right panel: ϕ_S dependence of the SIDIS cross section at $\phi_h = 0$. Also $x = 0.3$, $z = 0.2$, $P_{hT} = 0.5$ GeV, $Q^2 = 2.4$ GeV^2, and the beam energy $E_{beam} = 5.7$ GeV, averaged over beam helicities, transverse proton target polarization.

References

[1] A. Kotzinian, *New quark distributions and semiinclusive electroproduction on the polarized nucleons*, *Nucl. Phys.* **B441** (1995) 234–248, [`hep-ph/9412283`].

[2] P. J. Mulders and R. D. Tangerman, *The complete tree-level result up to order 1/Q for polarized deep-inelastic leptoproduction*, *Nucl. Phys.* **B461** (1996) 197–237, [`hep-ph/9510301`].

[3] D. Boer and P. J. Mulders, *Time-reversal odd distribution functions in leptoproduction*, *Phys. Rev.* **D57** (1998) 5780–5786, [`hep-ph/9711485`].

[4] K. Goeke, A. Metz and M. Schlegel, *Parameterization of the quark-quark correlator of a spin-1/2 hadron*, *Phys. Lett.* **B618** (2005) 90–96, [`hep-ph/0504130`].

[5] A. Bacchetta et al., *Semi-inclusive deep inelastic scattering at small transverse momentum*, *JHEP* **02** (2007) 093, [`hep-ph/0611265`].

[6] F. Stock et al., *The FILTEX / HERMES polarized hydrogen atomic beam source*, *Nucl. Instrum. Meth.* **A343** (1994) 334–342.

[7] D. G. Crabb and W. Meyer, *Solid polarized targets for nuclear and particle physics experiments*, *Ann. Rev. Nucl. Part. Sci.* **47** (1997) 67–109.

[8] S. Goertz, W. Meyer and G. Reicherz, *Polarized H, D and He-3 targets for particle physics experiments*, *Prog. Part. Nucl. Phys.* **49** (2002) 403–489.

[9] S. Arnold, A. Metz and M. Schlegel, *Dilepton production from polarized hadron hadron collisions*, `0809.2262`.

[10] A. Metz and A. Vossen, *Parton Fragmentation Functions*, *Prog. Part. Nucl. Phys.* **91** (2016) 136–202, [`1607.02521`].

[11] G. A. Miller, *Densities, Parton Distributions, and Measuring the Non-Spherical Shape of the Nucleon*, *Phys. Rev.* **C76** (2007) 065209, [0708.2297].

[12] M. Burkardt, *Spin-orbit correlations and single-spin asymmetries*, 0709.2966.

[13] M. Burkardt, *The g(2) Structure Function*, *AIP Conf.Proc.* **1155** (2009) 26–34, [0905.4079].

[14] A. Bacchetta, M. Boglione, A. Henneman and P. J. Mulders, *Bounds on transverse momentum dependent distribution and fragmentation functions*, *Phys. Rev. Lett.* **85** (2000) 712–715, [hep-ph/9912490].

[15] S. Wandzura and F. Wilczek, *Sum Rules for Spin Dependent Electroproduction: Test of Relativistic Constituent Quarks*, *Phys. Lett.* **B72** (1977) 195.

[16] R. Jaffe and X. Ji, *Chiral odd parton distributions and Drell–Yan processes*, *Nucl. Phys.* **B375** (1992) 527–560.

[17] R. Jaffe, *G(2): The Nucleon's Other Spin Dependent Structure Function*, *Comments Nucl. Part. Phys.* **19** (1990) 239.

[18] J. Balla, M. V. Polyakov and C. Weiss, *Nucleon matrix elements of higher twist operators from the instanton vacuum*, *Nucl. Phys.* **B510** (1998) 327–364, [hep-ph/9707515].

[19] B. Dressler and M. V. Polyakov, *On the twist-three contribution to h(L) in the instanton vacuum*, *Phys. Rev.* **D61** (2000) 097501, [hep-ph/9912376].

[20] M. Gockeler, R. Horsley, W. Kurzinger, H. Oelrich, D. Pleiter et al., *A Lattice calculation of the nucleon's spin dependent structure function g(2) revisited*, *Phys. Rev.* **D63** (2001) 074506, [hep-lat/0011091].

[21] Gockeler, M. and Horsley, R. and Pleiter, D. and Rakow, Paul E.L. and Schäfer, A. and others, *Investigation of the second moment of the nucleon's g(1) and g(2) structure functions in two-flavor lattice QCD*, *Phys. Rev.* **D72** (2005) 054507, [hep-lat/0506017].

[22] E143 collaboration, K. Abe et al., *Measurements of the proton and deuteron spin structure functions g_1 and g_2*, *Phys. Rev.* **D58** (1998) 112003, [hep-ph/9802357].

[23] E155 collaboration, P. L. Anthony et al., *Precision measurement of the proton and deuteron spin structure functions g2 and asymmetries A(2)*, *Phys. Lett.* **B553** (2003) 18–24, [hep-ex/0204028].

[24] HERMES collaboration, A. Airapetian et al., *Measurement of the virtual-photon asymmetry A_2 and the spin-structure function g_2 of the proton*, *Eur. Phys. J.* **C72** (2012) 1921, [1112.5584].

[25] A. M. Kotzinian and P. J. Mulders, *Longitudinal quark polarization in transversely polarized nucleons*, *Phys. Rev.* **D54** (1996) 1229–1232, [hep-ph/9511420].

[26] A. M. Kotzinian and P. J. Mulders, *Probing transverse quark polarization via azimuthal asymmetries in leptoproduction*, *Phys. Lett.* **B406** (1997) 373–380, [hep-ph/9701330].

[27] A. Kotzinian, B. Parsamyan and A. Prokudin, *Predictions for double spin asymmetry A(LT) in semi inclusive DIS*, *Phys. Rev.* **D73** (2006) 114017, [hep-ph/0603194].

[28] H. Avakian et al., *Are there approximate relations among transverse momentum dependent distribution functions?*, *Phys. Rev.* **D77** (2008) 014023, [0709.3253].

[29] A. Metz, P. Schweitzer and T. Teckentrup, *Lorentz invariance relations between parton distributions and the Wandzura-Wilczek approximation*, *Phys. Lett.* **B680** (2009) 141–147, [0810.5212].

[30] T. Teckentrup, A. Metz and P. Schweitzer, *Lorentz invariance relations and Wandzura-Wilczek approximation*, *Mod. Phys. Lett.* **A24** (2009) 2950–2959, [0910.2567].

[31] R. Tangerman and P. Mulders, *Polarized twist-three distributions g(T) and h(L) and the role of intrinsic transverse momentum*, hep-ph/9408305.

[32] H. Avakian, H. Matevosyan, B. Pasquini and P. Schweitzer, *Studying the information content of TMDs using Monte Carlo generators*, *J. Phys.* **G42** (2015) 034015.

[33] W. R. Inc., "Mathematica, Version 11.3."

[34] J. C. Collins, *Leading-twist single-transverse-spin asymmetries: Drell–Yan and deep-inelastic scattering*, *Phys. Lett.* **B536** (2002) 43–48, [hep-ph/0204004].

[35] J. P. Ralston and D. E. Soper, *Production of Dimuons from High-Energy Polarized Proton Proton Collisions*, *Nucl. Phys.* **B152** (1979) 109.

[36] J. C. Collins and D. E. Soper, *Back-To-Back Jets in QCD*, *Nucl. Phys.* **B193** (1981) 381.

[37] X. Ji, J.-p. Ma and F. Yuan, *QCD factorization for semi-inclusive deep-inelastic scattering at low transverse momentum*, *Phys. Rev.* **D71** (2005) 034005, [hep-ph/0404183].

[38] X. Ji, J.-P. Ma and F. Yuan, *QCD factorization for spin-dependent cross sections in DIS and Drell-Yan processes at low transverse momentum*, *Phys. Lett.* **B597** (2004) 299–308, [hep-ph/0405085].

[39] J. Collins, *Foundations of perturbative QCD*, *Camb. Monogr. Part. Phys. Nucl. Phys. Cosmol.* **32** (2011) 1–624.

[40] M. G. Echevarría, A. Idilbi and I. Scimemi, *Soft and Collinear Factorization and Transverse Momentum Dependent Parton Distribution Functions*, *Phys. Lett.* **B726** (2013) 795–801, [1211.1947].

[41] S. M. Aybat and T. C. Rogers, *TMD Parton Distribution and Fragmentation Functions with QCD Evolution*, *Phys. Rev.* **D83** (2011) 114042, [1101.5057].

[42] S. M. Aybat, J. C. Collins, J.-W. Qiu and T. C. Rogers, *The QCD Evolution of the Sivers Function*, *Phys. Rev.* **D85** (2012) 034043, [1110.6428].

[43] M. G. Echevarria, A. Idilbi, Z.-B. Kang and I. Vitev, *QCD Evolution of the Sivers Asymmetry*, *Phys. Rev.* **D89** (2014) 074013, [1401.5078].

[44] J. P. Ma and G. P. Zhang, *QCD Corrections of All Structure Functions in Transverse Momentum Dependent Factorization for Drell-Yan Processes*, *JHEP* **02** (2014) 100, [1308.2044].

[45] S. M. Aybat, A. Prokudin and T. C. Rogers, *Calculation of TMD Evolution for Transverse Single Spin Asymmetry Measurements*, *Phys. Rev. Lett.* **108** (2012) 242003, [1112.4423].

[46] Z.-B. Kang, A. Prokudin, P. Sun and F. Yuan, *Extraction of Quark Transversity Distribution and Collins Fragmentation Functions with QCD Evolution*, *Phys. Rev.* **D93** (2016) 014009, [1505.05589].

[47] A. Metz and M. Schlegel, *Twist three single spin asymmetries in semiinclusive deep inelastic scattering*, *Eur. Phys. J.* **A22** (2004) 489–494, [hep-ph/0403182].

[48] L. P. Gamberg, D. S. Hwang, A. Metz and M. Schlegel, *Light-cone divergence in twist-3 correlation functions*, *Phys. Lett.* **B639** (2006) 508–512, [hep-ph/0604022].

[49] A. P. Chen and J. P. Ma, *Light-Cone Singularities and Transverse-Momentum-Dependent Factorization at Twist-3*, *Phys. Lett.* **B768** (2017) 380–386, [1610.08634].

[50] A. Efremov and P. Schweitzer, *The Chirally odd twist 3 distribution e(a)(x)*, *JHEP* **0308** (2003) 006, [hep-ph/0212044].

[51] R. L. Jaffe, *Spin, twist and hadron structure in deep inelastic processes*, hep-ph/9602236.

[52] K. Kanazawa, Y. Koike, A. Metz, D. Pitonyak and M. Schlegel, *Operator Constraints for Twist-3 Functions and Lorentz Invariance Properties of Twist-3 Observables*, *Phys. Rev.* **D93** (2016) 054024, [1512.07233].

[53] E. V. Shuryak, *The Role of Instantons in Quantum Chromodynamics. 1. Physical Vacuum*, *Nucl. Phys.* **B203** (1982) 93.

[54] D. Diakonov and V. Y. Petrov, *Instanton Based Vacuum from Feynman Variational Principle*, *Nucl. Phys.* **B245** (1984) 259.

[55] D. Diakonov, M. V. Polyakov and C. Weiss, *Hadronic matrix elements of gluon operators in the instanton vacuum*, *Nucl. Phys.* **B461** (1996) 539–580, [hep-ph/9510232].

[56] A. Accardi, A. Bacchetta, W. Melnitchouk and M. Schlegel, *What can break the Wandzura–Wilczek relation?*, *JHEP* **11** (2009) 093, [0907.2942].

[57] M. Gluck, E. Reya and A. Vogt, *Dynamical parton distributions revisited*, *Eur. Phys. J.* **C5** (1998) 461–470, [hep-ph/9806404].

[58] A. V. Efremov, K. Goeke and P. Schweitzer, *Collins effect in semi-inclusive deeply inelastic scattering and in e^+e^- annihilation*, *Phys. Rev.* **D73** (2006) 094025.

[59] M. Anselmino et al., *Transversity and Collins functions from SIDIS and e^+e^- data*, *Phys. Rev.* **D75** (2007) 054032, [hep-ph/0701006].

[60] M. Anselmino et al., *Update on transversity and Collins functions from SIDIS and e^+e^- data*, *Nucl. Phys. Proc. Suppl.* **191** (2009) 98–107, [0812.4366].

[61] Y. Koike, K. Tanaka and S. Yoshida, *Drell-Yan double-spin asymmetry A(LT) in polarized p anti-p collisions: Wandzura-Wilczek contribution*, *Phys. Lett.* **B668** (2008) 286–292, [0805.2289].

[62] Hägler, Ph. and Musch, B. U. and Negele, J. W. and Schäfer, A., *Intrinsic quark transverse momentum in the nucleon from lattice QCD*, *Europhys. Lett.* **88** (2009) 61001, [0908.1283].

[63] Musch, Bernhard U. and Hägler, Philipp and Negele, John W. and Schäfer, Andreas, *Exploring quark transverse momentum distributions with lattice QCD*, *Phys. Rev.* **D83** (2011) 094507, [1011.1213].

[64] B. Yoon, M. Engelhardt, R. Gupta, T. Bhattacharya, J. R. Green, B. U. Musch et al., *Nucleon Transverse Momentum-dependent Parton Distributions in Lattice QCD: Renormalization Patterns and Discretization Effects*, *Phys. Rev.* **D96** (2017) 094508, [1706.03406].

[65] Engelhardt, M. and Hägler, P. and Musch, B. and Negele, J. and Schäfer, A., *Lattice QCD study of the Boer-Mulders effect in a pion*, *Phys. Rev.* **D93** (2016) 054501, [1506.07826].

[66] X. Ji, P. Sun, X. Xiong and F. Yuan, *Soft factor subtraction and transverse momentum dependent parton distributions on the lattice*, *Phys. Rev.* **D91** (2015) 074009, [1405.7640].

[67] Musch, B. U. and Hägler, Ph. and Engelhardt, M. and Negele, J. W. and Schäfer, A., *Sivers and Boer-Mulders observables from lattice QCD*, *Phys. Rev.* **D85** (2012) 094510, [1111.4249].

[68] LHPC collaboration, LHPC et al., *Transverse structure of nucleon parton distributions from lattice QCD*, *Phys. Rev. Lett.* **93** (2004) 112001, [hep-lat/0312014].

[69] LHPC Collaborations collaboration, Hägler, Ph. and others, *Nucleon Generalized Parton Distributions from Full Lattice QCD*, *Phys. Rev.* **D77** (2008) 094502, [0705.4295].

[70] QCDSF collaboration, M. Gockeler et al., *Quark helicity flip generalized parton distributions from two-flavor lattice QCD*, *Phys. Lett.* **B627** (2005) 113–123, [hep-lat/0507001].

[71] M. Burkardt and Y. Koike, *Violation of sum rules for twist three parton distributions in QCD*, *Nucl. Phys.* **B632** (2002) 311–329, [hep-ph/0111343].

[72] S. D. Bass, *Fixed poles, polarized glue and nucleon spin structure*, *Acta Phys. Polon.* **B34** (2003) 5893–5926, [hep-ph/0311174].

[73] M. Stratmann, *Bag model predictions for polarized structure functions and their Q**2 evolutions*, *Z. Phys.* **C60** (1993) 763–772.

[74] A. Signal, *Calculations of higher twist distribution functions in the MIT bag model*, *Nucl. Phys.* **B497** (1997) 415–434, [hep-ph/9610480].

[75] H. Avakian, A. Efremov, P. Schweitzer and F. Yuan, *The transverse momentum dependent distribution functions in the bag model*, *Phys. Rev.* **D81** (2010) 074035, [1001.5467].

[76] R. Jakob, P. Mulders and J. Rodrigues, *Modeling quark distribution and fragmentation functions*, *Nucl. Phys.* **A626** (1997) 937–965, [hep-ph/9704335].

[77] M. Wakamatsu, *Polarized structure functions g(2)(x) in the chiral quark soliton model*, *Phys. Lett.* **B487** (2000) 118–124, [hep-ph/0006212].

[78] B. Pasquini, S. Cazzaniga and S. Boffi, *Transverse momentum dependent parton distributions in a light-cone quark model*, *Phys. Rev.* **D78** (2008) 034025, [0806.2298].

[79] C. Lorcé, B. Pasquini and M. Vanderhaeghen, *Unified framework for generalized and transverse-momentum dependent parton distributions within a 3Q light-cone picture of the nucleon*, *JHEP* **1105** (2011) 041, [1102.4704].

[80] R. Kundu and A. Metz, *Higher twist and transverse momentum dependent parton distributions: A Light front Hamiltonian approach*, *Phys. Rev.* **D65** (2002) 014009, [hep-ph/0107073].

[81] M. Schlegel and A. Metz, *On the validity of Lorentz invariance relations between parton distributions*, hep-ph/0406289.

[82] K. Goeke, A. Metz, P. Pobylitsa and M. Polyakov, *Lorentz invariance relations among parton distributions revisited*, *Phys. Lett.* **B567** (2003) 27–30, [hep-ph/0302028].

[83] C. Lorcé, B. Pasquini and P. Schweitzer, *Unpolarized transverse momentum dependent parton distribution functions beyond leading twist in quark models*, *JHEP* **01** (2015) 103, [1411.2550].

[84] C. Lorcé, B. Pasquini and P. Schweitzer, *Transverse pion structure beyond leading twist in constituent models*, *Eur. Phys. J.* **C76** (2016) 415, [1605.00815].

[85] P. Zavada, *The Structure functions and parton momenta distribution in the hadron rest system*, *Phys. Rev.* **D55** (1997) 4290–4299, [hep-ph/9609372].

[86] A. V. Efremov, P. Schweitzer, O. V. Teryaev and P. Zavada, *The relation between TMDs and PDFs in the covariant parton model approach*, *Phys. Rev.* **D83** (2011) 054025, [1012.5296].

[87] A. V. Efremov, P. Schweitzer, O. V. Teryaev and P. Zavada, *Transverse momentum dependent distribution functions in a covariant parton model approach with quark orbital motion*, *Phys. Rev.* **D80** (2009) 014021, [0903.3490].

[88] P. Schweitzer, *The Chirally odd twist three distribution function e**alpha(x) in the chiral quark soliton model*, *Phys. Rev.* **D67** (2003) 114010, [hep-ph/0303011].

[89] Y. Ohnishi and M. Wakamatsu, *pi N sigma term and chiral odd twist three distribution function e(x) of the nucleon in the chiral quark soliton model*, *Phys. Rev.* **D69** (2004) 114002, [hep-ph/0312044].

[90] C. Cebulla, J. Ossmann, P. Schweitzer and D. Urbano, *The Twist-3 parton distribution function e**a(x) in large-N(c) chiral theory*, *Acta Phys. Polon.* **B39** (2008) 609–640, [0710.3103].

[91] S. Meissner, A. Metz and K. Goeke, *Relations between generalized and transverse momentum dependent parton distributions*, *Phys. Rev.* **D76** (2007) 034002, [hep-ph/0703176].

[92] A. Mukherjee, *Twist Three Distribution e(x): Sum Rules and Equation of Motion Relations*, *Phys. Lett.* **B687** (2010) 180–183, [0912.1446].

[93] A. Harindranath and W.-M. Zhang, *Examination of Wandzura-Wilczek relation for g2 (x, q**2) in pQCD*, *Phys. Lett.* **B408** (1997) 347–356, [hep-ph/9706419].

[94] D. Boer, P. J. Mulders and F. Pijlman, *Universality of T-odd effects in single spin and azimuthal asymmetries*, *Nucl. Phys.* **B667** (2003) 201–241, [hep-ph/0303034].

[95] X. Ji, J.-W. Qiu, W. Vogelsang and F. Yuan, *A unified picture for single transverse-spin asymmetries in hard processes*, *Phys. Rev. Lett.* **97** (2006) 082002, [hep-ph/0602239].

[96] M. Anselmino et al., *The role of Cahn and Sivers effects in deep inelastic scattering*, *Phys. Rev.* **D71** (2005) 074006, [hep-ph/0501196].

[97] J. C. Collins et al., *Sivers effect in semi-inclusive deeply inelastic scattering*, *Phys. Rev.* **D73** (2006) 014021, [hep-ph/0509076].

[98] U. D'Alesio and F. Murgia, *Azimuthal and Single Spin Asymmetries in Hard Scattering Processes*, *Prog. Part. Nucl. Phys. 61* **2008** (2008) 394–454, [0712.4328].

[99] P. Schweitzer, T. Teckentrup and A. Metz, *Intrinsic transverse parton momenta in deeply inelastic reactions*, *Phys. Rev.* **D81** (2010) 094019, [1003.2190].

[100] A. Signori, A. Bacchetta, M. Radici and G. Schnell, *Investigations into the flavor dependence of partonic transverse momentum*, *JHEP* **11** (2013) 194, [1309.3507].

[101] M. Anselmino, M. Boglione, J. O. Gonzalez Hernandez, S. Melis and A. Prokudin, *Unpolarised Transverse Momentum Dependent Distribution and Fragmentation Functions from SIDIS Multiplicities*, *JHEP* **04** (2014) 005, [1312.6261].

[102] A. Bacchetta, D. Boer, M. Diehl and P. J. Mulders, *Matches and mismatches in the*

descriptions of semi- inclusive processes at low and high transverse momentum, *JHEP* **08** (2008) 023, [0803.0227].

[103] F. Landry, R. Brock, P. M. Nadolsky and C. Yuan, *Tevatron Run-1 Z boson data and Collins-Soper-Sterman resummation formalism*, *Phys. Rev.* **D67** (2003) 073016, [hep-ph/0212159].

[104] A. D. Martin, W. J. Stirling, R. S. Thorne and G. Watt, *Parton distributions for the LHC*, *Eur. Phys. J.* **C63** (2009) 189–285, [0901.0002].

[105] D. de Florian, R. Sassot and M. Stratmann, *Global analysis of fragmentation functions for pions and kaons and their uncertainties*, *Phys. Rev.* **D75** (2007) 114010, [hep-ph/0703242].

[106] P. Schweitzer, M. Strikman and C. Weiss, *Intrinsic transverse momentum and parton correlations from dynamical chiral symmetry breaking*, *JHEP* **01** (2013) 163, [1210.1267].

[107] J. Collins, L. Gamberg, A. Prokudin, T. C. Rogers, N. Sato and B. Wang, *Relating Transverse Momentum Dependent and Collinear Factorization Theorems in a Generalized Formalism*, *Phys. Rev.* **D94** (2016) 034014, [1605.00671].

[108] CLAS collaboration, M. Osipenko et al., *Measurement of unpolarized semi-inclusive pi+ electroproduction off the proton*, *Phys. Rev.* **D80** (2009) 032004, [0809.1153].

[109] HERMES collaboration, A. Airapetian et al., *Multiplicities of charged pions and kaons from semi-inclusive deep-inelastic scattering by the proton and the deuteron*, *Phys. Rev.* **D87** (2013) 074029, [1212.5407].

[110] COMPASS collaboration, M. Aghasyan et al., *Transverse-momentum-dependent Multiplicities of Charged Hadrons in Muon-Deuteron Deep Inelastic Scattering*, 1709.07374.

[111] A. Bacchetta, F. Delcarro, C. Pisano, M. Radici and A. Signori, *Extraction of partonic transverse momentum distributions from semi-inclusive deep-inelastic scattering, Drell-Yan and Z-boson production*, *JHEP* **06** (2017) 081, [1703.10157].

[112] CLAS collaboration, H. Avakian et al., *Measurement of Single and Double Spin Asymmetries in Deep Inelastic Pion Electroproduction with a Longitudinally Polarized Target*, *Phys. Rev. Lett.* **105** (2010) 262002, [1003.4549].

[113] D. W. Sivers, *Single spin production asymmetries from the hard scattering of point-like constituents*, *Phys. Rev.* **D41** (1990) 83.

[114] M. Anselmino, M. Boglione, U. D'Alesio, S. Melis, F. Murgia and A. Prokudin, *New insight on the Sivers transverse momentum dependent distribution function*, *J. Phys. Conf. Ser.* **295** (2011) 012062, [1012.3565].

[115] M. Anselmino et al., *Extracting the sivers function from polarized sidis data and making predictions*, *Phys. Rev.* **D72** (2005) 094007, [hep-ph/0507181].

[116] M. Anselmino et al., *Comparing extractions of Sivers functions*, hep-ph/0511017.

[117] W. Vogelsang and F. Yuan, *Single-transverse spin asymmetries: From dis to hadronic collisions*, *Phys. Rev.* **D72** (2005) 054028.

[118] M. Anselmino et al., *Sivers Effect for Pion and Kaon Production in Semi- Inclusive Deep Inelastic Scattering*, *Eur. Phys. J.* **A39** (2009) 89–100, [0805.2677].

[119] A. Bacchetta and M. Radici, *Constraining quark angular momentum through semi-inclusive measurements*, *Phys. Rev. Lett.* **107** (2011) 212001, [1107.5755].

[120] M. Anselmino, M. Boglione, U. D'Alesio, S. Melis, F. Murgia and A. Prokudin, *Sivers Distribution Functions and the Latest SIDIS Data*, in *19th International Workshop on Deep-Inelastic Scattering and Related Subjects (DIS 2011) Newport News, Virginia, April 11-15, 2011*, 2011. 1107.4446.

[121] HERMES collaboration, A. Airapetian et al., *Observation of the Naive-T-odd Sivers Effect in Deep-Inelastic Scattering*, *Phys. Rev. Lett.* **103** (2009) 152002, [0906.3918].

[122] COMPASS collaboration, C. Adolph et al., *II Experimental investigation of transverse spin asymmetries in μ-p SIDIS processes: Sivers asymmetries*, *Phys. Lett.* **B717** (2012) 383–389, [1205.5122].

[123] A. Bacchetta and M. Radici, *Partial wave analysis of two hadron fragmentation functions*, *Phys. Rev.* **D67** (2003) 094002, [hep-ph/0212300].

[124] A. Bacchetta and M. Radici, *Two hadron semiinclusive production including subleading twist*, *Phys. Rev.* **D69** (2004) 074026, [hep-ph/0311173].

[125] A. Bacchetta, A. Courtoy and M. Radici, *First glances at the transversity parton distribution through dihadron fragmentation functions*, *Phys. Rev. Lett.* **107** (2011) 012001, [1104.3855].

[126] A. Bacchetta, A. Courtoy and M. Radici, *First extraction of valence transversities in a collinear framework*, *JHEP* **03** (2013) 119, [1212.3568].

[127] M. Radici, A. Courtoy, A. Bacchetta and M. Guagnelli, *Improved extraction of valence transversity distributions from inclusive dihadron production*, *JHEP* **05** (2015) 123, [1503.03495].

[128] M. Radici and A. Bacchetta, *First Extraction of Transversity from a Global Analysis of Electron-Proton and Proton-Proton Data*, *Phys. Rev. Lett.* **120** (2018) 192001, [1802.05212].

[129] J. C. Collins, *Fragmentation of transversely polarized quarks probed in transverse momentum distributions*, *Nucl. Phys.* **B396** (1993) 161–182.

[130] M. Anselmino, M. Boglione, U. D'Alesio, S. Melis, F. Murgia and A. Prokudin, *Simultaneous extraction of transversity and Collins functions from new SIDIS and e^+e^- data*, *Phys. Rev.* **D87** (2013) 094019, [1303.3822].

[131] Z.-B. Kang, A. Prokudin, P. Sun and F. Yuan, *Nucleon tensor charge from Collins azimuthal asymmetry measurements*, *Phys. Rev.* **D91** (2015) 071501, [1410.4877].

[132] M. Anselmino, M. Boglione, U. D'Alesio, J. O. Gonzalez Hernandez, S. Melis, F. Murgia et al., *Collins functions for pions from SIDIS and new e^+e^- data: a first glance at their transverse momentum dependence*, *Phys. Rev.* **D92** (2015) 114023, [1510.05389].

[133] HERMES collaboration, A. Airapetian et al., *Effects of transversity in deep-inelastic scattering by polarized protons*, *Phys. Lett.* **B693** (2010) 11–16, [1006.4221].

[134] COMPASS collaboration, C. Adolph et al., *Collins and Sivers asymmetries in muonproduction of pions and kaons off transversely polarised protons*, *Phys. Lett.* **B744** (2015) 250–259, [1408.4405].

[135] V. Barone, S. Melis and A. Prokudin, *The Boer-Mulders effect in unpolarized SIDIS: An Analysis of the COMPASS and HERMES data on the cos2phi asymmetry*, *Phys. Rev.* **D81** (2010) 114026, [0912.5194].

[136] HERMES collaboration, A. Airapetian et al., *Azimuthal distributions of charged hadrons, pions, and kaons produced in deep-inelastic scattering off unpolarized protons and deuterons*, *Phys. Rev.* **D87** (2013) 012010, [1204.4161].

[137] COMPASS collaboration, C. Adolph et al., *Measurement of azimuthal hadron asymmetries in semi-inclusive deep inelastic scattering off unpolarised nucleons*, *Nucl. Phys.* **B886** (2014) 1046–1077, [1401.6284].

[138] R. N. Cahn, *Azimuthal Dependence in Leptoproduction: A Simple Parton Model Calculation*, *Phys. Lett.* **B78** (1978) 269.

[139] V. Barone, S. Melis and A. Prokudin, *Azimuthal asymmetries in unpolarized Drell-Yan processes and the Boer-Mulders distributions of antiquarks*, *Phys. Rev.* **D82** (2010) 114025, [1009.3423].

[140] V. Barone, M. Boglione, J. O. Gonzalez Hernandez and S. Melis, *Phenomenological analysis of azimuthal asymmetries in unpolarized semi-inclusive deep inelastic scattering*, *Phys. Rev.* **D91** (2015) 074019, [1502.04214].

[141] H. Avakian, A. V. Efremov, P. Schweitzer and F. Yuan, *Transverse momentum dependent distribution function $h_{1T}^{\perp}$ and the single spin asymmetry $A_{UT}^{\sin(3\phi-\phi_S)}$*, *Phys. Rev.* **D78** (2008) 114024, [0805.3355].

[142] J. She, J. Zhu and B.-Q. Ma, *Pretzelosity h(1T)**perpendicular and quark orbital angular momentum*, *Phys. Rev.* **D79** (2009) 054008, [0902.3718].

[143] C. Lorce and B. Pasquini, *Pretzelosity TMD and Quark Orbital Angular Momentum*, *Phys. Lett.* **B710** (2012) 486–488, [1111.6069].

[144] B. Parsamyan, *Transverse spin dependent azimuthal asymmetries at COMPASS*, *J. Phys. Conf. Ser.* **295** (2011) 012046, [1012.0155].

[145] HERMES collaboration, G. Schnell, *The Sivers and other semi-inclusive single-spin asymmetries at HERMES*, *PoS* **DIS2010** (2010) 247.

[146] C. Lefky and A. Prokudin, *Extraction of the distribution function $h_{1T}^{\perp}$ from experimental data*, *Phys. Rev.* **D91** (2015) 034010, [1411.0580].

[147] A. Kotzinian, *SIDIS Asymmetries in Quark-Diquark Model*, in *Transversity 2008: 2nd International Workshop on Transverse Polarization Phenomena in Hard Processes Ferrara, Italy, May 28-31, 2008*, 2008. 0806.3804. DOI.

[148] S. Boffi, A. V. Efremov, B. Pasquini and P. Schweitzer, *Azimuthal spin asymmetries in light-cone constituent quark models*, *Phys. Rev.* **D79** (2009) 094012, [0903.1271].

[149] NNPDF collaboration, R. D. Ball et al., *Parton distributions for the LHC Run II*, *JHEP* **04** (2015) 040, [1410.8849].

[150] B. Parsamyan, *Transverse spin azimuthal asymmetries in SIDIS at COMPASS: Multidimensional analysis*, *Int. J. Mod. Phys. Conf. Ser.* **40** (2016) 1660029, [1504.01599].

[151] Jefferson Lab Hall A collaboration, J. Huang et al., *Beam-Target Double Spin Asymmetry A_{LT} in Charged Pion Production from Deep Inelastic Scattering on a Transversely Polarized He-3 Target at $1.4 < Q^2 < 2.7 GeV^2$*, *Phys. Rev. Lett.* **108** (2012) 052001, [1108.0489].

[152] HERMES collaboration, L. L. Pappalardo and M. Diefenthaler, *Measurements of*

Double-Spin Asymmetries in SIDIS of Longitudinally Polarized Leptons off Transversely Polarized Protons, 1107.4227.

[153] HERMES collaboration, L. L. Pappalardo, *Accessing TMDs at HERMES*, *AIP Conf. Proc.* **1441** (2012) 229–232.

[154] HERMES collaboration, A. Airapetian et al., *Observation of a single spin azimuthal asymmetry in semiinclusive pion electro production*, *Phys. Rev. Lett.* **84** (2000) 4047–4051, [hep-ex/9910062].

[155] S. Jawalkar et al., *Semi-Inclusive π_0 target and beam-target asymmetries from 6 GeV electron scattering with CLAS*, 1709.10054.

[156] HERMES collaboration, A. Airapetian et al., *Measurement of single spin azimuthal asymmetries in semiinclusive electroproduction of pions and kaons on a longitudinally polarized deuterium target*, *Phys. Lett.* **B562** (2003) 182–192, [hep-ex/0212039].

[157] CLAS collaboration, H. Avakian et al., *Measurement of beam-spin asymmetries for pi + electroproduction above the baryon resonance region*, *Phys. Rev.* **D69** (2004) 112004, [hep-ex/0301005].

[158] HERMES collaboration, A. Airapetian et al., *Beam-Spin Asymmetries in the Azimuthal Distribution of Pion Electroproduction*, *Phys. Lett.* **B648** (2007) 164–170, [hep-ex/0612059].

[159] W. Gohn, H. Avakian, K. Joo and M. Ungaro, *Beam spin asymmetries from semi-inclusive pion electroproduction in deep inelastic scattering*, *AIP Conf. Proc.* **1149** (2009) 461–464.

[160] M. Aghasyan, H. Avakian, P. Rossi, E. De Sanctis, D. Hasch et al., *Precise Measurements of Beam Spin Asymmetries in Semi-Inclusive π^0 production*, *Phys. Lett.* **B704** (2011) 397–402, [1106.2293].

[161] CLAS collaboration, W. Gohn et al., *Beam-spin asymmetries from semi-inclusive pion electroproduction*, *Phys. Rev.* **D89** (2014) 072011, [1402.4097].

[162] A. V. Efremov, K. Goeke and P. Schweitzer, *Azimuthal asymmetries at CLAS: extraction of e**a(x) and prediction of A(UL)*, *Phys. Rev.* **D67** (2003) 114014, [hep-ph/0208124].

[163] A. Afanasev and C. E. Carlson, *Single spin beam asymmetry in semiexclusive deep inelastic electroproduction*, in *Intersections of particle and nuclear physics. Proceedings, 8th Conference, CIPANP 2003, New York, USA, May 19-24, 2003*, 2003. hep-ph/0308163.

[164] F. Yuan, *The Beam single spin asymmetry in semiinclusive deep inelastic scattering*, *Phys. Lett.* **B589** (2004) 28–34, [hep-ph/0310279].

[165] L. P. Gamberg, D. S. Hwang and K. A. Oganessyan, *Chiral odd fragmentation functions in single pion inclusive electroproduction*, *Phys. Lett.* **B584** (2004) 276–284, [hep-ph/0311221].

[166] A. V. Afanasev and C. E. Carlson, *Beam Single-Spin Asymmetry in Semi-Inclusive Deep Inelastic Scattering*, *Phys. Rev.* **D74** (2006) 114027, [hep-ph/0603269].

[167] W. Mao and Z. Lu, *Beam single spin asymmetry of neutral pion production in semi-inclusive deep inelastic scattering*, *Phys. Rev.* **D87** (2013) 014012, [1210.4790].

[168] W. Mao and Z. Lu, *On the beam spin asymmetries of electroproduction of charged hadrons off the nucleon targets*, *Eur. Phys. J.* **C74** (2014) 2910, [1401.4653].

[169] A. Courtoy, *Phenomenology of hadron structure — why low energy physics matters*, *J. Phys. Conf. Ser.* **651** (2015) 012007, [1405.6567].

[170] Y. Yang, Z. Lu and I. Schmidt, *Twist-3 T-odd fragmentation functions $G^{\perp}$ and $\tilde{G}^{\perp}$ in a spectator model*, *Phys. Lett.* **B761** (2016) 333–339, [1607.01638].

[171] M. Anselmino, A. Efremov, A. Kotzinian and B. Parsamyan, *Transverse momentum dependence of the quark helicity distributions and the Cahn effect in double-spin asymmetry A(LL) in semi inclusive DIS*, *Phys. Rev.* **D74** (2006) 074015, [hep-ph/0608048].

[172] W. Mao, X. Wang, X. Du, Z. Lu and B.-Q. Ma, *On the $\cos\phi_h$ asymmetry in electroproduction of pions in double longitudinally polarized process*, *Nucl. Phys.* **A945** (2016) 153–167.

[173] HERMES collaboration, A. Airapetian et al., *Subleading-twist effects in single-spin asymmetries in semi-inclusive deep-inelastic scattering on a longitudinally polarized hydrogen target*, *Phys. Lett.* **B622** (2005) 14–22, [hep-ex/0505042].

[174] HERMES collaboration, A. Airapetian et al., *Single spin azimuthal asymmetries in electroproduction of neutral pions in semiinclusive deep inelastic scattering*, *Phys. Rev.* **D64** (2001) 097101, [hep-ex/0104005].

[175] T. P. Cheng and A. Zee, *Coincidence electroproduction and scaling in the regge region*, *Phys. Rev.* **D6** (1972) 885–893.

[176] European Muon collaboration, J. J. Aubert et al., *Measurement of Hadronic Azimuthal Distributions in Deep Inelastic Muon Proton Scattering*, *Phys. Lett.* **130B** (1983) 118–122.

[177] J. T. Dakin, G. J. Feldman, W. L. Lakin, F. Martin, M. L. Perl, E. W. Petraske et al., *Preliminary results on the inclusive electroproduction of hadrons*, 1972.

[178] H. Mkrtchyan, P. Bosted, G. Adams, A. Ahmidouch, T. Angelescu et al., *Transverse momentum dependence of semi-inclusive pion production*, *Phys. Lett.* **B665** (2008) 20–25, [0709.3020].

[179] M. Anselmino, M. Boglione, U. D'Alesio, S. Melis, F. Murgia et al., *General Helicity Formalism for Polarized Semi-Inclusive Deep Inelastic Scattering*, *Phys. Rev.* **D83** (2011) 114019, [1101.1011].

[180] A. V. Efremov, K. Goeke, S. Menzel, A. Metz and P. Schweitzer, *Sivers effect in semi-inclusive DIS and in the Drell-Yan process*, *Phys. Lett.* **B612** (2005) 233–244, [hep-ph/0412353].

[181] L. Gamberg, Z.-B. Kang and A. Prokudin, *Indication on the process-dependence of the Sivers effect*, *Phys. Rev. Lett.* **110** (2013) 232301, [1302.3218].

[182] M. Anselmino, M. Boglione and S. Melis, *A Strategy towards the extraction of the Sivers function with TMD evolution*, *Phys. Rev.* **D86** (2012) 014028, [1204.1239].

[183] P. Sun and F. Yuan, *Energy Evolution for the Sivers Asymmetries in Hard Processes*, *Phys. Rev.* **D88** (2013) 034016, [1304.5037].

[184] M. Gluck, E. Reya, M. Stratmann and W. Vogelsang, *Models for the polarized parton distributions of the nucleon*, *Phys. Rev.* **D63** (2001) 094005, [hep-ph/0011215].

[185] A. Buckley, J. Ferrando, S. Lloyd, K. Nordström, B. Page, M. Rüfenacht et al., *LHAPDF6: parton density access in the LHC precision era*, *Eur. Phys. J.* **C75** (2015) 132, [1412.7420].

[186] B. Berthou et al., *PARTONS: PARtonic Tomography Of Nucleon Software*, *Eur. Phys. J.* **C78** (2018) 478, [1512.06174].

[187] F. Hautmann, H. Jung, M. Krämer, P. J. Mulders, E. R. Nocera, T. C. Rogers et al., *TMDlib and TMDplotter: library and plotting tools for transverse-momentum-dependent parton distributions*, *Eur. Phys. J.* **C74** (2014) 3220, [1408.3015].